Spring 5-15-2015

Single-chain RANKL Provides Insights into RANK Receptor Oligomerization and a Novel Approach to Osteoclast Inhibition

Julia Therese Warren
Washington University in St. Louis

WASHINGTON UNIVERSITY IN ST. LOUIS
Division of Biology and Biomedical Sciences
Immunology

Dissertation Examination Committee:
Steven L. Teitelbaum, Chair
Marco Colonna
Roberta Faccio
Daved H. Fremont
Philip Stahl
Wojciech Swat

Single-chain RANKL Provides Insights into RANK Receptor Oligomerization and a Novel Approach to Osteoclast Inhibition

by

Julia Therese Warren

A dissertation presented to the
Graduate School of Arts and Sciences
of Washington University in
partial fulfillment of the
requirements for the degree
of Doctor of Philosophy

May 2015
St. Louis, Missouri

Table of Contents

List of Figures

List of Tables

Acknowledgements

The completion of this thesis would not have been possible without the scientific and personal support of many. First, I would like to thank my mentor Dr. Steven Teitelbaum, whose commitment to asking new questions and finding unexpected answers, combined with a passion for mentoring the next generation of scientists, has made it a pleasure to work with him for the past several years. Working in the Teitelbaum lab has also provided me with the opportunity to have as my colleagues a wonderful group of inquisitive and supportive people. Specifically, I would like to thank Jean Chappel and Cheryl Adles for their expert technical assistance, Monica Croke for her patience in teaching me many things about the osteoclast and about being a graduate student, Nidhi Rohatgi and Wei Zou for their constant encouragements and input, and Tomo Fukunaga for tolerating my physical proximity as a desk-mate, bench-mate, and hood-mate. Working in the Teitelbaum lab has also given me the chance to receive input from many of the world's leading experts in bone biology through formal and impromptu meetings. Their input and advice have made this project more rigorous and exciting. Finally, working at the Musculoskeletal Center has given me the chance to interact with a number of scientists who I now feel privileged call my friends.

I also received excellent guidance on the goals and execution of this thesis from my committee, chaired by Phil Stahl, who has provided guidance both within and outside of committee meetings. This work was largely a collaboration between the Teitelbaum and Fremont labs, and Daved's commitment to scientific rigor has challenged me to grow as a scientist. Portions of this work necessitated my almost daily presence in the Fremont lab at times, and I would like to thank the members, especially Chris Nelson, for their willingness to offer experimental advice and to exchange ideas.

I would like to thank my friends from this and other stages of my life for their support through this process. They have been there to celebrate the successes and hear about the failures, all the while providing encouragement and a source of laughter (and occasionally food). In addition, my family have included my biggest cheerleaders no matter what the correlation to actual accomplishments. I would especially like to thank my mother, father, sister, Aunt Lynnie, Aunt Beth, and our extended family Judy and Bob for their constant belief in my potential and their unwavering support. I also would like to thank my grandmother Lucille, who would have been so proud of this document that, the next time I visited, all of her friends would be quoting from my abstract.

Finally, I have received unwavering support and love from my partner, Bob. He has tolerated strange hours away at the lab, inspired me to work harder, and motivated me to come home each day.

This work was supported by the Medical Scientist Training Program T32 training grant and a National Institute of Health F30 training grant.

ABSTRACT OF THE DISSERTATION

Single-chain RANKL Provides Insights into RANK Receptor Oligomerization and a Novel Approach to Osteoclast Inhibition

by

Julia Therese Warren

Doctor of Philosophy in Biology and Biomedical sciences

(Immunology)

Washington University in St. Louis, 2015

Professor Steven L. Teitelbaum, Chairperson

Osteoporosis is a skeletal disease characterized by bone resorption in excess of bone formation. The osteoclast is the sole bone resorbing cell and therefore provides an important avenue for novel therapeutic development. The mature osteoclast is derived from the monocyte/macrophage lineage, and its proper differentiation and function requires the interaction of receptor activator of NF-kB Ligand (RANKL) with its receptor RANK. RANKL exists as a homotrimer, with classical models of receptor activation assuming trimeric clustering of receptor as necessary for signal transduction. We have designed a novel single-chain RANKL (scRANKL) construct to test the assumption that the recruitment of three RANK receptors is necessary for downstream signaling. scRANKL consists of all three RANKL monomers connected by short, protease-resistant linkers, enabling individual manipulation of each RANK binding site and assessment of the receptor clustering state necessary for downstream signaling. We used our co-crystal structure of RANK/RANKL to design mutations in RANKL that abolish binding to RANK. After inserting these variants at one scRANKL site, to create a single-

blocked ligand capable of recruiting only two RANK receptors, we still observe RANK signaling and osteoclast formation, although only at high ligand concentrations. In contrast, double-blocked scRANKL does not form osteoclasts. Hence, dimeric engagement of RANK by RANKL is sufficient and necessary for downstream signaling. Although double-blocked scRANKL may potentially antagonize RANK/RANKL signaling, it competes poorly with endogenous RANKL due to loss of receptor avidity. Therefore, we identified mutations in RANKL, using yeast surface display, that dramatically increase its affinity for RANK. Concurrently, we sorted for loss of binding to OPG, the RANKL endogenous decoy receptor, with the hypothesis that this trait would allow scRANKL to more efficiently function as a competitive antagonist, in vivo. When inserted at the intact RANK binding sites in single- or double-blocked scRANKL, these novel constructs are highly efficient inhibitors of wild-type RANKL-induced osteoclastogenesis. Our work demonstrates that the manipulation of RANK receptor oligomerization, and the subsequent blockade in signaling, may provide a novel avenue to develop anti-resorptive drugs. Additionally, the design of single-chain TNFSF ligands with individually manipulated receptor binding sites can more broadly inform our knowledge of how these receptors, with diverse biological functions, initiate signal transduction.

Chapter 1

Introduction

1.1 Background

Bone homeostasis

The skeletal system in mammals acts not only as a scaffold whose biomechanical properties are crucial for movement and mineral homeostasis, but also as a key site for the development and maintenance of hematopoietic lineage cells (*1*). More recently, it has been suggested that the skeleton acts as an endocrine organ to regulate whole organism metabolism (*2*). Classically, basal conditions within the skeleton were thought to be maintained by a balance between the bone anabolic osteoblast and the bone resorptive osteoclast (*3*). It is now appreciated that the osteocyte, itself a terminally differentiated osteoblast, plays a critical role in sensing mechanical stress and perhaps in regulating other cell types within the bone marrow cavity (*4*). Both the osteoblast and the osteocyte are derived from bone marrow stromal cells, and their crucial roles in the synthesis and mineralization of bone matrix have been extensively studied (*5*).

The osteoclast is a multinucleated cell derived from hematopoietic lineage monocyte/macrophages precursors (*6*). Osteoclasts act to resorb bone by attaching via the recognition of matrix-embedded "RGD" ligands binding to the avb3 integrin (*7-9*). Subsequent signaling leads to actin cytoskeletal organization, the formation of an actin-rich sealing zone, and finally the generation of a ruffled plasmalemma border juxtaposed to bone (*10, 11*). The directional secretion of acid- and collagenolytic enzyme-containing vesicles into the resorptive area promotes dissolution of the inorganic phase of bone, followed by proteolytic cleavage of the demineralized, organic component (*12*).

A long-standing question regarding skeletal homeostasis is how osteoclastic bone resorption and osteoblastic bone formation are coupled in time and space. It is believed that

bone formation is directed to areas of recent, active bone resorption thus providing a mechanism by which older, less mechanically sound bone can be equally replaced by new bone (*13, 14*). This phenomenon has been recognized for decades (*15*), and recent efforts have pointed to several candidate factors that may act to link these two processes (*16-20*). Although the precise molecular mechanisms governing this aspect of bone homeostasis, it is clear that a balance between these two processes is essential.

Diseases Resulting in Low Bone Mass

Although in basal conditions of skeletal homeostasis the actions of the bone anabolic osteoblast and the bone catabolic osteoclast are quantitatively balanced to maintain skeletal mass, many diseases reflect an imbalance toward osteoclast activity. Among these are osteoporosis or the lytic lesions of skeletal metastases, and rheumatoid arthritis. In particular, post-menopausal low bone mass and osteoporosis are estimated to affect roughly over 50 million Americans. Decreased bone mass attending a decline in estrogen levels fuels primarily an increase in osteoclastic bone resorption that osteoblastic bone formation is unable to compensate for (*21*). These diseases predispose to fragility fractures, likely reflecting not only a decrease in bone mineral density but also compromised bone quality reflected in such parameters as thinning of trabeculae and loss of trabecular connectivity. Additionally, pathologies such as Paget's disease of the bone reflect focal, increase bone turnover with a balance toward resorption (*22*).

Role of RANK, RANKL and OPG in regulating osteoclasts

Several cytokines influence the formation and function of osteoclasts, but nearly 15 years ago a series of genetic studies demonstrated the interaction of receptor activator of NF-kB ligand

(RANKL) with its receptor RANK to be key molecular events necessary for these processes (*23-26*). Around the same time, osteoprotegerin (OPG) was described as a decoy receptor for RANKL, preventing its association with RANK and thus inhibiting osteoclast formation and function (*27*, *28*). Reflecting the role of the RANK/RANKL/OPG axis in bone homeostasis, humans with inactivating mutations in RANK or RANKL can present with osteoclast-poor autosomal recessive osteopetrosis (ARO) (*29*). This disease is characterized by impaired remodeling, retention of mineralized cartilage, high bone mass and an absence of tartrate-resistant acid phosphatase (TRAP)-positive osteoclasts on histological sections (*30*). Conversely, mutations in OPG result in idiopathic hyperphosphatasia, also known as juvenile Paget's disease (*31*). This diminished functionality of OPG causes a state of high bone turnover with hyperactivated osteoclasts and concomitant increased osteoblast activity. Progressive long bone deformities and predisposition to fracture are the result of overall low bone mass. Table 1.1 summarizes currently identified mutations affecting the regions encoding the cytokine/receptor interface.

Tumor Necrosis Factor Superfamily

RANKL is a member of the tumor necrosis factor superfamily (TNFSF) and both RANK and OPG are members of the TNF receptor superfamily (TNFRSF). There are at least 19 TNFSF cytokines and 30 receptors in humans displaying low sequence conservation with high degrees of structural homology (*32*). The available TNFSF structures all show the cytokine as homotrimers (reviewed in (*33*), see also (*34-39*)) composed of two layered beta sheets named from N- to C-terminal as the A through H sheets with connected loops likewise termed the AA', A'B, BC etc. loops. The A'/A/H/C/F sheet is mostly buried, forming a hydrophobic core thought

to be important for trimer stability, whereas the B'/B/G/D/E is less buried. Loops connecting the beta sheets face outward from the core of the protein, comprising most of the binding interface formed between two adjacent monomers. All TNFSF members are Type II transmembrane proteins, and in some cases are thought to take on soluble forms after either cleavage off of the cell surface or through alternative splicing.

RANKL is a member of the so-called "conventional" TNFSF ligands, along with TNFα, lymphotoxin alpha (LTα), LTβ, tumor necrosis factor-related apoptosis inducing ligand (TRAIL), FasL, TNF-like ligand 1A (TL1A), lymphotoxin exhibiting inducible expression and competing with herpes simplex virus glycoprotein D for herpesvirus entry mediator a receptor expressed by T lymphocytes (LIGHT), and CD40L. Conserved elements among this family are hydrophobic residues in the DE loop, relatively long CD, DE, and EF loops, and a footprint for the receptor with two clustered contact areas (*33*, *40*). The other loop making substantial contact with receptor, the AA' loop, varies in length wildly among TNFSF members from 6 residues (TNFα) to 22 (TRAIL). Among TNFSF member, RANKL is most closely related to TRAIL, sharing 25% sequence identity between murine and 27% between human cytokines (aligned using ClustalW (*41*)). The structures of human RANKL (3URF) and human TRAIL (1DG6) align with a Cα root mean square difference (RMSD) of 1.31Å, indicating substantial overall structural homology (alignments performed using PDBeFold (*42*)). Indeed, TRAIL likely is also capable of binding OPG, though at low affinity (*43*, *44*), and clusters phylogenetically with RANKL as a distinct family among the TNFSF (*45*).

Tumor Necrosis Factor Receptor Superfamily

The extracellular portion of TNF receptors consists of modular cysteine-rich domains (CRDs) with varying numbers of intramolecular disulfide bonds (*46*). These receptors are primarily type I transmembrane proteins and take on an elongated, rod-like shape of between one and four CRDs. Although less well structurally studied than the TNF ligands, most TNF receptors are thought to be monomeric in nature. A notable exception is the observation of a TNFR1 dimer when crystallized alone, either in a head-to-head or head-to-tail orientation (*47*). How relevant this TNFR1 dimer is to the control of receptor signaling remains to be established.

RANK and OPG both contain four extracellular CRDs, and despite having only 34% sequence similarity, individual superposition of the CRDs yields Ca RMSDs between 0.9 and 1.5Å (*34*). Though they occupy a similar overall binding grove, we were able to identify several key differences in the individual residues used to make contact with RANKL. Specifically, OPG makes more extensive contacts to the DE loop and also possesses a key binding determinant at residue, F96. This residue participates in pi-stacking interactions with portions of the RANKL CD loop, which undergo a significant rearrangement in this area to accommodate OPG. Indeed, the corresponding residue F117 in humans is mutated in several reported cases of juvenile idiopathic hyperphosphatasia (Table 1.1). Conversely, the interaction with RANK requires no substantial rearrangements of RANKL and the receptor appears to be shifted slightly away from the RANKL DE-loop side of the interface.

Additionally, a key difference between RANK and OPG lies in their C-terminal regions. Following its CRDs, RANK contains a transmembrane region and a long cytoplasmic motif with TNF receptor-associated factor (TRAF) recruitment motifs (*48*, *49*). Its signaling is described below. OPG, however, is secreted and capable of forming a homo-dimer through its C-terminal region, especially the death-like domains and the penultimate C400 residue (*50*). OPG also

contains a heparin-binding basic region, which has been implicated in the sub-cellular localization of RANKL in osteoblastic cells (*51*). Interestingly, several patients with juvenile Paget's diseases have mutations disrupting both the death-like domain and the heparin binding domains (*31*, *52-54*). However, these patients are also missing the crucial regions for OPG dimerization. It remains to be seen which role of OPG (as a highly avid decoy receptor or as regulator of RANKL trafficking) are functionally significant in light of these mutations.

Binding of RANKL to RANK or OPG

We previously determined the single-site binding affinities of RANKL for both RANK and OPG (*34*) using surface plasmon resonance (SPR). In these experiments, the monomeric fragments of each receptors containing the cytokine-binding CRDs was used as the analyte, thus allowing us to measure the kinetics of how RANK or OPG bind to an individual cleft within the trimer. From these experiments, we observed that RANKL binds to RANK with approximately 2uM affinity. This is reflected in a relatively slow on-rate and fast off-rate (see Table 1.2). Conversely, the single-site affinity of OPG for RANKL is almost 500-fold higher at approximately 5nM. For OPG, association and dissociation rates are 30-fold faster and 20-fold slower, respectively. These values are consistent with the function of OPG as a decoy receptor. Measuring single-site affinities of OPG for RANKL necessitated using only the ligand-binding, CRDs of OPG rather than the full-length molecule which is known to form a homodimer. From our data, we cannot determine whether one full-length OPG homodimer is capable of binding to grooves on two separate RANKL trimers, or whether each arm of the full-length OPG dimer binds to two distinct grooves within one RANKL homotrimer.

The values that we measured for these interactions varied from previously reported ones (*35, 36*). It is important to note that our experiments address single-site binding, rather than the apparently much higher affinities reported using trimeric ligand as analyte (a reflection of the effects of avidity and measurements of an apparent Kd). Indeed, the issue or measuring single-site affinities versus apparent affinities of oligomeric interactions plagues the TNFSF literature. Table 1.2 outlines the reported binding affinities of RANKL for RANK and OPG, as well as the affinity of TRAIL for OPG. Within the RANK/RANKL interaction alone, the affinities vary from 2.0 uM to 68 pM. This nearly 30,000-fold difference in affinity could be explained by experimental design alone, as the extraordinarily high affinity measurement reflects SPR-determination by immobilizing monomeric ligand and flowing over trimeric ligand as the analyte. Variation in other measurements could be due to different purification systems yielding glycosylated or non-glycosylated versions, or due to differences between murine and human variants. Ultimately, single-site affinity measurements by SPR are substantially more quantitative and therefore all binding data presented in this dissertation will reflect this type of analysis.

Signaling downstream of RANKL binding to RANK

Despite its long cytoplasmic tail, RANK receptor possesses no intrinsic enzymatic activity and instead recruits signaling adaptors via conserved motifs, including TNF-receptor associated factors (TRAFs). Indeed, recruitment (*48*) and subsequent ubiquitin ligase activity (*55*) of TRAF6 is required for osteoclast differentiation. Following activation of TRAF6, TAB2 and TAK1 are recruited (*56, 57*) which allows for the ubiquitination and activation of IKKg or NEMO (*58*). Eventually, active IKK complex phosphorylates the NF-κB repressor IκBa,

leading to its proteasomal degradation and allowing NF-κB to translocate to the nucleus (*59*) where it regulates the expression of several osteoclast-specific genes. Additionally, during differentiation RANK signaling via TRAF6 can activate the MAP kinases p38, JNK, and ERK (*60*). Together, these kinases activate the transcription factors c-fos and c-Jun, which can act in concert to promote the upregulation of several crucial genes, including NFATc1 (*61*). The crucial step of NFATc1 activation (*62*) by RANK signaling occurs in conjunction with co-stimulatory ITAM signals (*63*) acting via PLCgamma2 and calcium signaling (*64*). In addition to TRAF-binding motifs, other regions of the RANK cytoplasmic motif have been implicated in its signaling. Several groups have pointed to a crucial "IVVY" motif as being important for osteoclastogenic signals (*65*, *66*), perhaps through the recruitment of PLCgamma2 and the scaffold protein Gab2 (*67*).

RANK signaling not only induces differentiation of macrophages into osteoclasts, it can also activate the mature cell to resorb bone (*68*). In mature cells, this occurs via organization of the cytoskeleton to form actin rings (*69*). The binding of TRAF6, but not other TRAFs, is essential for proper cytoskeletal organization (*70*). Indeed, mice lacking a molecule that serves to negatively regulate the association of TRAF6 and RANK exhibit not only enhanced osteoclastogenesis, but also enhanced activation of the cytoskeleton in response to RANKL treatment (*71*). RANKL mediated actin ring formation is also dependent upon Src kinase activity (*72*, *73*) and the ability to induce Src-mediated formation of a cytoskeletal organizing RANK/Src/avB3 complex (*74*).

Initiating Signal Transduction

Although the signaling cascades described above have been extensively characterized, the precise mechanism that transforms extracellular ligand binding into intracellular, receptor-initiated signaling cascades remains a fascinating question. For G-protein coupled receptors (GPCRs), ligand binding is thought to induce a conformational change that recruits heterotrimeric G-proteins and promotes the exchange of GDP for GTP, thus initiating signaling (*75*). The classic example of oligomeric ligand causing receptor activation is in the epidermal growth factor receptor (EGFR). At resting state, monomeric and dimeric receptor species are in equilibrium but ligation by dimeric EGF stabilizes the oligomer, promoting its intrinsic kinase activity and inducing autophosphorylation/activation (*76*). No known TNF receptor contains instrinsic enzymatic activity or directly recruits an intracellular enzyme. It has been largely assumed that ligand-induced trimerization of individual monomer receptor chains is the initiating event for signal transduction. For some TNF receptor members, it has been proposed that multimers of receptor are pre-formed in the absence of ligand (*77-80*), and that ligand binding allows for a conformational change that brings the intracellular adapter-recruitment motifs into proximity (*81*). Although there exists a crystal structure of TNFR1 in a dimeric state with extensive contacts form at the proposed "pre-ligand association domain" (*47*), the crystal structures of several TRAFs alone or bound to the receptor pepties site show formation of a trimeric species (*82*). Therefore, the exact oligomeric nature of receptor required for the initiating of downstream signaling remains to be fully elucidated. More recently, higher order clustering has been proposed for several TNFRs (*83-85*).

Several studies have attempted to address the issue of receptor oligomerization necessary for RANK signal initiation. In one study, a chimeric protein consisting of RANK cytoplasmic domain fused to the erythropoietin extracellular portion was transfected into the immortalized

macrohpage cell line RAW264.7 (*86*). Agonist antibody ligation purportedly results in dimeric clustering of receptor, and in this context the authors observed decreased osteoclast formation and function. However, a separate group reported that the overexpression of differentially tagged RANK receptor could lead to its ligand-independent clustering and activation (*87*). This group identified the same IVVY cytoplasmic motif described above as recruiting Gab2 and PLCg as being responsible for pre-ligand receptor association. However, careful titration of RANK in a subsequent overexpression study (*88*) failed to reproduce ligand-independent receptor clustering and signal transduction, highlighting the need for tools to address this fundamental issue using unmanipulated, primary cells.

Single-chain TNFSF

The ligands of the TNFSF fold in such a way that the N- and C-termini of neighboring monomers are immediately adjacent. This fact has been used by several groups to create versions of TNFa (*89*) or TRAIL (*90, 91*) that contain each monomer covalently linked by short, flexible amino acid stretches. These constructs have been termed "single-chain" because the trimeric ligand is synthesized as one, single polypeptide chain. Additionally, Boschert *et al* (*92*) demonstrated that in principle it is possible to individually mutate the receptor recruitment sites within single-chain TNF. Although they used these constructs to probe the differences in TNFR1-Fas or TNFR2-Fas chimeric receptor overexpressing cell lines, it is easy to conceive a scenario where these proteins could be used to address issues of receptor multimerization in unmanipulated cells using TNFR1 or TNFR2 selective variants.

1.2 Rationale for the thesis

We reasoned that construction of a single-chain RANKL (scRANKL) would allow us to probe the receptor oligomeric state of RANK necessary and sufficient for downstream signaling in osteoclast precursors. To this end, we constructed and optimized the expression of scRANKL. We utilized our previously described co-crystal structures to generate mutations in RANKL incapable of recruiting RANK receptor and introduced this mutation into scRANKL. Additionally, we reasoned that we could identify a version of scRANKL capable of binding RANK receptor yet incapable of generating osteoclastogenic signals thus providing a novel mechanism for inhibition. Not surprisingly, scRANKL variants incapable of binding receptor at one or two sites were unable to compete with the avidity afforded to trimeric, WT-RANKL. An additional aim of this work was to identify mutations in RANKL that increased the affinity for RANK. Upon insertion into the intact receptor recruitment sites, we were able to generate a highly effective RANKL inhibitor. We tested this ability of this protein to antagonize RANKL-mediated osteoclast formation both *in vitro* and *in vivo*.

From our attempts to identify high affinity RANKL, we generated a panel of mutants with a wide range of affinities for RANK. We observed that there was not a simple linear relationship between receptor binding and osteoclastogenic capacity. Rather, supraphysiologic binding mediated by extremely long off-rates is not equally capable of agonist activity as variants with only modest increases in affinity. This biphasic effect suggests a mechanism for receptor activation that relies on the ability not only to associate, but also to dissociate from receptor, as being crucial for activation.

1.3 Tables

Table 1.1 RANK, OPG, and RANKL mutations at the ligand/receptor interface

	Mutation (Human)	Residue (Murine)	Location in structure	Structural predictions	Disease Association	Reference
OPG	C44R	C23	CRD1	Disulfide bond to C62 disrupted -> improper folding	Idiopathic hyperphosphatasia (juvenile Paget's disease)	(*54*)
	C65R	C44	CRD2 – A1	Disulfide bond to C87 disrupted -> improper folding	Idiopathic hyperphosphatasia (juvenile Paget's disease)	(*31*)
	C87Y	C66	CRD2 – B2	Disulfide to C113 disrupted -> improper folding	Idiopathic hyperphosphatasia (juvenile Paget's disease)	(*31*)
	F117L	F96L	CRD3 – A1	Loss of crucial hydrophobic and aromatic ring stacking energetics -> decreased affinity for RANKL	Idiopathic hyperphosphatasia (juvenile Paget's disease)	(*31*)
	ΔD182 (in frame)	D161	CRD4 – B1	Equivalent RANK residue involved in intramolecular salt bridge to conserved T174, loss of salt bridge could lead to protein instability. Alternatively, this may displace nearby C195 needed for disulfide bond to C175	Idiopathic hyperphosphatasia (juvenile Paget's disease)	(*93*)
RANK	G53R	G24	CRD1 – B2	Needed to make a tight turn. Probably disrupts folding of CRD1	ARO	(*94*)
	R129C	R100	CRD3 A->B X2	Salt bridge to $RANKL^{E225}$, hydrogen bonds to $RANKL^{N266, E268}$ disrupted interactions -> decreased affinity	ARO (Compound heterozygote with C175R)	(*94*)
	A134V	A105	CRD3 – B1	Adjacent to C104, may disrupt disulfide bond to C151	ARO	(*95*)
	D148V	D119	CRD3 – B1	Intramolecular salt bridge to mainchain T102 and His90, may be important for folding or stability	ARO	(*95*)
	R170G	K141	CRD4 A->B X2	Forms intramolecular salt bridge to D162 which may be important for folding or stability	ARO	(*94*)
	C175R	C146	CRD4 – B1	Disulfide to C195 disrupted -> improper folding	ARO (Compound heterozygote with R129C)	(*94*)
RANKL	Δ145-177	146-176	A strand into AA' loop	Important contacts to RANK, likely impact binding. Not heavily contacted by OPG.	ARO	(*96*)
	M199K	M198	A''-B' loop	No contacts to RANK or OPG, no inter-monomer RANKL contacts. Core residue that may be important for monomer folding.	ARO	(*96*)
	Frameshift at V277	V276	F strand	Missing F, G, and H strands likely critical for proper folding or trimer assembly	ARO	(*96*)

Table 1.2. Reported murine or human RANK/RANKL, OPG/RANKL or OPG/TRAIL binding affinities.

Immobilized	Analyte	ka (1/Ms)	kd (1/s)	KD (M)	Reference
mRANKL	mRANK (CRDs)	4.7×10^{4}	1.1×10^{-1}	2.6×10^{-6}	(*34*)
mRANK	mRANKL	NR	NR	6.8×10^{-11}	(*35*)
mRANK*	mRANKL*	NR	NR	2.3×10^{-7}	(*36*)
hRANK	hRANKL	NR	NR	2.1×10^{-9}	(*97*)
hRANK	hRANKL	NR	NR	1.1×10^{-10}	(*98*)
RANK-Fc	RANKL	4.9×10^{5}	3.3×10^{-4}	6.7×10^{-10}	(*99*)
mRANKL	mOPG (CRDs)	1.4×10^{6}	1.1×10^{-3}	5.1×10^{-9}	(*34*)
hRANKL	hOPG (CRDs)	6.5×10^{6}	4.2×10^{-3}	6.5×10^{-10}	(*38*)
hOPG-Fc	hRANKL	7.6×10^{5}	1.3×10^{-3}	1.7×10^{-9}	(*50*)
hRANKL	hOPG (FL)	3.0×10^{5}	2.0×10^{-3}	1.0×10^{-8}	(*50*)
hRANKL	hOPG (CRDs)	1.6×10^{3}	5.0×10^{-3}	3.0×10^{-6}	(*50*)
hOPG-Fc	hRANKL	NR	NR	6.7×10^{-9}	(*100*)
hOPG-Fc	hTRAIL	NR	NR	4.5×10^{-8}	(*101*)
hOPG-Fc	hTRAIL	NR	NR	4.0×10^{-7}	(*43*)
hOPG-Fc	hTRAIL	NR	NR	1.0×10^{-9}	(*102*)
hOPG-Fc	hTRAIL	6.6×10^{4}	2.0×10^{-4}	3.0×10^{-9}	(*44*)

*Indicates isothermal calorimetry (ITC) experiment with TNFSF member injected into a stirred cell of TNFRSF member. All other experiments were performed using surface plasmon resonance (SPR).

1.4 References

1. M. Zaidi, Skeletal remodeling in health and disease, *Nat. Med.* **13**, 791–801 (2007).

2. G. Karsenty, M. Ferron, The contribution of bone to whole-organism physiology, *Nature* **481**, 314–320 (2012).

3. S. C. Manolagas, R. L. Jilka, Bone marrow, cytokines, and bone remodeling. Emerging insights into the pathophysiology of osteoporosis, *N. Engl. J. Med.* **332**, 305–311 (1995).

4. L. F. Bonewald, The amazing osteocyte, *J Bone Miner Res* **26**, 229–238 (2011).

5. F. Long, Building strong bones: molecular regulation of the osteoblast lineage, *Nat. Rev. Mol. Cell Biol.* **13**, 27–38 (2012).

6. N. Kurihara, C. Chenu, M. Miller, C. Civin, G. D. Roodman, Identification of committed mononuclear precursors for osteoclast-like cells formed in long term human marrow cultures, *Endocrinology* **126**, 2733–2741 (1990).

7. M. H. Helfrich, S. A. Nesbitt, E. L. Dorey, M. A. Horton, Rat osteoclasts adhere to a wide range of RGD (Arg-Gly-Asp) peptide-containing proteins, including the bone sialoproteins and fibronectin, via a beta 3 integrin, *J Bone Miner Res* **7**, 335–343 (1992).

8. S. B. Rodan, G. A. Rodan, Integrin function in osteoclasts, *J. Endocrinol.* **154 Suppl**, S47–56 (1997).

9. X. Feng *et al.*, A Glanzmann's mutation in beta 3 integrin specifically impairs osteoclast function, *J. Clin. Invest.* **107**, 1137–1144 (2001).

10. K. P. McHugh *et al.*, Mice lacking beta3 integrins are osteosclerotic because of dysfunctional osteoclasts, *J. Clin. Invest.* **105**, 433–440 (2000).

11. K. A. Szewczyk, K. Fuller, T. J. Chambers, Distinctive subdomains in the resorbing surface of osteoclasts, *PLoS ONE* **8**, e60285 (2013).

12. S. L. Teitelbaum, Bone resorption by osteoclasts, *Science* **289**, 1504–1508 (2000).

13. B. F. Boyce, L. Xing, Functions of RANKL/RANK/OPG in bone modeling and remodeling, *Arch. Biochem. Biophys.* **473**, 139–146 (2008).

14. A. Leibbrandt, J. M. Penninger, TNF conference 2009: beyond bones - RANKL/RANK in the immune system, *Adv. Exp. Med. Biol.* **691**, 5–22 (2011).

15. Z. F. Jaworski, C. Hooper, Study of cell kinetics within evolving secondary Haversian systems, *J. Anat.* **131**, 91–102 (1980).

16. Y. Tang *et al.*, TGF-beta1-induced migration of bone mesenchymal stem cells couples bone resorption with formation, *Nat. Med.* **15**, 757–765 (2009).

17. C. Zhao *et al.*, Bidirectional ephrinB2-EphB4 signaling controls bone homeostasis, *Cell Metab.* **4**, 111–121 (2006).

18. J. Ryu *et al.*, Sphingosine 1-phosphate as a regulator of osteoclast differentiation and osteoclast-osteoblast coupling, *EMBO J.* **25**, 5840–5851 (2006).

19. L. Pederson, M. Ruan, J. J. Westendorf, S. Khosla, M. J. Oursler, Regulation of bone formation by osteoclasts involves Wnt/BMP signaling and the chemokine sphingosine-1-

phosphate, *Proceedings of the National Academy of Sciences* **105**, 20764–20769 (2008).

20. S. Takeshita *et al.*, Osteoclast-secreted CTHRC1 in the coupling of bone resorption to formation, *J. Clin. Invest.* **123**, 3914–3924 (2013).

21. L. A. G. Armas, R. R. Recker, Pathophysiology of osteoporosis: new mechanistic insights, *Endocrinol. Metab. Clin. North Am.* **41**, 475–486 (2012).

22. S. H. Ralston, R. Layfield, Pathogenesis of Paget disease of bone, *Calcif. Tissue Int.* **91**, 97–113 (2012).

23. Y. Y. Kong *et al.*, OPGL is a key regulator of osteoclastogenesis, lymphocyte development and lymph-node organogenesis, *Nature* **397**, 315–323 (1999).

24. W. C. Dougall *et al.*, RANK is essential for osteoclast and lymph node development, *Genes Dev.* **13**, 2412–2424 (1999).

25. N. Kim, P. R. Odgren, D. K. Kim, S. C. Marks, Y. Choi, Diverse roles of the tumor necrosis factor family member TRANCE in skeletal physiology revealed by TRANCE deficiency and partial rescue by a lymphocyte-expressed TRANCE transgene, *Proc Natl Acad Sci USA* **97**, 10905–10910 (2000).

26. J. Li *et al.*, RANK is the intrinsic hematopoietic cell surface receptor that controls osteoclastogenesis and regulation of bone mass and calcium metabolism, *Proc Natl Acad Sci USA* **97**, 1566–1571 (2000).

27. W. S. Simonet *et al.*, Osteoprotegerin: a novel secreted protein involved in the regulation of bone density, *Cell* **89**, 309–319 (1997).

28. N. Bucay *et al.*, osteoprotegerin-deficient mice develop early onset osteoporosis and arterial calcification, *Genes Dev.* **12**, 1260–1268 (1998).

29. C. Sobacchi, A. Schulz, F. P. Coxon, A. Villa, M. H. Helfrich, Osteopetrosis: genetics, treatment and new insights into osteoclast function, *Nat Rev Endocrinol* **9**, 522–536 (2013).

30. J. C. Crockett, D. J. Mellis, D. I. Scott, M. H. Helfrich, New knowledge on critical osteoclast formation and activation pathways from study of rare genetic diseases of osteoclasts: focus on the RANK/RANKL axis, *Osteoporos Int* **22**, 1–20 (2011).

31. B. Chong *et al.*, Idiopathic hyperphosphatasia and TNFRSF11B mutations: relationships between phenotype and genotype, *J Bone Miner Res* **18**, 2095–2104 (2003).

32. T. Hehlgans, K. Pfeffer, The intriguing biology of the tumour necrosis factor/tumour necrosis factor receptor superfamily: players, rules and the games, *Immunology* **115**, 1–20 (2005).

33. H. Wu, S. G. Hymowitz, in *Handbook of Cell Signaling*, R. Bradshaw, E. Dennis, Eds. (Academic Press, 2009), vol. 1, pp. 265–275.

34. C. A. Nelson, J. T. Warren, M. W.-H. Wang, S. L. Teitelbaum, D. H. Fremont, RANKL employs distinct binding modes to engage RANK and the osteoprotegerin decoy receptor, *Structure/Folding and Design* **20**, 1971–1982 (2012).

35. C. Liu *et al.*, Structural and functional insights of RANKL-RANK interaction and signaling, *The Journal of Immunology* **184**, 6910–6919 (2010).

36. H. M. Ta *et al.*, Structure-based development of a receptor activator of nuclear factor-kappaB ligand (RANKL) inhibitor peptide and molecular basis for osteopetrosis, *Proceedings of the*

National Academy of Sciences **107**, 20281–20286 (2010).

37. C. Zhan *et al.*, Decoy strategies: the structure of TL1A:DcR3 complex, *Structure* **19**, 162–171 (2011).

38. X. Luan *et al.*, Crystal structure of human RANKL complexed with its decoy receptor osteoprotegerin, *The Journal of Immunology* **189**, 245–252 (2012).

39. Y. Mukai *et al.*, Solution of the structure of the TNF-TNFR2 complex, *Sci Signal* **3**, ra83 (2010).

40. J.-L. Bodmer, P. Schneider, J. Tschopp, The molecular architecture of the TNF superfamily, *Trends Biochem. Sci.* **27**, 19–26 (2002).

41. M. Goujon *et al.*, A new bioinformatics analysis tools framework at EMBL-EBI, *Nucleic Acids Res.* **38**, W695–9 (2010).

42. E. Krissinel, K. Henrick, Secondary-structure matching (SSM), a new tool for fast protein structure alignment in three dimensions, *Acta Crystallogr. D Biol. Crystallogr.* **60**, 2256–2268 (2004).

43. A. Truneh *et al.*, Temperature-sensitive differential affinity of TRAIL for its receptors. DR5 is the highest affinity receptor, *J. Biol. Chem.* **275**, 23319–23325 (2000).

44. J. G. Emery *et al.*, Osteoprotegerin is a receptor for the cytotoxic ligand TRAIL, *J. Biol. Chem.* **273**, 14363–14367 (1998).

45. Y. Collette, A. Gilles, P. Pontarotti, D. Olive, A co-evolution perspective of the TNFSF and

TNFRSF families in the immune system, *Trends Immunol.* **24**, 387–394 (2003).

46. J. H. Naismith, S. R. Sprang, Modularity in the TNF-receptor family, *Trends Biochem. Sci.* **23**, 74–79 (1998).

47. J. H. Naismith, T. Q. Devine, T. Kohno, S. R. Sprang, Structures of the extracellular domain of the type I tumor necrosis factor receptor, *Structure/Folding and Design* **4**, 1251–1262 (1996).

48. B. G. Darnay, J. Ni, P. A. Moore, B. B. Aggarwal, Activation of NF-κB by RANK Requires Tumor Necrosis Factor Receptor-associated Factor (TRAF) 6 and NF-κB-inducing Kinase IDENTIFICATION OF A NOVEL TRAF6 INTERACTION MOTIF, *J. Biol. Chem.* **274**, 7724–7731 (1999).

49. W. Liu *et al.*, Functional identification of three receptor activator of NF-kappa B cytoplasmic motifs mediating osteoclast differentiation and function, *J. Biol. Chem.* **279**, 54759–54769 (2004).

50. L. A. Schneeweis, D. Willard, M. E. Milla, Functional dissection of osteoprotegerin and its interaction with receptor activator of NF-kappaB ligand, *J. Biol. Chem.* **280**, 41155–41164 (2005).

51. S. Aoki *et al.*, Function of OPG as a traffic regulator for RANKL is crucial for controlled osteoclastogenesis, *J Bone Miner Res* **25**, 1907–1921 (2010).

52. K. Janssens, M. C. de Vernejoul, F. de Freitas, F. Vanhoenacker, W. Van Hul, An intermediate form of juvenile Paget's disease caused by a truncating TNFRSF11B mutation, *Bone* **36**, 542–548 (2005).

53. M. P. Whyte *et al.*, Juvenile Paget's disease: the second reported, oldest patient is homozygous for the TNFRSF11B ‘Balkan’ mutation (966_969delTGACinsCTT), which elevates circulating immunoreactive osteoprotegerin levels, *J Bone Miner Res* **22**, 938–946 (2007).

54. F. Saki *et al.*, Juvenile paget's disease in an Iranian kindred with vitamin D deficiency and novel homozygous TNFRSF11B mutation, *J Bone Miner Res* **28**, 1501–1508 (2013).

55. B. Lamothe *et al.*, TRAF6 ubiquitin ligase is essential for RANKL signaling and osteoclast differentiation, *Biochem. Biophys. Res. Commun.* **359**, 1044–1049 (2007).

56. J. Mizukami *et al.*, Receptor activator of NF-κB ligand (RANKL) activates TAK1 mitogen-activated protein kinase kinase kinase through a signaling complex containing RANK, TAB2, and TRAF6, *Mol. Cell. Biol.* **22**, 992–1000 (2002).

57. A. Besse *et al.*, TAK1-dependent signaling requires functional interaction with TAB2/TAB3, *J. Biol. Chem.* **282**, 3918–3928 (2007).

58. C.-J. Wu, D. B. Conze, T. Li, S. M. Srinivasula, J. D. Ashwell, Sensing of Lys 63-linked polyubiquitination by NEMO is a key event in NF-kappaB activation [corrected], *Nat. Cell Biol.* **8**, 398–406 (2006).

59. Z. J. Chen, Ubiquitin signalling in the NF-κB pathway, *Nat. Cell Biol.* **7**, 758–765 (2005).

60. N. Kobayashi *et al.*, Segregation of TRAF6-mediated signaling pathways clarifies its role in osteoclastogenesis, *EMBO J.* **20**, 1271–1280 (2001).

61. F. Ikeda *et al.*, Critical roles of c-Jun signaling in regulation of NFAT family and RANKL-regulated osteoclast differentiation, *J. Clin. Invest.* **114**, 475–484 (2004).

62. H. Takayanagi *et al.*, Induction and activation of the transcription factor NFATc1 (NFAT2) integrate RANKL signaling in terminal differentiation of osteoclasts, *Developmental cell* **3**, 889–901 (2002).

63. T. Koga *et al.*, Costimulatory signals mediated by the ITAM motif cooperate with RANKL for bone homeostasis, *Nature* **428**, 758–763 (2004).

64. M. Shinohara *et al.*, Tyrosine kinases Btk and Tec regulate osteoclast differentiation by linking RANK and ITAM signals, *Cell* **132**, 794–806 (2008).

65. D. Xu, S. Wang, W. Liu, J. Liu, X. Feng, A novel receptor activator of NF-kappaB (RANK) cytoplasmic motif plays an essential role in osteoclastogenesis by committing macrophages to the osteoclast lineage, *J. Biol. Chem.* **281**, 4678–4690 (2006).

66. H. Kim *et al.*, Selective inhibition of RANK blocks osteoclast maturation and function and prevents bone loss in mice, *The Journal of clinical investigation* **119**, 813 (2009).

67. Y. Taguchi, J. Gohda, T. Koga, H. Takayanagi, J.-I. Inoue, A unique domain in RANK is required for Gab2 and PLCgamma2 binding to establish osteoclastogenic signals, *Genes Cells* **14**, 1331–1345 (2009).

68. D. L. Lacey *et al.*, Osteoprotegerin ligand is a cytokine that regulates osteoclast differentiation and activation, *Cell* **93**, 165–176 (1998).

69. T. L. Burgess *et al.*, The ligand for osteoprotegerin (OPGL) directly activates mature osteoclasts, *J. Cell Biol.* **145**, 527–538 (1999).

70. A. P. Armstrong *et al.*, A RANK/TRAF6-dependent signal transduction pathway is essential

for osteoclast cytoskeletal organization and resorptive function, *J. Biol. Chem.* **277**, 44347–44356 (2002).

71. S. Bai *et al.*, FHL2 inhibits the activated osteoclast in a TRAF6-dependent manner, *J. Clin. Invest.* **115**, 2742–2751 (2005).

72. O. Destaing *et al.*, The tyrosine kinase activity of c-Src regulates actin dynamics and organization of podosomes in osteoclasts, *Mol. Biol. Cell* **19**, 394–404 (2008).

73. T. Miyazaki *et al.*, Src kinase activity is essential for osteoclast function, *J. Biol. Chem.* **279**, 17660–17666 (2004).

74. T. Izawa *et al.*, c-Src links a RANK/αvβ3 integrin complex to the osteoclast cytoskeleton, *Mol. Cell. Biol.* **32**, 2943–2953 (2012).

75. R. J. Lefkowitz, Seven transmembrane receptors: something old, something new, *Acta Physiol (Oxf)* **190**, 9–19 (2007).

76. M. A. Lemmon, J. Schlessinger, Regulation of signal transduction and signal diversity by receptor oligomerization, *Trends Biochem. Sci.* **19**, 459–463 (1994).

77. G. Papoff *et al.*, Identification and characterization of a ligand-independent oligomerization domain in the extracellular region of the CD95 death receptor, *J. Biol. Chem.* **274**, 38241–38250 (1999).

78. R. M. Siegel *et al.*, Fas preassociation required for apoptosis signaling and dominant inhibition by pathogenic mutations, *Science* **288**, 2354–2357 (2000).

79. F. K. Chan *et al.*, A domain in TNF receptors that mediates ligand-independent receptor assembly and signaling, *Science* **288**, 2351–2354 (2000).

80. F. K.-M. Chan, Three is better than one: pre-ligand receptor assembly in the regulation of TNF receptor signaling, *Cytokine* **37**, 101–107 (2007).

81. F. K. Chan *et al.*, Fluorescence resonance energy transfer analysis of cell surface receptor interactions and signaling using spectral variants of the green fluorescent protein, *Cytometry* **44**, 361–368 (2001).

82. H. Wu, Assembly of post-receptor signaling complexes for the tumor necrosis factor receptor superfamily, *Adv. Protein Chem.* **68**, 225–279 (2004).

83. R. M. Siegel *et al.*, SPOTS: signaling protein oligomeric transduction structures are early mediators of death receptor-induced apoptosis at the plasma membrane, *J. Cell Biol.* **167**, 735–744 (2004).

84. N. Holler *et al.*, Two adjacent trimeric Fas ligands are required for Fas signaling and formation of a death-inducing signaling complex, *Mol. Cell. Biol.* **23**, 1428–1440 (2003).

85. H. Wu, Higher-order assemblies in a new paradigm of signal transduction, *Cell* **153**, 287–292 (2013).

86. K. Iwamoto *et al.*, Dimer formation of receptor activator of nuclear factor kappaB induces incomplete osteoclast formation, *Biochem. Biophys. Res. Commun.* **325**, 229–234 (2004).

87. K. Kanazawa, A. Kudo, Self-assembled RANK induces osteoclastogenesis ligand-independently, *J Bone Miner Res* **20**, 2053–2060 (2005).

88. J. C. Crockett *et al.*, Signal peptide mutations in RANK prevent downstream activation of NF-κB, *J Bone Miner Res* **26**, 1926–1938 (2011).

89. A. Krippner-Heidenreich *et al.*, Single-chain TNF, a TNF derivative with enhanced stability and antitumoral activity, *J. Immunol.* **180**, 8176–8183 (2008).

90. B. Schneider *et al.*, Potent antitumoral activity of TRAIL through generation of tumor-targeted single-chain fusion proteins, *Cell Death and Disease* **1**, e68 (2010).

91. D. Spitzer *et al.*, A genetically encoded multifunctional TRAIL trimer facilitates cell-specific targeting and tumor cell killing, *Molecular Cancer Therapeutics* **9**, 2142–2151 (2010).

92. V. Boschert *et al.*, Single chain TNF derivatives with individually mutated receptor binding sites reveal differential stoichiometry of ligand receptor complex formation for TNFR1 and TNFR2, *Cell. Signal.* **22**, 1088–1096 (2010).

93. T. Cundy *et al.*, A mutation in the gene TNFRSF11B encoding osteoprotegerin causes an idiopathic hyperphosphatasia phenotype, *Hum. Mol. Genet.* **11**, 2119–2127 (2002).

94. M. M. Guerrini *et al.*, Human osteoclast-poor osteopetrosis with hypogammaglobulinemia due to TNFRSF11A (RANK) mutations, *Am. J. Hum. Genet.* **83**, 64–76 (2008).

95. A. Pangrazio *et al.*, RANK-dependent autosomal recessive osteopetrosis: characterization of five new cases with novel mutations, *J Bone Miner Res* **27**, 342–351 (2012).

96. C. Sobacchi *et al.*, Osteoclast-poor human osteopetrosis due to mutations in the gene encoding RANKL, *Nat. Genet.* **39**, 960–962 (2007).

97. S. Theoleyre *et al.*, Cellular activity and signaling induced by osteoprotegerin in osteoclasts: involvement of receptor activator of nuclear factor κB ligand and MAPK, *Biochimica et Biophysica Acta (BBA)-Molecular Cell Research* **1644**, 1–7 (2004).

98. S. Zhang *et al.*, The affinity of human RANK binding to its ligand RANKL, *Arch. Biochem. Biophys.* **487**, 49–53 (2009).

99. C. R. Reis, A. H. G. Van Assen, W. J. Quax, R. H. Cool, Unraveling the Binding Mechanism of Trivalent Tumor Necrosis Factor Ligands and Their Receptors, *Molecular & Cellular Proteomics* **10**, M110.002808–M110.002808 (2011).

100. D. Willard *et al.*, Expression, purification, and characterization of the human receptor activator of NF-kappaB ligand (RANKL) extracellular domain, *Protein Expr. Purif.* **20**, 48–57 (2000).

101. S. Vitovski, J. S. Phillips, J. Sayers, P. I. Croucher, Investigating the Interaction between Osteoprotegerin and Receptor Activator of NF- B or Tumor Necrosis Factor-related Apoptosis-inducing Ligand: EVIDENCE FOR A PIVOTAL ROLE FOR OSTEOPROTEGERIN IN REGULATING TWO DISTINCT PATHWAYS, *Journal of Biological Chemistry* **282**, 31601–31609 (2007).

102. M. E. Gasparian *et al.*, Generation of new TRAIL mutants DR5-A and DR5-B with improved selectivity to death receptor 5, *Apoptosis* **14**, 778–787 (2009).

Chapter 2

Manipulation of Receptor Oligomerization as a Novel Strategy for TNF Superfamily Inhibition

Portions of this chapter are adapted from the manuscript submitted to *Science* for consideration, November, 2013.

Julia T. Warren, Christopher A. Nelson, Corinne E. Decker, Daved H. Fremont, Steven L. Teitelbaum

2.1 Abstract

Receptor activator of NF-kB ligand (RANKL) is the key cytokine regulating osteoclast formation and is therefore a therapeutic target for treatment of disorders such as osteoporosis and skeletal metastasis. The molecular details initiating osteoclastogenesis and thus bone resorption, particularly the state of RANKL receptor (RANK) oligomerization, are unclear. We describe a novel RANKL construct, with all three monomers covalently linked as a single polypeptide chain, which enables delineation of the receptor oligomeric state necessary and sufficient to form bone resorptive cells. We find RANKL-induced trimeric clustering of its receptor, RANK, to be a prerequisite for optimal osteoclast formation, although dimeric clustering is also capable of less efficiently generating the cell. We used this information to modify the affinity of individual single-chain RANKL monomers for RANK as well as for the decoy receptor, osteoprotegerin (OPG). This approach yielded an effective inhibitor of osteoclastogenesis, in vitro and in vivo, thus providing a novel strategy for anti- resorptive therapy. As RANKL is a member of the tumor necrosis factor superfamily (TNFSF), our observations may also inform the design of inhibitors for other TNFSF members.

2.2 Introduction

The TNFSF and its associated receptors represent a protein family with wide-ranging roles in physiology and homeostasis (*1*). Excess activation of TNF superfamily (TNFSF) receptors induces a myriad of pathological conditions such as psoriasis, inflammatory joint disease and osteoporosis (*2*, *3*). While biological agents such as humanized monoclonal antibodies and decoy receptors have positively impacted the course of these diseases, each has limitations including acquired resistance, predisposition to infectious diseases and malignancy as well as marked suppression of skeletal remodeling (*4*). The TNFSF member RANKL is the key cytokine regulating osteoclast formation and function (*5*, *6*) and excess activation of its receptor, RANK, promotes pathological bone loss (*7*). RANKL exists as a homotrimer in solution (*8*) with each of the three interfaces separating the monomers containing a binding groove that can accept a single copy of RANK or the anti-osteoclastogenic decoy receptor, OPG (*9*-*11*).

Despite the trimeric nature of the cytokine, the assumption that osteoclastic signaling is initiated by clustering of three RANK monomers is controversial. This largely reflects the fact that previous studies have relied on the overexpression of RANK or of various RANK/extracellular receptor chimeras. Enforced dimerization of RANK by overexpression of a RANK cytoplasmic domain fused to the extracellular portion of the Epo receptor and ligation of this chimera with anti-Epo antibody led to decreased osteoclast formation (*12*). However, this study, and a subsequent publication using a RANK overexpression system (*13*), show that even in the absence of RANKL, TRAP-positive osteoclasts can be observed. The relevance of this ligand-independent RANK functionality is uncertain, as mice and humans lacking functional RANKL fail to form osteoclasts (*5*, *6*, *14*). Additionally, the careful selection of stable cell lines expressing similar levels of RANK as found in osteoclast precursors did not lead to ligand-

independent signaling (*1*, *15*). Together, these studies highlight the need for tools to examine these fundamental questions in the context of primary, unmanipulated cells.

Indeed, the receptor oligomeric state necessary and sufficient for signaling has been an area of interest more broadly within the TNF superfamily. For some TNF receptor members, it has been proposed that multimers of receptor are pre-formed in the absence of ligand (*2*, *3*, *16-19*), and that ligand binding allows for a conformational change that brings the intracellular adapter-recruitment motifs into proximity (*4*, *20*). Similar to RANK overexpression, ligand-independent TNFR1-mediated apoptosis actually prevents generation of cells overexpressing this receptor (*5*, *6*, *21*). Although there exists a crystal structure of TNFR1 in a dimeric state with extensive contacts formed at the proposed "pre-ligand association domain" (*7*, *22*), the crystal structures of several TRAFs alone or bound to receptor fragments show formation of a trimeric species (*8*, *23*). Therefore, the exact oligomeric nature of receptor required for the initiating of downstream signaling remains to be fully elucidated.

Recently, several groups have described the use of "single-chain" protein variants within the TNFSF containing each monomer covalently linked by short, flexible amino acid stretches (*9-11*, *24-26*). This is possible because the ligands of the TNFSF fold such that the N- and C-termini of neighboring monomers are in close physical proximity. Indeed, a single-chain version of TNFα with individually mutated receptor recruitment sites was generated and used to show that TNFR1 needs only one available recruitment site to promote cell death of a TNFR1 extracellular / Fas intracellular chimeric receptor (*12*, *27*). Though the authors propose a mechanism whereby pre-associated TNFR1 dimers become signaling competent via the binding of two separate TNF homotrimers to each TNFR1 dimer, their surprising finding may be confounded by the chimeric and overexpressed nature of the receptor.

In the present study, we created a single-chain version of RANKL (scRANKL) by covalently linking each monomer with flexible glycine-serine repeats. We designed mutations to prevent RANK receptor recruitment and introduced them individually into each scRANKL monomer, generating versions capable of recruiting only two or one RANK monomer to each scRANKL. Our examination of these scRANKL variants using primary, bone marrow macrophages with endogenous levels of RANK receptor allow us to comment on the receptor oligomeric state necessary and sufficient for downstream signaling and osteoclast formation. Additionally, we used a non-biased, forward genetic approach to delineate RANKL variants with high affinity for RANK and decreased binding to the decoy receptor osteoprotegerin (OPG). Insertion of these novel RANKL mutants into the intact receptor recruitment sites of single- or double-block scRANKL generated an effective inhibitor of WT RANKL-mediated osteoclast formation and function. This combined strategy of single-chain trimers with high affinity intact sites may be broadly applicable to other TNF receptor signaling systems.

2.3 Materials and Methods:

Construction of single-chain RANKL vector: Initially, scRANKL was cloned into the pGEX vector (GE-Healthcare) by PCR amplification of mouse RANKL monomer (residues 162–316 of NCBI Reference Sequence NP_035743) using primer pairs that yielded the following restriction sites: *5' SmaI*-RANKL-*3'BspEI, 5'BspE*I-RANKL-*3'BamHI*, *5'BamHI*-RANKL-*3'NotI*. The primers were designed such that the three monomers are separated by a linker sequence ([Gly-Gly-Ser-Gly] x 3). Each insert was double-digested with the appropriate restriction enzymes (Fermentas) and ligated into the pGEX vector between the SmaI and NotI sites. The entire scRANKL gene was subcloned into a mammalian protein expression vector (pFM (*13, 28*), gift of Dr. Filipo Mancia) downstream of the signal peptide from pHLsec (MGILPSPGMPALLSLVSLLSVLLMGCVA) (*5*, *6*, *14*, *29*). To aid protein recovery a TEV protease cleavage site and 6-histidine tag were added at the c-terminus (SSGRENLYFQGHHHHHH). In brief, the construct encodes: a signal-peptide, RANKL (aa 162-316) linker- RANKL (aa 162-316) linker - RANKL (aa 162-316) - TEV cleavage site - 6xHis. Expression is driven by the CMV promoter. Transfection efficiency is monitored as red fluorescent protein production, which initiates downstream of scRANKL at an internal ribosomal entry site.

Production of mammalian RANKL protein: Suspension adapted 293-Freestyle cells (Life Technologies) were maintained in serum-free Freestyle 293 expression medium (Life Technologies) according to the manufacturer's protocol. For transfection of RANKL variants, DNA was prepared using an endotoxin-free maxiprep kit (Qiagen). Cells were seeded at a density of $0.5x10^6$/mL in 200mL volume 24 hours prior to transfection. On the day of transfection, DNA and polyethylenimine (*29*)were mixed at a ratio of 1:3 (WT RANKL or triple-

chain variants, 200ug:600ug) or 1:2 (single-chain RANKL variants, 200ug:400ug) in opti-mem(Life Technologies), incubated for 15 minutes at room temperature, and added directly to cells. Supernatant was harvested four and seven days after transfection, 0.22uM filtered and equilibrated by the addition of 1/10 volume 10X phosphate buffered saline (Gibco) and 10mM imidazole. The protein was captured on Ni-NTA Superflow resin (Qiagen) and washed using 10mM imidazole in PBS. Protein was eluted in steps from 25-500mM imidazole. Fractions containing purified protein were identified on coomassie stained SDS-PAGE. Positive fractions were pooled and concentrated using a disposable YM30 centricon (Millipore). All proteins were sterile filtered for use in cell culture.

Chemical cross-linking: Purified WT-RANKL (500ng) was incubated with varying concentrations (0-500uM) of the chemical cross-linker bis-(sulfosuccinimidyl)-suberate (BS^3, Pierce) in PBS at room temperature for 30 minutes, at which time the reaction was stopped by the addition of 10mM Tris-HCl, pH=7.0. Samples were boiled in reducing conditions and loaded onto SDS-PAGE gels (10%) alongside 500ng of scRANKL protein. Bands were stained using the coomassie derivative Imperial protein stain (Pierce) and visualized using the Odyssey scanner (Licor).

Multi-angle light scattering (MALS): Purified RANKL proteins were applied to a Wyatt WTC-030S5 size exclusion column mounted on a Waters HPLC system attached to a multi-angle light scattering device. The light detectors, a Dawn HELEOS-II 18-angle light scattering detector, and an Optilab rEX refractive index, were previously calibrated against monomeric bovine serum album. MALS was monitored during the experiments and the resulting data analyzed using associated software. For each experiment, 250 ug of sample was applied at 1

mg/ml in running buffer (25mM HEPES pH 7.4, 150 mM NaCL, 0.01% sodium azide) at 20°C and a flow rate of 0.5 ml per minute.

Identification of RANKL mutants which do not bind RANK. RANKL residues forming salt bridges or hydrogen bonds with RANK were targeted for site directed mutagenesis using the program PISA and the RANK/RANKL co-crystal structure (*9*). Loops at the RANK/RANKL interface were disrupted by amino acid insertion. Mutations were introduced into the expression construct, pGEX- GST-RANKL, by PCR using Phusion polymerase (NEB). After verification by nucleic acid sequencing, the mutant RANKL-encoding constructs were transformed into *E. coli* strain BL21-CodonPlus (DE3)-RIL competent cells (Agilent Technologies) for protein production. Correctly-folded soluble protein was purified from cell lysate on glutathione sepharose (*8*).

Bio-layer interferometry (BLI): All BLI experiments were performed on an Octet RED system (ForteBio). GST-RANKL proteins were biotinylated using NHS-PEG4-biotin (Pierce) according to manufacturer's protocol, and excess biotin was removed by desalting over Zeba Spin Columns (7KD molecular weight cutoff, Pierce). Biotinylated proteins were adsorbed onto super-streptavidin sensor pins (ForteBio). Binding of RANK-Fc or OPG-Fc was measured in HBS-EP containing 1% BSA. Due to the dimeric nature of Fc-tagged receptors, only apparent Kd values were observed.

Surface Plasmon Resonance (SPR): All SPR experiments were performed on a Biacore T-100 (GE Healthcare) using CM5 sensor chips and HBS-EP buffer. To confirm receptor recruitment using scRANKL variants, 4,000 RU of WT-scRANKL or variant scRANKL were coupled to individual lanes, leaving one reference flow cell uncoupled. Monomeric RANK (20uM) was flowed over until saturation. Total RUs bound at equilibrium were calculated using

BIAEvaluation software. Experiments to determine kinetic affinity constants of RANKL variants for RANK or OPG were performed and analyzed as previously described (*9*).

Generation of osteoclasts from primary bone marrow macrophages: Long bones of eight week-old mice were flushed and the marrow subjected to red blood cell lysis. The remainder of the whole marrow was cultured on petri dishes maintained at 37°C with 6% CO2 in alpha-mem containing 10% inactivated fetal bovine serum, 100 U/ml penicillin, 100 μg/ml streptomycin, (α-10 medium) supplemented with 1:10 CMG (conditioned medium supernatant containing recombinant M-CSF) (*30*). Osteoclasts were differentiated in α-10 medium with 1:50 CMG and the relevant RANKL variant.

Detection of osteoclast formation: Cells were fixed in 4% paraformaldehyde in PBS for 15 minutes and stained for the tartrate resistant acid phosphatase (TRAP) using a kit (Sigma). Additionally, osteoclasts were quantified by a solution assay of TRAP enzyme levels. Cells were fixed and lysed in 90mM citrate buffer pH=5.2, 80mM sodium tartrate, 0.1% Triton-X 100 for 10 minutes at room temperature. Colorimetric nitrophenylphosphate (substrate of TRAP enzyme) was added and visualized after 15 minutes by the addition of sodium hydroxide. Data was acquired using the 405nM absorbance filter on a Bio-rad plate reader. Because of the limited range of the TRAP solution assay, a more quantitative assessment of TRAP activity was performed using the fluorescent phosphatase substrate ELF-97 (Molecular Probes). Fixed cells were incubated with 100uM ELF-97 in 90mM citrate buffer pH 4.8, 80mM sodium tartrate for 15 minutes at room temperature. The reaction was stopped by the addition of sodium hydroxide and fluorescence was visualized using the 345/530 excitation/emission filter on a Spectramax M2 plate reader.

Quantitative real-time PCR: To quantitate mRNA markers of osteoclast formation, RNA was isolated from cultured cells according to the manufacturer's protocol (Qiagen RNeasy miniprep kit). Equal amounts of RNA were used to perform reverse transcription (Bio-rad iScript) and quantitative real-time PCR was performed using Eva Sso fast qPCR Sybr green kit (Bio-rad) using a 7500 fast machine (ABI). Data was analyzed according to the delta-delta Ct method and normalized to a control containing no RANKL addition (labeled BMM). Primers used were as follows: CatK (Forward: 5'-ATGTGGGTGTTCAAGTTTCTGC-3', Reverse: 5'-CCACAAGATTCTGGGGACTC-3'), NFATc1 (Forward: 5'-CCCGTCACATTCTGGTCCAT-3', Reverse: 5'-CAAGTAACCGTGTAGCTGCACAA-3'), TRAP (Forward: 5'-CAGCTCCCTAGAAGATGGATTCAT-3', Reverse: 5'GTCAGGAGTGGGAGCCATATG), beta3 (Forward: 5'-TTCGACTACGGCCAGATGATT-3', Reverse: 5'-GGAGAAAGACAGGTCCATCAAGT-3').

Western blot: Cells were washed three times in ice-cold PBS and lysed with RIPA buffer (Millipore) supplemented with protease and phosphatase inhibitor cocktail (Pierce). After 10 minutes of incubation on ice, cell lysates were cleared of debris by pelleting for 15 minutes at 21,000g. 40-50ug of protein were loaded onto SDS-PAGE gels (10%), transferred onto PVDF membrane, and incubated with primary antibody overnight. After extensive washing and incubation with near-infrared labeled secondary antibody, membranes were visualized using the Odyssey scanner (Licor). Primary antibodies to detect phosphorylated or total NF-kB or p38 were from Cell Signaling, antibody directed against actin was from Sigma, and fluorescently labeled secondary antibodies were from Rockland.

Yeast surface display of RANKL and staining with receptor: WT-SM RANKL was cloned into the pYD1 yeast display vector (Life Technologies) using *5' NheI* and *3' XhoI*

restriction sites, yielding the yeast mating protein Aga2p fused to the RANKL N-terminus and having at the C-terminus a V5-epitope tag. The pYD1-RANKL construct was transformed into EBY100 yeast as described and colonies selected in tryptophan-deficient, glucose-based media at 30˚C. Display of RANKL protein was induced by inoculating into galactose-based selective media and incubating at 30˚C with shaking for 24-48 hours. Surface expression of RANKL was detecting using an anti-V5- FITC antibody (Invitrogen). After incubation with RANK-Fc or OPG-Fc for 10 minutes at room temperature and washing with ice-cold PBS, receptor binding was detecting using an anti-human Fc-APC antibody (Molecular Probes). All experiments were performed using LSR II or Canto II flow cytometers (BD Biosciences) and analyzed using the FlowJo software package (Tree Star, Inc.). Alternatively, RANK-6xHis or OPG-6xHis were detected using APC-labeled anti-6xHis antibody (MBL International).

Generation of RANKL library and selection: Primers annealing immediately 5' or 3' to RANKL in the pYD1 vector were designed and used in error-prone PCR amplification (Gene Morph II, Agilent). A lower and higher mutation rate was accomplished by manipulating the amount of starting template and the number of amplification cycles. The resulting product was further amplified using the high fidelity Phusion polymerase (Finnzymes). Simultaneously, pYD1 vector backbone was amplified using primers that extended outward from the regions surrounding RANKL-V5, leaving 24 base pairs of overlap between the vector backbone and the amplified, mutant RANKL-V5 insert. These purified PCR products were transformed into EBY100 cells according to established protocols (*31*), yielding a library of approximately $1x10^6$ transformants. Selections were made using magnetic assisted cell sorting (MACS, Miltenyi). Roughly $1x10^7$ cells were induced from either the low or high mutation rate libraries, and both were first sorted for the expression of the V5 C-terminal tag indicating proper folding and full-

length protein. This was performed by incubating cells with FITC-labeled anti-V5 antibody and selecting cells using anti-FITC mibrobeads for cell separation. After growth of the selected clones, cells were again induced to display RANKL protein, incubated with OPG-Fc, washed, and clones that did not bind OPG were collected as the flow-through on a Protein A magnetic bead column. These cells were then labeled with RANK-Fc, and this time those clones that retained binding to the Protein A column were collected. After sorting, cells were expanded in selective media and this strategy repeated two additional times yielding clones termed "LM3S" and "HM3S". Roughly 200 individual colonies were isolated from the libraries and stained with OPG-Fc. Those clones with little to no detectable staining were then assessed for their ability to bind RANK-Fc. DNA was extracted from the top scoring clones of interest using a yeast miniprep kit (Zymoprep) and transformed into DH5alpha E. coli chemically competent cells (Invitrogen) for sequencing. Individual point mutations were then added to RANKL using site-directed mutagenesis, and subsequent combinations were cloned in a similar fashion. A second round of error-prone PCR utilized the identical primers and protocol as above, but starting template of either F164Y/Q236H/F269Y or K194N/Q236H/F269Y triple mutants. Clones were selected over three rounds of sorting using three sequentially lower amounts of monomeric RANK-6xHis and anti-6xHis microbeads. Finally, the resulting library was incubated with RANK-6xHis at room temperature for 10 minutes and then tested for the ability to outcompete the presence of unlabeled OPG at room temperature for 5 minutes. Residual RANK binding was detecting using APC-labeled anti-6xHis antibody. In the course of sorting, K194E was identified and used to replace K194N, which introduced a potential N-linked glycosylation site at the interface with RANK or OPG.

Intraperitoneal RANKL Injection: Balb/c 8-week old female mice were purchased from NIH Frederickson, housed in the animal facility at Washington University School of Medicine and maintained according to the guidelines set by the Association for Assessment and Accreditation of Laboratory Animal Care. All animal studies were approved by the Animal Studies Committee of Washington University School of Medicine. PBS, WT-SM RANKL (0.5mg/kg), or WT-SM RANKL + single-block, $RANK^{high}$ scRANKL (0.5mg/kg) were injected intraperitoneally at 0, 24, and 48 hours as described (*32*). Mice were sacrificed 1.5 hours after the third injection and serum was collected by cardiac puncture. CTx ELISA was performed according to the manufacturer's protocol (Immunodiagnostics Systems).

2.4 Results

To assess the oligomeric state of receptor clustering required for efficient initiation of signal transduction, we covalently linked three RANKL monomers by two short glycine-rich linkers (Figure 2.1). This single-chain version of trimeric RANKL (scRANKL) permits individual modification of RANK and OPG affinity at each of the three binding sites. Two additional surface "solubility" mutations (C220S/E246I "WT-SM RANKL"), which do not impact RANK binding, were introduced to improve protein expression (Figure 2.2). Whereas chemical cross-linking of wild-type homotrimeric RANKL (WT RANKL) is necessary to observe the trimer in a denaturing gel, scRANKL has a molecular weight consistent with three covalently-linked RANKL monomers (Figure 2.3A). Because the predominant scRANKL species migrates on the gel at a position slightly below chemically cross-linked trimeric RANKL, we calculated molecular weights using multi-angle light scattering (Figure 2.3B). Importantly, scRANKL induces bone marrow macrophage (BMM)-derived osteoclastogenesis as effectively as WT (Figure 2.3C).

To manipulate the number of individual RANK receptors recruited to scRANKL, we sought to identify mutations in RANKL incapable of binding RANK. To this end, we took advantage of the RANKL/RANK co-crystal structure detailing the key loops of the cytokine contacting its receptor. We inserted short sequences into each RANKL loop as well as designing individual, salt bridge-disrupting, point mutations and quantitated apparent affinities for Fc-tagged versions of the RANK or OPG cysteine-rich domain cytokine binding fragments (Figure 2.4A). One mutant of interest, with three amino acids (GGS) inserted into the CD-loop (CDins RANKL), fails to bind recombinant RANK-Fc despite proper folding established by its binding of OPG-Fc in a dose dependent manner (Figure 2.4A,B). Indeed, all mutants with no detectable

binding to RANK-Fc contained mutations in this RANKL loop. Interestingly, this same loop is the target for Denosumab, a humanized monoclonal antibody targeting RANKL and currently approved for the treatment of osteoporosis.

Although we observe overall an excellent correlation between apparent affinity for RANK-Fc and capacity to generate osteoclasts as assessed by TRAP stain, TRAP solution assay, and osteoclastogenic mRNA markers (Figure 2.5A-C), it is noteworthy that several variants with no apparent biological activity still had detectable binding to RANK-Fc. This is significant, as attempts to manipulate receptor oligomerization necessitate the complete absence of receptor recruitment. This property is not readily detected by *in vitro* functional assays or measurements of affinity using the monomeric fragment of RANK which binds to WT RANKL with relatively low affinity (1uM). Lastly, to confirm its failure to ligand RANK, we demonstrate that CDins RANKL is incapable of promoting RANK signaling (Figure 2.5D).

Next, we generated single-block and double-block scRANKL by inserting CDins into one or two monomers, respectively (Figure 2.6A). To demonstrate that we had selectively manipulated the number of receptors bound to the single chain protein, we coupled equal amounts of WT, single-block or double-block scRANKL, to individual lanes of a surface plasmon resonance (SPR) chip. After flowing monomeric RANK, as an analyte, we measured the degree of receptor binding at saturation. As expected, each monomer block results in the loss of approximately one-third of the receptor binding (Figure 2.6B).

To test the hypothesis that recruitment of three RANK receptors is necessary to initiate osteoclastogenesis, we added the scRANKL variants to cultures of BMMs. Whereas WT-scRANKL increases osteoclast number in a saturable, dose-dependent manner, triple-block scRANKL, containing CDins mutation in all three monomers, fails to generate any osteoclasts

(Figure 2.6C). Double-block scRANKL also yields no osteoclasts, establishing that more than one RANK monomer is required. Surprisingly, however, single-block scRANKL is capable of generating osteoclasts although less effectively than WT. This phenomenon is dose-dependent and saturable, maximizing at approximately 85% of control (Figure 2.6D). Mirroring osteoclastogenesis, single-block, but not double- or triple-block, scRANKL phosphorylates the effector molecules NF-kB and p38 (Figure 2.6E). To confirm that this unexpected observation was not due to higher order clustering by aggregated protein, we further purified single-block scRANKL to more stringent molecular weight homogeneity. We still observe osteoclast formation, albeit at lower levels (not shown). Therefore, recruitment of two RANK receptors is sufficient and necessary to initiate osteoclast-forming signals, although it is less efficient than recruitment of three receptors.

The capacity of double-block scRANKL to bind RANK, yet not produce osteoclasts, suggests it may function as a competitive antagonist of WT-RANKL. To test this possibility, we induced osteoclast formation using WT RANKL and added increasing amounts of single- or double-block scRANKL, or OPG, a known inhibitor of osteoclastogenesis. While OPG dose-dependently inhibits osteoclast formation, neither version of scRANKL was able to antagonize this process (Figure 2.7). This lack of inhibitory effectiveness likely reflects failure of the one or two intact binding site(s) to overcome the avidity afforded by the three sites of WT RANKL. We reasoned that we might generate effective inhibitors by compensating for the reduced avidity of single- or double-block scRANKL through increasing the affinity for RANK at the intact site(s).

This required identifying presently unknown RANKL mutations which increase RANK affinity. To this end, we performed two generations of *in vitro* evolution through yeast surface display (YSD) (*33*). The first generation involved creating a library of RANKL mutants using

error-prone PCR and sorting for clones that retain binding to RANK-Fc. Notably, OPG, the principal biological inhibitor of RANK-induced osteoclastogenesis (*34-36*), exerts its effects by competing for RANKL. Because both RANK and OPG bind the same groove, it is possible that increasing the affinity of RANKL for RANK would simultaneously increase binding to the decoy receptor. To obviate this possibility, we simultaneously sorted the library for clones recognizing RANK with high affinity and with decreased capacity to bind OPG-Fc and identified five clones of interest (Figure 2.8A). Reversion mutagenesis yielded RANKL individual point mutations (K194E, Q236H, F269Y) which, when expressed in combination (KQF), substantially increase RANK-Fc and decrease OPG-Fc binding (Figure 2.8B-D).

The goal of the second generation of evolution was to select RANKL variants with long RANK kinetic half-lives while still not recognizing OPG. We again constructed a RANKL mutant library using error-prone PCR, this time using high affinity KQF RANKL as a starting template. Due to the rapid off-rate, monomeric RANK does not stain yeast-displayed WT-RANKL, despite their established interaction. We therefore sorted the second library using sequentially limiting amounts of monomeric RANK. Staining at each stage of sorting demonstrated the emergence of a population now capable of binding monomeric RANK (Figure 9A).

Next, we selected RANKL variants which continue to bind limiting amounts of RANK after five minutes at room temperature, in the presence of unlabeled OPG (Figure 2.9B). Together, these strategies yielded an additional RANKL point mutant (H270Y) that further increases RANK recognition without detectable binding to OPG (Figure 2.9C,D). We then determined the affinities and kinetic parameters of an intermediate and a high RANK binding variant by SPR. Interestingly, although the two solubility mutations, introduced for production

of scRANKL, have no effect on RANK recognition, they induce an approximately ten-fold decrease in OPG binding (Figure 2.10). Another point mutant, Q236H, yields a further 100-fold decrease in OPG and a roughly 15-fold increase in RANK binding as compared to WT RANKL (Figure 2.11A,B). Finally, KQFH recognizes RANK with approximately 500-fold greater affinity than does WT RANKL while failing to meaningfully bind OPG (Figure 2.11C). These alterations in affinity largely reflect a prolonged half-life, changing from relatively rapid dissociation time (WT-SM RANKL $t_{1/2}$=3 seconds) to a value more than 200-times longer (KQFH-SM RANKL $t_{1/2}$=675 seconds).

We next used our mutational analysis to generate scRANKL constructs in which RANK and OPG recognition is blocked by a combination of CDins and Q236H as confirmed by yeast surface display (Figure 12A) and failure to form osteoclasts or induce signaling (Figure 2.12B,C). To enhance RANK binding at the intact site(s), we used either intermediate (Q236H) or high affinity (KQFH) mutations, neither of which meaningfully recognize OPG, and generated all possible version of single- or double-block scRANKL. All versions of double-block scRANKL remain incapable of generating osteoclasts (Figure 2.13A). Furthermore, the decreased osteoclast formation and associated signals induced by single-block scRANKL variants reflect an inverse relationship with RANK affinity of the intact binding sites (Figure 2.13B-D). Because the $RANK^{med}$ and $RANK^{high}$ differ primarily in RANK off-rate (Figure 2.11), our data suggest that the ability to dissociate from the receptor is crucial for initiating signal transduction in the face of sub-optimal receptor clustering.

In contrast to the failure of single or double-block scRANKL containing unaltered residual monomer(s) to blunt RANK signaling and osteoclast formation, double-block, $RANK^{high}$ scRANKL effectively inhibits with an IC_{50} approximating 10 nM (Figure 2.13E).

When two sites are available to bind RANK with high affinity (single-block, $RANK^{high}$), the potency increases to an IC_{50} of 0.2 nM. Lastly, we sought to test the effectiveness of single-block, $RANK^{high}$ scRANKL at blocking WT-RANKL induced osteoclastic bone resorption *in vivo*. Intraperitoneal injection of WT-SM RANKL into 8-week old BALB/c mice increases osteoclast function as determined by the serum marker CTx (Figure 2.13F). Suggesting therapeutic relevance of our observations, this increase in bone resorption is completely abrogated by an equal amount of single-block, $RANK^{high}$.

2.5 Discussion

The oligomeric state of cytokines often leads to the assumption of an identical oligomeric receptor clustering as the driving force for initiating signal transduction. Our use of scRANKL with individually mutated receptor binding sites has allowed us to examine this assumption in unmanipulated primary cells. Despite the trimeric nature of RANKL cytokine, the recruitment of only two RANK receptors is sufficient to generate osteoclasts. The decreased osteoclastogenic capacity of single-block scRANKL indicates that this state of receptor clustering is, however, sub-optimal. This data mirrors the observations made using an Epo/RANK chimeric receptor clustered by agonistic antibody treatment (*12*). It is also reminiscent of an observed drop in the EC_{50} using single-chain TNF that blocks recruitment of one TNFR2/Fas chimeric receptor (*27*). Although our observations are strengthened by the use of primary, unmanipulated cells that avoid the confounding factors of receptor overexpression, we cannot eliminate the possibility that the flexibility within our scRANKL linkers may allow for higher order multimerization of ligand and thus recruitment of additional RANK receptors in the context of single-block scRANKL. Regardless, our data using double-block scRANKL, which is incapable of generating osteoclasts and inducing signals, stands in contrast to the observation that single-chain TNF blocking recruitment of two TNFR1/Fas chimeric receptors is equally capable of inducing cell death as WT TNF. There are several possibilities for this difference, including the absence of overexpression in our system, the lack of compelling evidence for RANK pre-ligand association, or the recruitment of different intracellular signaling components.

Interestingly, an increase in affinity at the two receptor recruitment sites in single-block scRANKL generates fewer osteoclasts. As the primary difference in kinetics between WT-

RANKL and our high affinity variants lies in the off-rate, it appears that the ability of single-block scRANKL to generate osteoclasts may be facilitated by the rapid off rate at the two receptor binding sites. This may allow for the recruitment of additional RANK receptor, ultimately leading to higher order clustering which has been implicated for other TNF receptor family members (*37-42*). Our data demonstrating that increasing the time required for single-block scRANKL variants to dissociate diminishes osteoclastogenesis supports this model.

Lastly, our observations establish that single-chain RANKL, in combination with blocked or high affinity RANK binding sites, allows arrest of RANK signaling, thus generating an effective inhibitor of RANKL-mediated osteoclast formation and function. Indeed, single-block, $RANK^{high}$ scRANKL inhibits osteoclast formation *in* vitro with an IC_{50} value of 0.2 nM, which is almost 10-fold lower than the reported IC_{50} value for Denosumab (IC_{50} = 1.64 nM), the anti-human RANKL antibody approved for the treatment of osteoporosis (*43*). RANKL, a member of the TNF superfamily (TNFSF), binds to multiple receptors (RANK and OPG) with different biological effects. Within the TNFSF, there are several examples of cytokines demonstrating receptor promiscuity (*44*). For example, TNFα, which recognizes TNFR1 and TNFR2, is central to the pathogenesis of disabling disorders such as rheumatoid arthritis and psoriasis (*2*). In fact, treatment of these diseases has been greatly facilitated by global TNFα blockade using humanized antibodies or soluble receptor (*45*). As effective as these drugs are, they carry major complications such as predisposition to malignancy and serious infections, including tuberculosis (*46, 47*). Current evidence indicates that the positive effects of anti-TNFa therapy reflects suppressed activation of TNFR1, while negative consequences are due to inhibition of the pro-immune properties of TNFR2 (*48*). TNF and RANKL interact with their receptors in a homologous fashion (*49*). Our data demonstrate that the strategy of combining high affinity and

blocking mutations into a single-chain can be used to construct an effective inhibitor that is receptor selective. This suggests a potential mechanism for blocking TNFR1 while sparing TNFR2, thereby reducing systemic complications. Indeed, this strategy may be broadly applicable to all members of the pathologically important TNF superfamily.

2.6 References

1. T. Hehlgans, K. Pfeffer, The intriguing biology of the tumour necrosis factor/tumour necrosis factor receptor superfamily: players, rules and the games, *Immunology* **115**, 1–20 (2005).

2. M. Croft *et al.*, TNF superfamily in inflammatory disease: translating basic insights, *Trends Immunol.* **33**, 144–152 (2012).

3. D. S. Vinay, B. S. Kwon, The tumour necrosis factor/TNF receptor superfamily: therapeutic targets in autoimmune diseases, *Clin. Exp. Immunol.* **164**, 145–157 (2011).

4. M. G. Tansey, D. E. Szymkowski, The TNF superfamily in 2009: new pathways, new indications, and new drugs, *Drug Discov. Today* **14**, 1082–1088 (2009).

5. Y. Y. Kong *et al.*, OPGL is a key regulator of osteoclastogenesis, lymphocyte development and lymph-node organogenesis, *Nature* **397**, 315–323 (1999).

6. N. Kim, P. R. Odgren, D. K. Kim, S. C. Marks, Y. Choi, Diverse roles of the tumor necrosis factor family member TRANCE in skeletal physiology revealed by TRANCE deficiency and partial rescue by a lymphocyte-expressed TRANCE transgene, *Proc Natl Acad Sci USA* **97**, 10905–10910 (2000).

7. M. Zaidi, Skeletal remodeling in health and disease, *Nat. Med.* **13**, 791–801 (2007).

8. J. Lam, C. A. Nelson, F. P. Ross, S. L. Teitelbaum, D. H. Fremont, Crystal structure of the TRANCE/RANKL cytokine reveals determinants of receptor-ligand specificity, *J. Clin. Invest.* **108**, 971–979 (2001).

9. C. A. Nelson, J. T. Warren, M. W.-H. Wang, S. L. Teitelbaum, D. H. Fremont, RANKL employs distinct binding modes to engage RANK and the osteoprotegerin decoy receptor, *Structure/Folding and Design* **20**, 1971–1982 (2012).

10. C. Liu *et al.*, Structural and functional insights of RANKL-RANK interaction and signaling, *The Journal of Immunology* **184**, 6910–6919 (2010).

11. H. M. Ta *et al.*, Structure-based development of a receptor activator of nuclear factor-kappaB ligand (RANKL) inhibitor peptide and molecular basis for osteopetrosis, *Proceedings of the National Academy of Sciences* **107**, 20281–20286 (2010).

12. K. Iwamoto *et al.*, Dimer formation of receptor activator of nuclear factor kappaB induces incomplete osteoclast formation, *Biochem. Biophys. Res. Commun.* **325**, 229–234 (2004).

13. K. Kanazawa, A. Kudo, Self-assembled RANK induces osteoclastogenesis ligand-independently, *J Bone Miner Res* **20**, 2053–2060 (2005).

14. C. Sobacchi *et al.*, Osteoclast-poor human osteopetrosis due to mutations in the gene encoding RANKL, *Nat. Genet.* **39**, 960–962 (2007).

15. J. C. Crockett *et al.*, Signal peptide mutations in RANK prevent downstream activation of NF-κB, *J Bone Miner Res* **26**, 1926–1938 (2011).

16. G. Papoff *et al.*, Identification and characterization of a ligand-independent oligomerization domain in the extracellular region of the CD95 death receptor, *J. Biol. Chem.* **274**, 38241–38250 (1999).

17. R. M. Siegel *et al.*, Fas preassociation required for apoptosis signaling and dominant inhibition by pathogenic mutations, *Science* **288**, 2354–2357 (2000).

18. F. K. Chan *et al.*, A domain in TNF receptors that mediates ligand-independent receptor assembly and signaling, *Science* **288**, 2351–2354 (2000).

19. F. K.-M. Chan, Three is better than one: pre-ligand receptor assembly in the regulation of TNF receptor signaling, *Cytokine* **37**, 101–107 (2007).

20. F. K. Chan *et al.*, Fluorescence resonance energy transfer analysis of cell surface receptor interactions and signaling using spectral variants of the green fluorescent protein, *Cytometry* **44**, 361–368 (2001).

21. M. P. Boldin *et al.*, Self-association of the "death domains" of the p55 tumor necrosis factor (TNF) receptor and Fas/APO1 prompts signaling for TNF and Fas/APO1 effects, *J. Biol. Chem.* **270**, 387–391 (1995).

22. J. H. Naismith, T. Q. Devine, T. Kohno, S. R. Sprang, Structures of the extracellular domain of the type I tumor necrosis factor receptor, *Structure/Folding and Design* **4**, 1251–1262 (1996).

23. H. Wu, Assembly of post-receptor signaling complexes for the tumor necrosis factor receptor superfamily, *Adv. Protein Chem.* **68**, 225–279 (2004).

24. A. Krippner-Heidenreich *et al.*, Single-chain TNF, a TNF derivative with enhanced stability and antitumoral activity, *J. Immunol.* **180**, 8176–8183 (2008).

25. B. Schneider *et al.*, Potent antitumoral activity of TRAIL through generation of tumor-targeted single-chain fusion proteins, *Cell Death and Disease* **1**, e68 (2010).

26. D. Spitzer *et al.*, A genetically encoded multifunctional TRAIL trimer facilitates cell-specific targeting and tumor cell killing, *Molecular Cancer Therapeutics* **9**, 2142–2151 (2010).

27. V. Boschert *et al.*, Single chain TNF derivatives with individually mutated receptor binding sites reveal differential stoichiometry of ligand receptor complex formation for TNFR1 and TNFR2, *Cell. Signal.* **22**, 1088–1096 (2010).

28. F. Mancia *et al.*, Optimization of protein production in mammalian cells with a coexpressed fluorescent marker, *Structure/Folding and Design* **12**, 1355–1360 (2004).

29. A. R. Aricescu, W. Lu, E. Y. Jones, A time- and cost-efficient system for high-level protein production in mammalian cells, *Acta Crystallogr. D Biol. Crystallogr.* **62**, 1243–1250 (2006).

30. S. Takeshita, K. Kaji, A. Kudo, Identification and characterization of the new osteoclast progenitor with macrophage phenotypes being able to differentiate into mature osteoclasts, *J Bone Miner Res* **15**, 1477–1488 (2000).

31. R. D. Gietz, R. H. Schiestl, Large-scale high-efficiency yeast transformation using the LiAc/SS carrier DNA/PEG method, *Nat Protoc* **2**, 38–41 (2007).

32. Y. Tomimori *et al.*, Evaluation of pharmaceuticals with a novel 50-hour animal model of bone loss, *J Bone Miner Res* **24**, 1194–1205 (2009).

33. S. A. Gai, K. D. Wittrup, Yeast surface display for protein engineering and characterization, *Curr. Opin. Struct. Biol.* **17**, 467–473 (2007).

34. H. Yasuda *et al.*, Identity of osteoclastogenesis inhibitory factor (OCIF) and osteoprotegerin (OPG): a mechanism by which OPG/OCIF inhibits osteoclastogenesis in vitro, *Endocrinology* **139**, 1329–1337 (1998).

35. W. S. Simonet *et al.*, Osteoprotegerin: a novel secreted protein involved in the regulation of bone density, *Cell* **89**, 309–319 (1997).

36. L. A. Schneeweis, D. Willard, M. E. Milla, Functional dissection of osteoprotegerin and its interaction with receptor activator of NF-kappaB ligand, *J. Biol. Chem.* **280**, 41155–41164 (2005).

37. F. Henkler *et al.*, The extracellular domains of FasL and Fas are sufficient for the formation of supramolecular FasL-Fas clusters of high stability, *J. Cell Biol.* **168**, 1087–1098 (2005).

38. R. M. Siegel *et al.*, SPOTS: signaling protein oligomeric transduction structures are early mediators of death receptor-induced apoptosis at the plasma membrane, *J. Cell Biol.* **167**, 735–744 (2004).

39. L. Wang *et al.*, The Fas-FADD death domain complex structure reveals the basis of DISC assembly and disease mutations, *Nat. Struct. Mol. Biol.* **17**, 1324–1329 (2010).

40. Y. Liu *et al.*, Crystal structure of sTALL-1 reveals a virus-like assembly of TNF family ligands, *Cell* **108**, 383–394 (2002).

41. A. Krippner-Heidenreich *et al.*, Control of receptor-induced signaling complex formation by the kinetics of ligand/receptor interaction, *J. Biol. Chem.* **277**, 44155–44163 (2002).

42. Z. Zhou *et al.*, Human glucocorticoid-induced TNF receptor ligand regulates its signaling activity through multiple oligomerization states, *Proceedings of the National Academy of Sciences* **105**, 5465–5470 (2008).

43. P. J. Kostenuik *et al.*, Denosumab, a fully human monoclonal antibody to RANKL, inhibits bone resorption and increases BMD in knock-in mice that express chimeric (murine/human) RANKL, *J Bone Miner Res* **24**, 182–195 (2009).

44. J.-L. Bodmer, P. Schneider, J. Tschopp, The molecular architecture of the TNF superfamily, *Trends Biochem. Sci.* **27**, 19–26 (2002).

45. B. B. Aggarwal, S. C. Gupta, J. H. Kim, Historical perspectives on tumor necrosis factor and its superfamily: 25 years later, a golden journey, *Blood* **119**, 651–665 (2012).

46. M. Crawford, J. R. Curtis, Tumor necrosis factor inhibitors and infection complications, *Curr Rheumatol Rep* **10**, 383–389 (2008).

47. T. Bongartz *et al.*, Anti-TNF antibody therapy in rheumatoid arthritis and the risk of serious infections and malignancies: systematic review and meta-analysis of rare harmful effects in randomized controlled trials, *JAMA* **295**, 2275–2285 (2006).

48. F. Van Hauwermeiren, R. E. Vandenbroucke, C. Libert, Treatment of TNF mediated diseases by selective inhibition of soluble TNF or TNFR1, *Cytokine Growth Factor Rev.* **22**, 311–319 (2011).

49. H. Wu, S. G. Hymowitz, in *Handbook of Cell Signaling*, R. Bradshaw, E. Dennis, Eds. (Academic Press, 2009), vol. 1, pp. 265–275.

Acknowledgements: We thank Dr. S. Kyle Austen and Dr. Michelle Sabo for experimental advice, as well as Jean Chappel for technical assistance. This work was supported by the National Institutes of Health Grant Numbers AR032788 (to S.L.T. and D.H.F.) and F30 AG039896 (to J.T.W.).

2.7 Figure Legends

Figure 2.1. Construction and validation of single-chain RANKL. WT-RANKL is depicted as three individual polypeptides (monomers), whereas WT single-chain RANKL (scRANKL) exists as a single polypeptide with [GGSG]x3 amino acid linkers.

Figure 2.2. Effect of solubility mutations on RANKL function. Kinetic affinities for RANK of WT-RANKL or WT RANKL containing two solubility mutations (C220S/E246I, "WT-SM RANKL") were determined using surface plasmon resonance (SPR).

Figure 2.3. Characterization of scRANKL. (A) Coomassie-stained SDS-PAGE gel of WT RANKL and scRANKL (500ng each) chemically cross-linked by increasing concentrations of BS3. (B) Multi-angle light scattering (MALS) of non-covalently linked RANKL or single-chain RANKL. Precise molecular weights of homotrimerically assembled RANKL (left) or single-chain RANKL (right) determined using MALS. The differences in calculated and measured molecular weights reflect the presence of significant glycosylation on these mammalian cell-produced, secreted proteins. (C) Osteoclasts were generated from BMMs in the presence of recombinant WT RANKL or scRANKL and TRAP stained.

Figure 2.4. Design of RANKL mutants that prevent binding to RANK. (A) Binding of RANKL variants to RANK-Fc or OPG-Fc as assessed by BLI. Due to the dimeric nature of the analyte, K_D values represent approximate affinity constants. (B) Representative BLI curves showing binding of WT-SM RANKL, CDins RANKL, or GST control to RANK-Fc or OPG-Fc.

Figure 2.5. Functional characterization of RANKL mutants with varying degrees of RANK binding. Osteoclastogenic capacity of recombinant RANKL variants *in vitro* assessed by (A) TRAP stain, (B) TRAP-solution assay and (C) osteoclastogenic marker mRNAs. (D) Signal transudction of WT-SM RANKL and CDins RANKL assessed by IκB phosphorylation.

Figure 2.6. Degree of RANK monomer recruitment necessary and sufficient for osteoclastogenesis. (A) Individual monomer(s) of single- or double-block scRANKL are mutated to inhibit binding to RANK. Thus, single–blocked scRANKL contains two intact receptor recruitment sites and double- blocked, one. (B) Triplicate curves showing equal amounts of scRANKL variants coupled to an SPR chip with RANK as analyte. The average number of RU for each binding curve at saturation is displayed. (C) Osteoclastogenesis induced by scRANKL variants assessed by TRAP activity. (D) EC_{50} values of osteoclast generation and percent maximum osteoclastogenesis relative to WT-scRANKL. (E) RANK-mediated signaling induced by WT- and various sc-RANKL constructs (500ng/ml).

Figure 2.7. Ability of single- or double-block scRANKL to inhibit osteoclastogenesis. (A) BMMs were cultured with WT-SM RANKL (200ng/mL) and increasing amounts of single- or double-block scRANKL. Four days later osteoclastogenesis was assessed by TRAP activity. The addition of OPG monomeric fragment (4ug/mL) was used as positive control for inhibition of osteoclastogenesis. (B) Representative TRAP stains of the highest scRANKL concentrations from part (A).

Figure 2.8. Reversion mutagenesis of YSD RANKL clones. Binding to RANK-Fc (blue) or OPG-Fc (red) is expressed relative to WT-SM RANKL. (A) Top scoring clones from low (LM3S) or high (HM3S) mutation rate libraries with (B) individual point mutations of these clones. (C) A second mutation was added to the most effective individual point mutant (Q236H). (D) A third mutation was added to closely approximate the ideal phenotype.

Figure 2.9. Yeast-surface display generation of high affinity RANKL mutants. (A) Flow cytometry-based histogram showing staining with 1uM RANK at each phase of library sorting. To select for clones with increased RANK binding, the three rounds of sorting were

initiated (Sort#1) with a concentration of RANKL 10-fold greater than the K_D of RANK and was terminated (Sort#3) with a concentration 10-fold less. (C) Kinetic and equilibrium affinities of WT-SM RANKL, SM RANKL^{Q236H}, and SM RANKL^{KQFH} were determined using SPR. RANKL variants were coupled to a sensor chip and RANK or OPG monomeric fragments served as analyte. (B) Schematic representing competitive OPG YSD screen. In the context of wild-type RANKL (left side), RANK (purple) fused to 6-His is readily displaced by OPG (yellow) due to its higher affinity. Alternatively, in the context of an increased affinity RANKL clone that has lost the capacity to bind decoy receptor, OPG is incapable of displacing RANK (right side). Additionally, only those clones that have an increased half-life will have sustained binding after room temperature washing. (C) Individual point-mutated RANKL clones retaining high RANK binding, detected by an anti-6His mAb, after 5 minutes of OPG competition. (B, C) Data are expressed as percent RANKL bound to RANK with time, relative to that bound in the absence of OPG. Additionally, binding of RANK (APC) is normalized to the level of RANKL yeast surface induction (FITC) expressed as the median fluorescence intensity (MFI) ratio (APC/FITC). (D) RANKL point mutants generated by YSD K_D values are estimated using titrating amounts of RANK binding to yeast surface-displayed RANKL and fitting median fluorescence intensity values to a one-site binding model. ND = not enough data points to fit K_D values, despite low levels of detectable staining at the highest concentrations.

Figure 2.10. Effect of RANKL solubility mutations on OPG binding. Kinetic affinities of WT-RANKL or WT-SM RANKL were determined by SPR.

Figure 2.11. Kinetic parameters of RANKL high affinity variants. Kinetic and equilibrium affinities of WT-SM RANKL (A), Q236H-SM RANKL (B), and KQFH-SM RANKL (C) were determined using SPR. RANKL variants were coupled to a sensor chip and RANK or OPG monomeric fragments served as analyte.

Figure 2.12. Combined mutations of RANKL and OPG which block RANK binding. (A) Titration curves of $RANKL^{CDins}$ and $RANKL^{CDins/Q236H}$ binding to RANK or OPG assessed by flow cytometry of RANKL-displaying yeast cells. Binding of RANK or OPG (APC) is normalized to the level of RANKL yeast surface induction (FITC) expressed as the median fluorescence intensity (MFI) ratio (APC/FITC). (B) Capacity of $RANKL^{CDins}$ and $RANKL^{CDins/Q236H}$ to generate osteoclasts in vitro. (C) Phosphorylation of IkB by $RANKL^{CDins}$ and $RANKL^{CDins/Q236H}$ (500ng/mL).

Figure 2.13. Development of a competitive antagonist scRANKL. (A) Induction of osteoclastogenesis, *in vitro*, by double-block scRANKL variants compared to WT scRANKL. (B) Induction of osteoclastogenesis by double-block, $RANK^{high}$ or single-block scRANKL variants with WT, medium or high RANK affinity at the intact binding sites quantitated by a fluorescent TRAP activity assay. (C) EC_{50} of osteoclast generation and percent maximum number of osteoclasts relative to WT-scRANKL. (D) Capacity of increasing amounts of single-block, $RANK^{high}$ (orange squares) or double-block, $RANK^{high}$ (orange triangles) scRANKL to inhibit WT-SM RANKL-induced osteoclastogenesis. WT-SM only (open diamond) serves as a positive control for osteoclast formation. (E) Mice were injected with WT-SM RANKL +/- 0.5mg/kg single-block, $RANK^{high}$ scRANKL. Two days later serum CTx was measured.

Figure 2.1

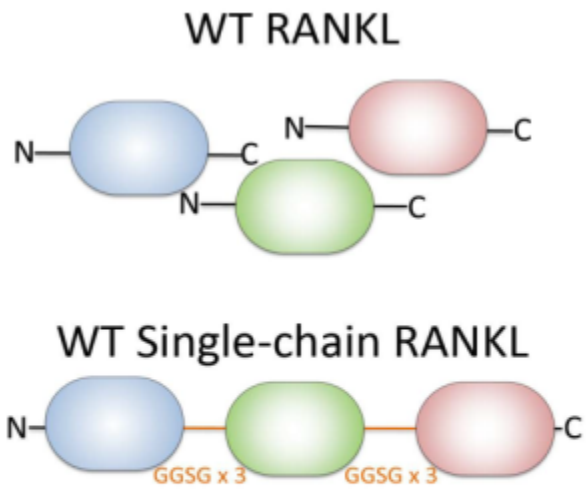

Figure 2.2

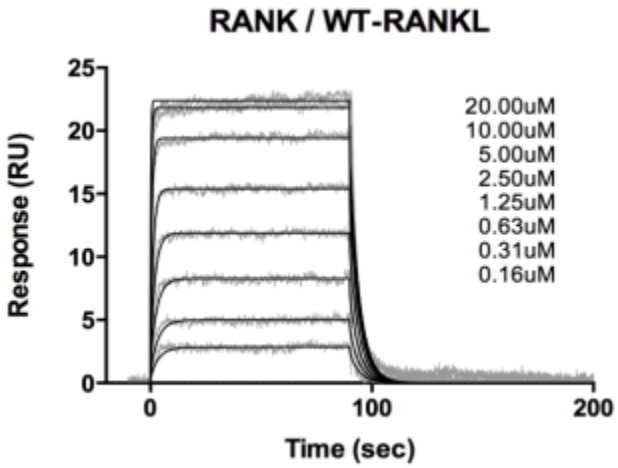

ka (1/Ms) = $2.04 \pm 0.09 \times 10^{5}$

kd (1/s) = $2.52 \pm 0.43 \times 10^{-1}$

$K_{D\text{-kinetic}}$ (M) = $1.23 \pm 0.17 \times 10^{-6}$

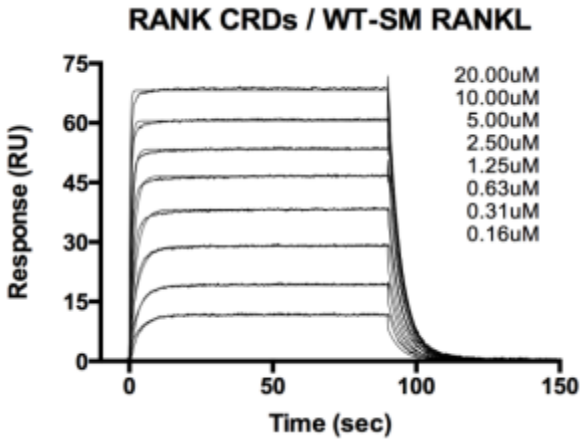

ka (1/Ms) = $1.51 \pm 0.38 \times 10^{5}$

kd (1/s) = $2.08 \pm 0.09 \times 10^{-1}$

$K_{D\text{-kinetic}}$ (M) = $1.40 \pm 0.31 \times 10^{-6}$

Figure 2.3

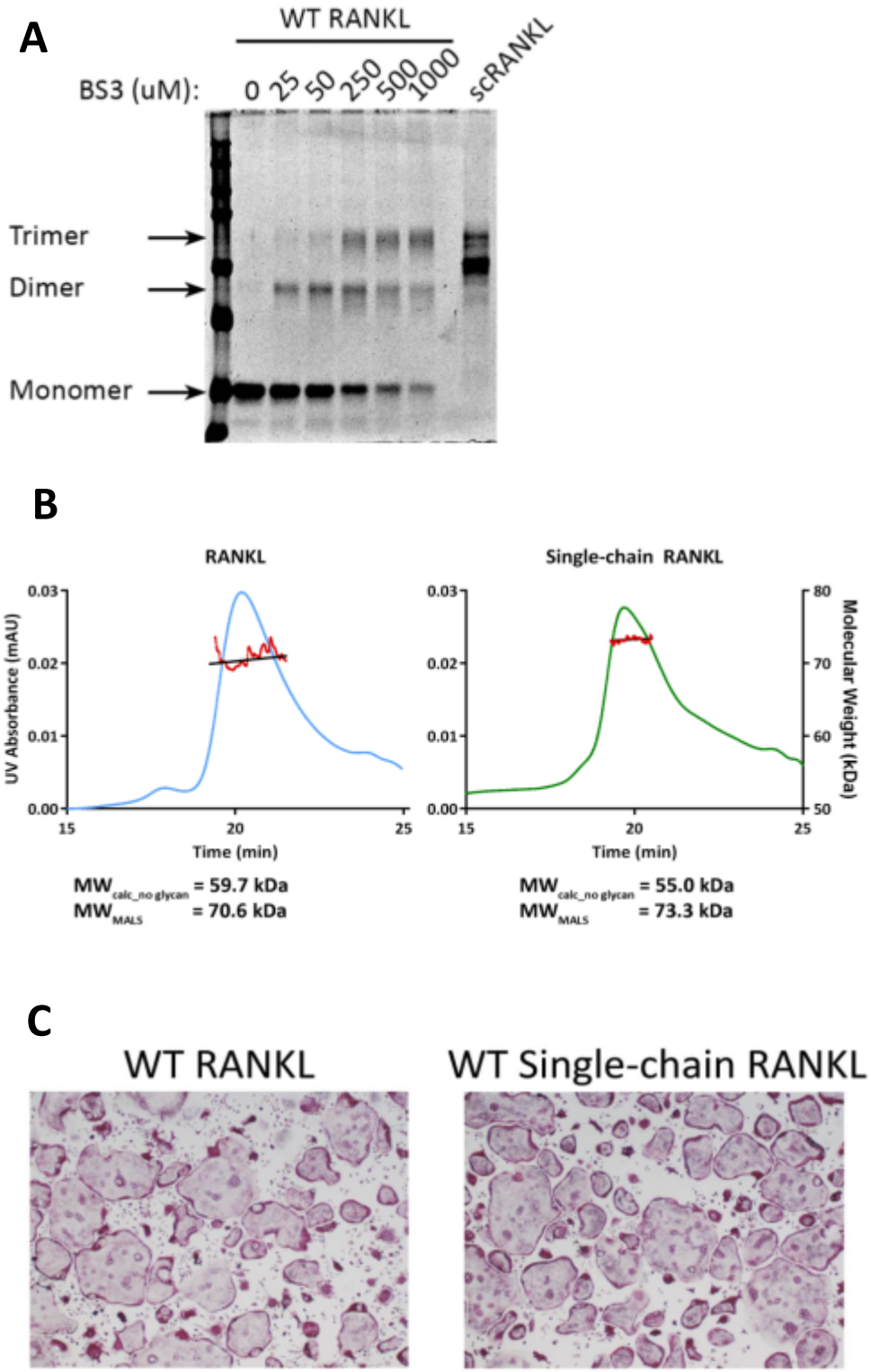
A
WT RANKL
BS3 (uM):
0 25 50 250 500 1000
scRANKL
Trimer
Dimer
Monomer
B
RANKL
Single-chain RANKL
UV Absorbance (mAU)
Molecular Weight (kDa)
Time (min)
MW calc_no glycan = 59.7 kDa
MW MALS = 70.6 kDa
MW calc_no glycan = 55.0 kDa
MW MALS = 73.3 kDa
C
WT RANKL
WT Single-chain RANKL

Figure 2.4

A

		K_D (RANK-Fc)*	K_D (OPG-Fc)*
WT		5.24E-10	1.96E-11
Mut1	R190G	6.79E-09	4.53E-10
Mut2	G191D	7.31E-09	7.05E-10
Mut3	AA'-1 WYHDggsRGW	1.32E-08	8.77E-10
Mut4	AA'-2 WYHDssRGW	1.05E-08	3.89E-10
Mut5	AA'-3 WYHDsRGW	1.22E-08	1.48E-10
Mut6	AA'-4 WYHDsRsGW	2.17E-08	9.40E-10
Mut7	AA'-5 WYssHDRGW	1.36E-08	3.84E-10
Mut8	AA'-6 WYsHDRGW	1.43E-08	1.85E-11
Mut9	R222A	1.35E-08	1.09E-09
Mut10	R222Y	2.34E-09	5.30E-10
Mut11	E268Y	1.12E-08	1.61E-10
Mut12	E268Yggs	9.16E-09	2.40E-12
Mut13	R222Y/E268Y	6.59E-09	1.48E-09
Mut14	H224E	2.07E-08	4.73E-11
Mut15	E225R	1.53E-08	9.35E-12
Mut16	CD-1 FRggsHHET	Not Detectable	6.10E-11
Mut17	CD-2 FRhggsHHET	Not Detectable	3.56E-12
Mut21	E225R/E268Y	1.14E-08	1.02E-11
Mut22	AA'-1/CD-1	Not Detectable	1.07E-09
Mut23	AA'-1/CD-2	Not Detectable	2.20E-09
Mut24	AA'-2/CD-1	Not Detectable	9.78E-10
Mut25	AA'2/CD-2	Not Detectable	1.39E-09
Mut28	R222A/E268A	1.85E-08	1.48E-09

CDins RANKL: ggs inserted after R222 (Mut16)

B

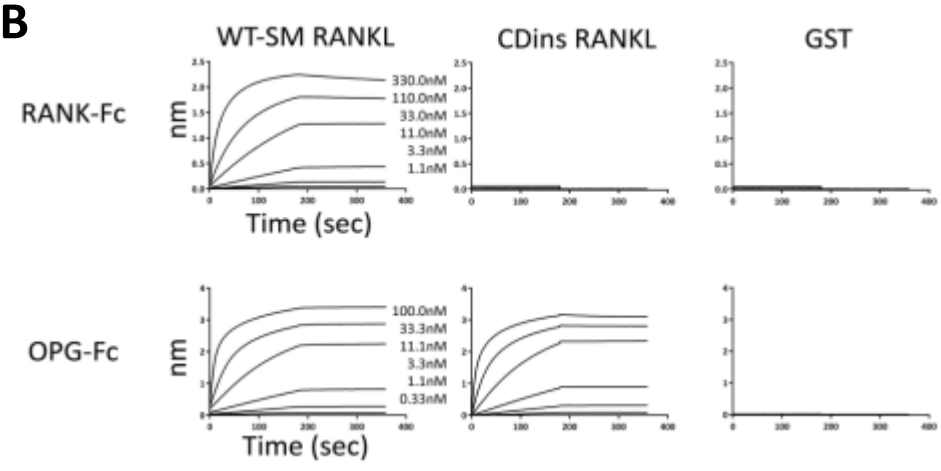

Figure 2.5

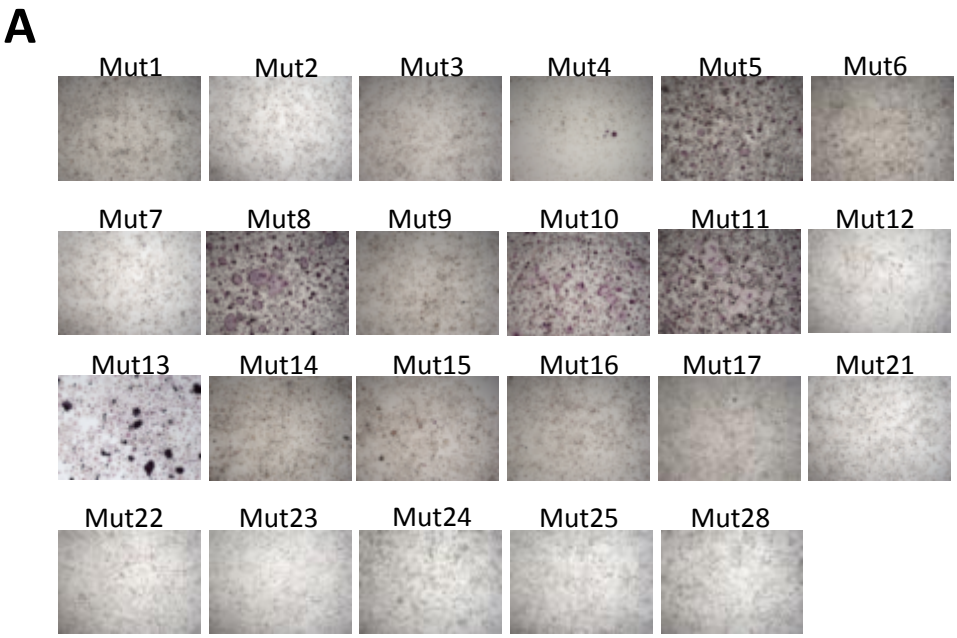
A
Mut1
Mut2
Mut3
Mut4
Mut5
Mut6
Mut7
Mut8
Mut9
Mut10
Mut11
Mut12
Mut13
Mut14
Mut15
Mut16
Mut17
Mut21
Mut22
Mut23
Mut24
Mut25
Mut28

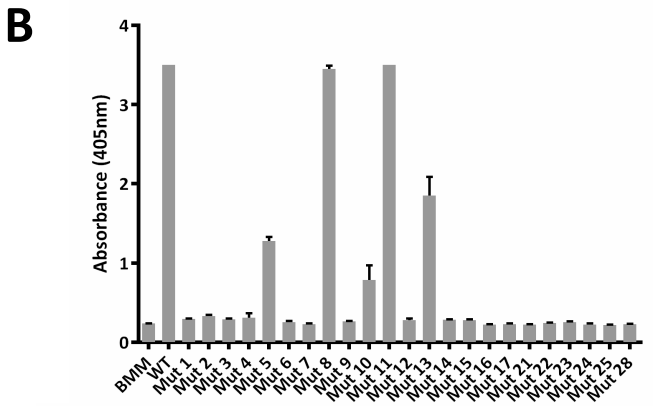
B
Absorbance (405nm)
0
1
2
3
4
BMM
WT
Mut 1
Mut 2
Mut 3
Mut 4
Mut 5
Mut 6
Mut 7
Mut 8
Mut 9
Mut 10
Mut 11
Mut 12
Mut 13
Mut 14
Mut 15
Mut 16
Mut 17
Mut 21
Mut 22
Mut 23
Mut 24
Mut 25
Mut 28

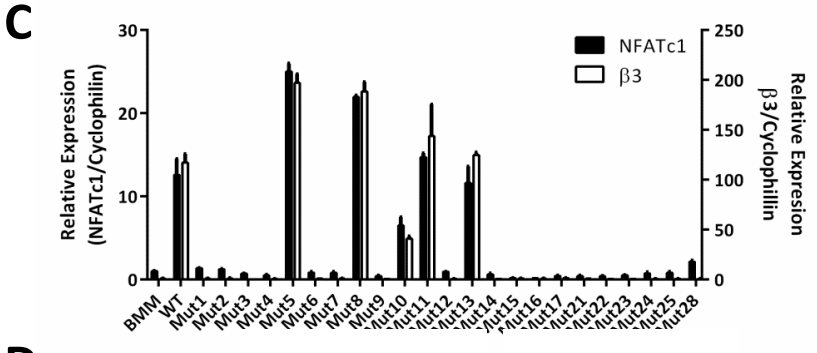
C
NFATc1
β3
Relative Expression
(NFATc1/Cyclophilin)
Relative Expresion
β3/Cyclophillin
0
10
20
30
0
50
100
150
200
250
BMM
WT
Mut1
Mut2
Mut3
Mut4
Mut5
Mut6
Mut7
Mut8
Mut9

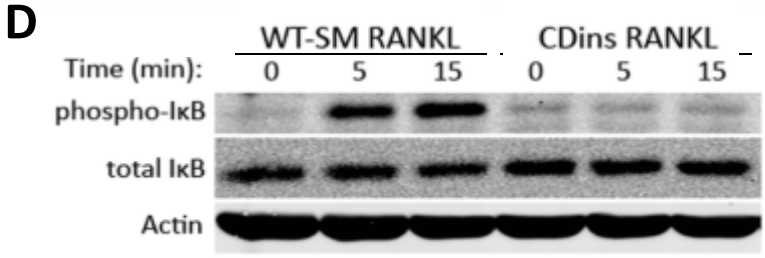
D
WT-SM RANKL
CDins RANKL
Time (min):
0
5
15
0
5
15
phospho-IκB
total IκB
Actin

Figure 2.6

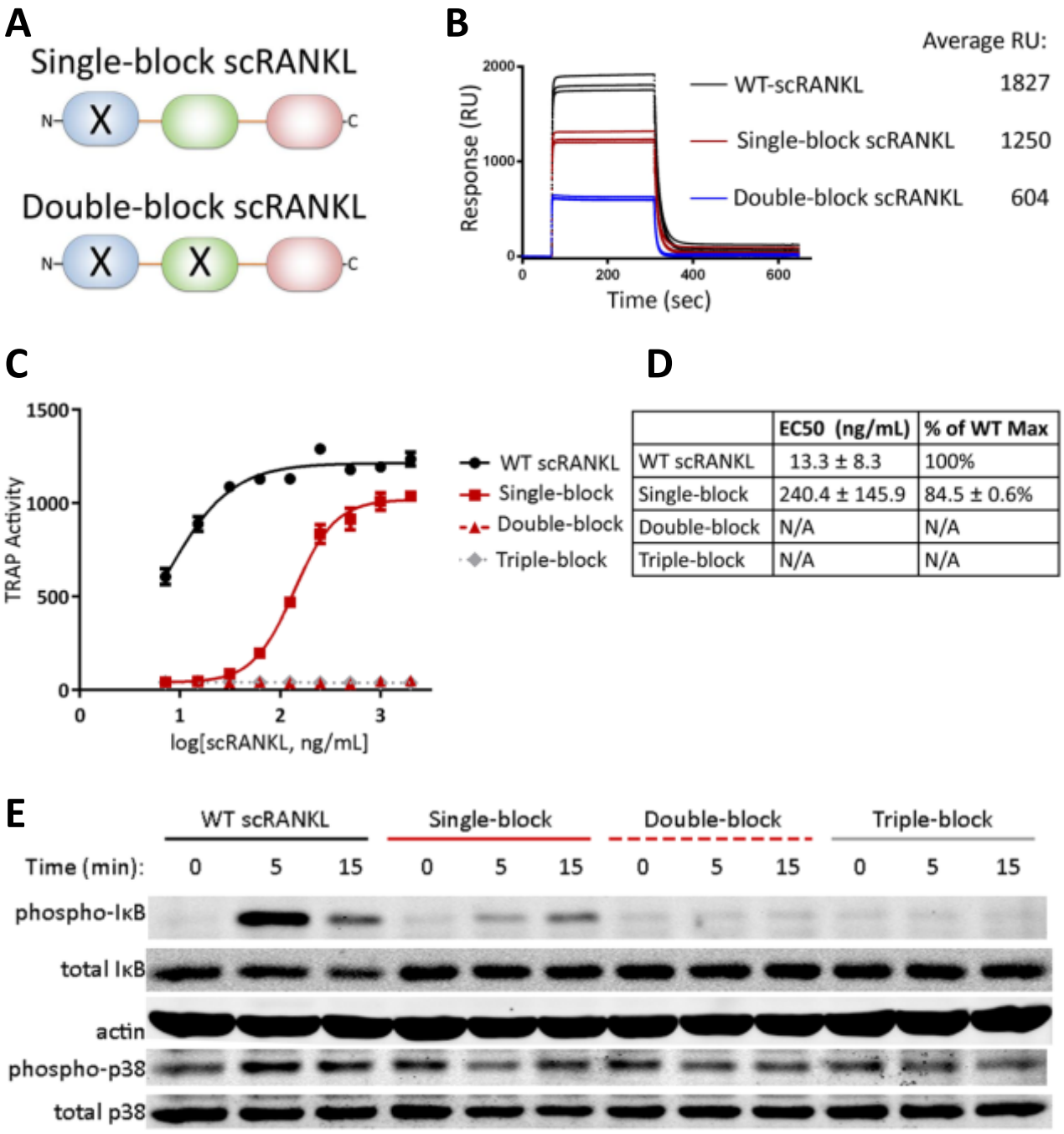

	EC50 (ng/mL)	% of WT Max
WT scRANKL	13.3 ± 8.3	100%
Single-block	240.4 ± 145.9	84.5 ± 0.6%
Double-block	N/A	N/A
Triple-block	N/A	N/A

Figure 2.7

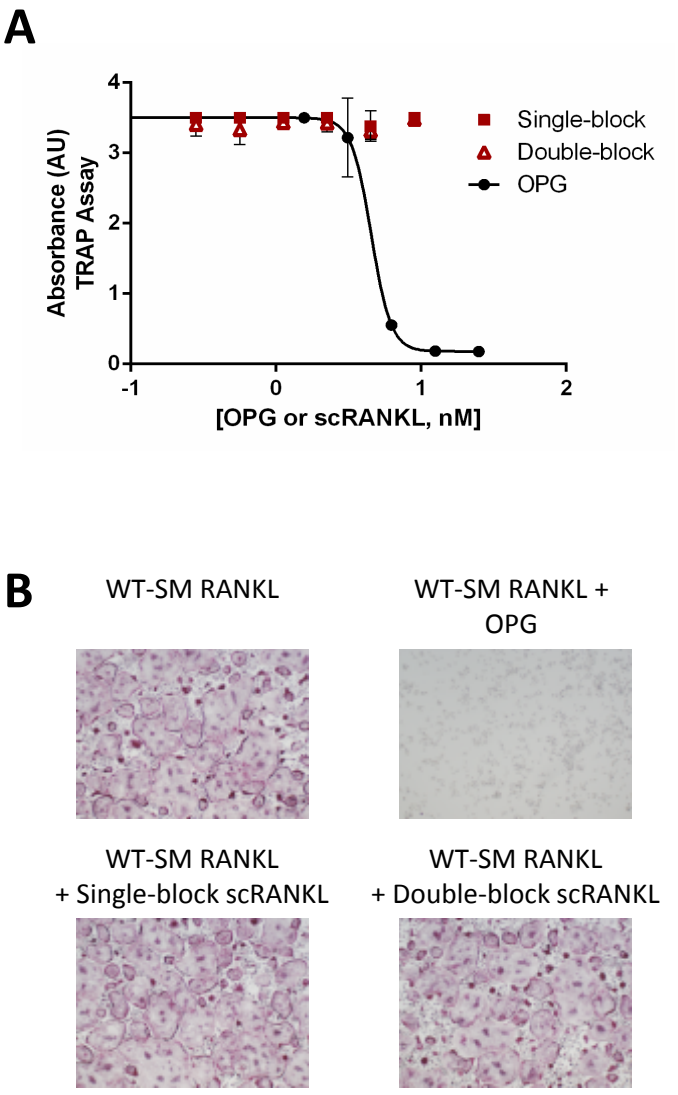
A
Absorbance (AU)
TRAP Assay
4
3
2
1
0
-1
0
1
2
[OPG or scRANKL, nM]
Single-block
Double-block
OPG
B
WT-SM RANKL
WT-SM RANKL +
OPG
WT-SM RANKL
+ Single-block scRANKL
WT-SM RANKL
+ Double-block scRANKL

Figure 2.8

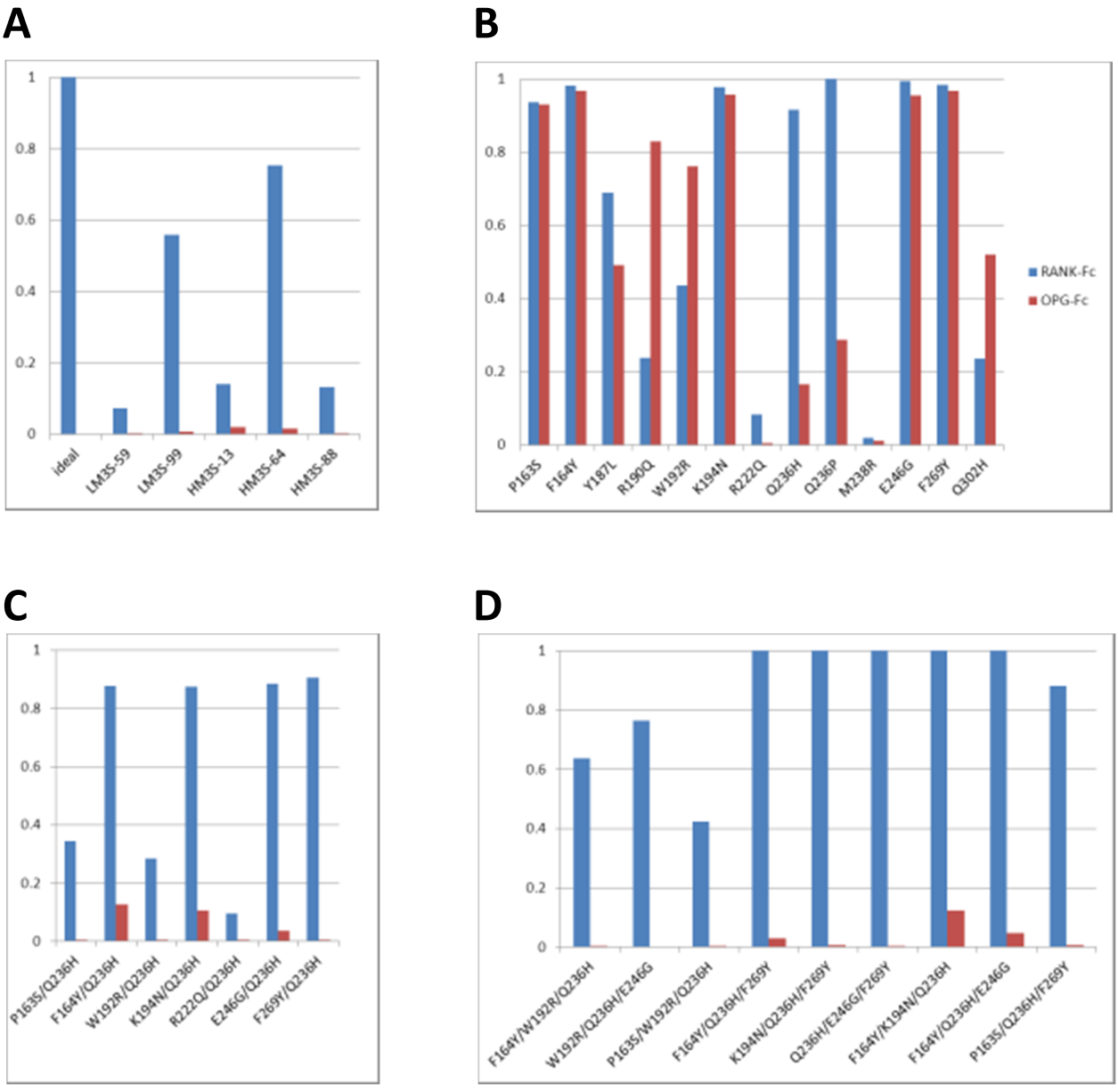
A
B
C
D
1
0.8
0.6
0.4
0.2
0
ideal
LM3S-59
LM3S-99
HM3S-13
HM3S-64
HM3S-88
P163S
F164Y
Y187L
R190Q
W192R
K194N
R222Q
Q236H
Q236P
M238R
E246G
F269Y
Q302H
RANK-Fc
OPG-Fc
P163S/Q236H
F164Y/Q236H
W192R/Q236H
K194N/Q236H
R222Q/Q236H
E246G/Q236H
F269Y/Q236H
F164Y/W192R/Q236H
W192R/Q236H/E246G
P163S/W192R/Q236H
F164Y/Q236H/F269Y
K194N/Q236H/F269Y
Q236H/E246G/F269Y
F164Y/K194N/Q236H
F164Y/Q236H/E246G
P163S/Q236H/F269Y

Figure 2.9

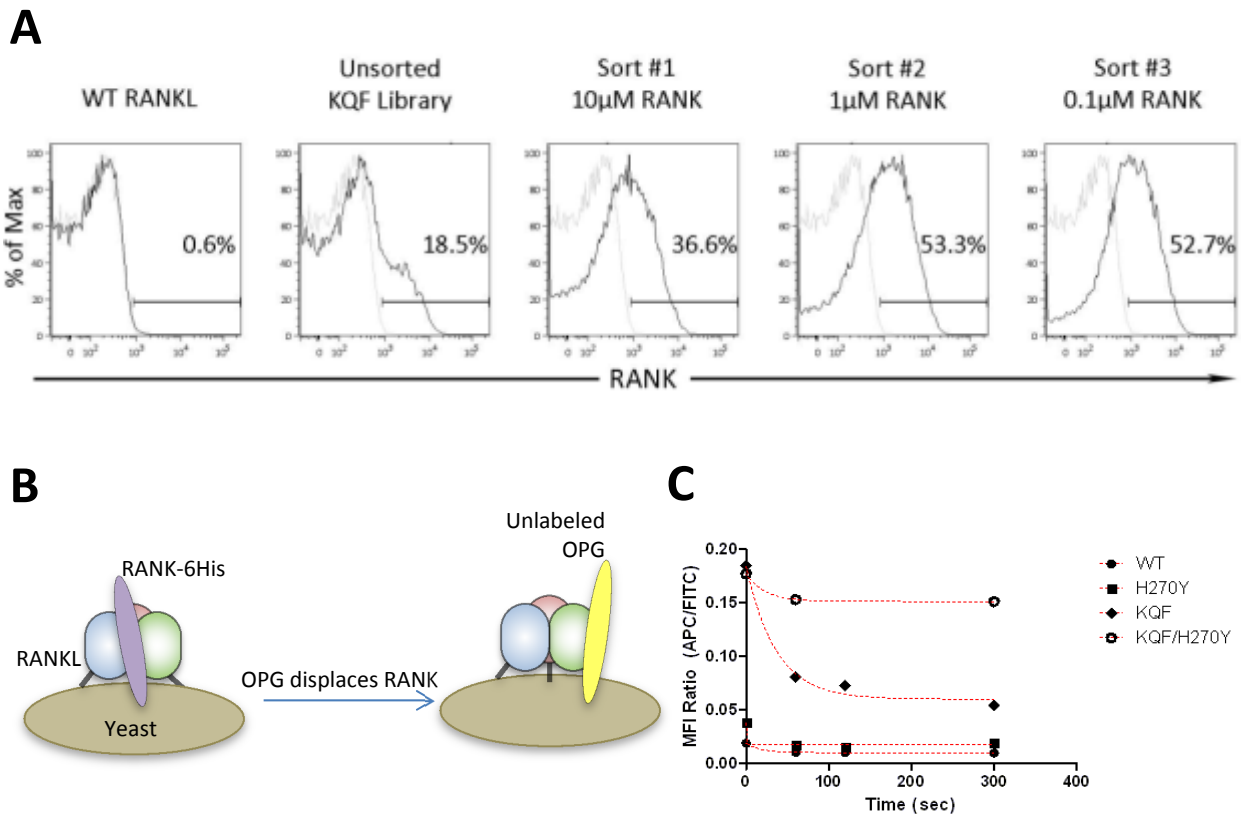

D

					YSD Approximated K_D (nM)	
Residue no.	194	236	269	270	RANK	OPG
WT RANKL	K	Q	F	H	ND	32.8
K194E	E				ND	71.7
Q236H		H			346.5	ND
F269Y			Y		ND	33.3
H270Y				Y	464.7	275.9
K/Q	E	H			69.7	ND
K/Q/F	E	H	Y		23.6	ND
K/Q/F/H	E	H	Y	Y	1.4	ND

Figure 2.10

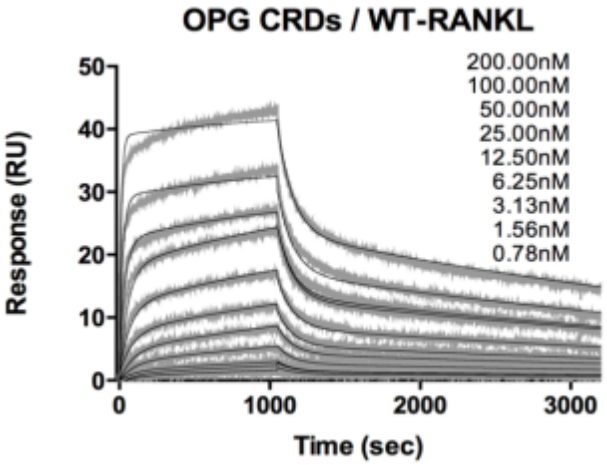

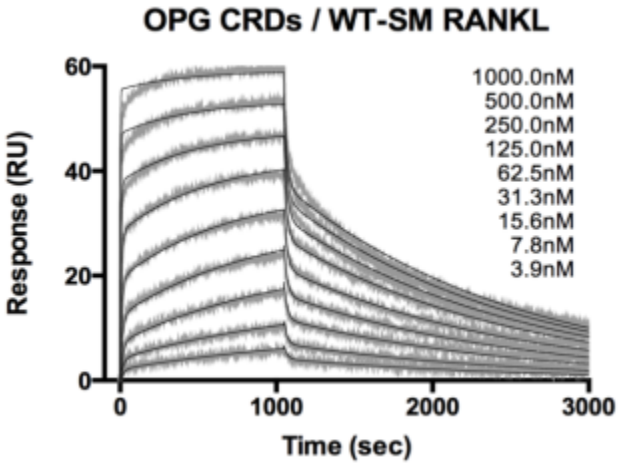

ka (1/Ms) =	$3.90 \pm 0.79 \times 10^{5}$
kd (1/s) =	$8.52 \pm 0.37 \times 10^{-3}$
$K_{D\text{-kinetic}}$ (M) =	$4.75 \pm 0.93 \times 10^{-9}$

ka (1/Ms) =	$4.14 \pm 0.68 \times 10^{5}$
kd (1/s) =	$4.57 \pm 0.60 \times 10^{-2}$
$K_{D\text{-kinetic}}$ (M) =	$3.05 \pm 0.30 \times 10^{-8}$

Figure 2.11

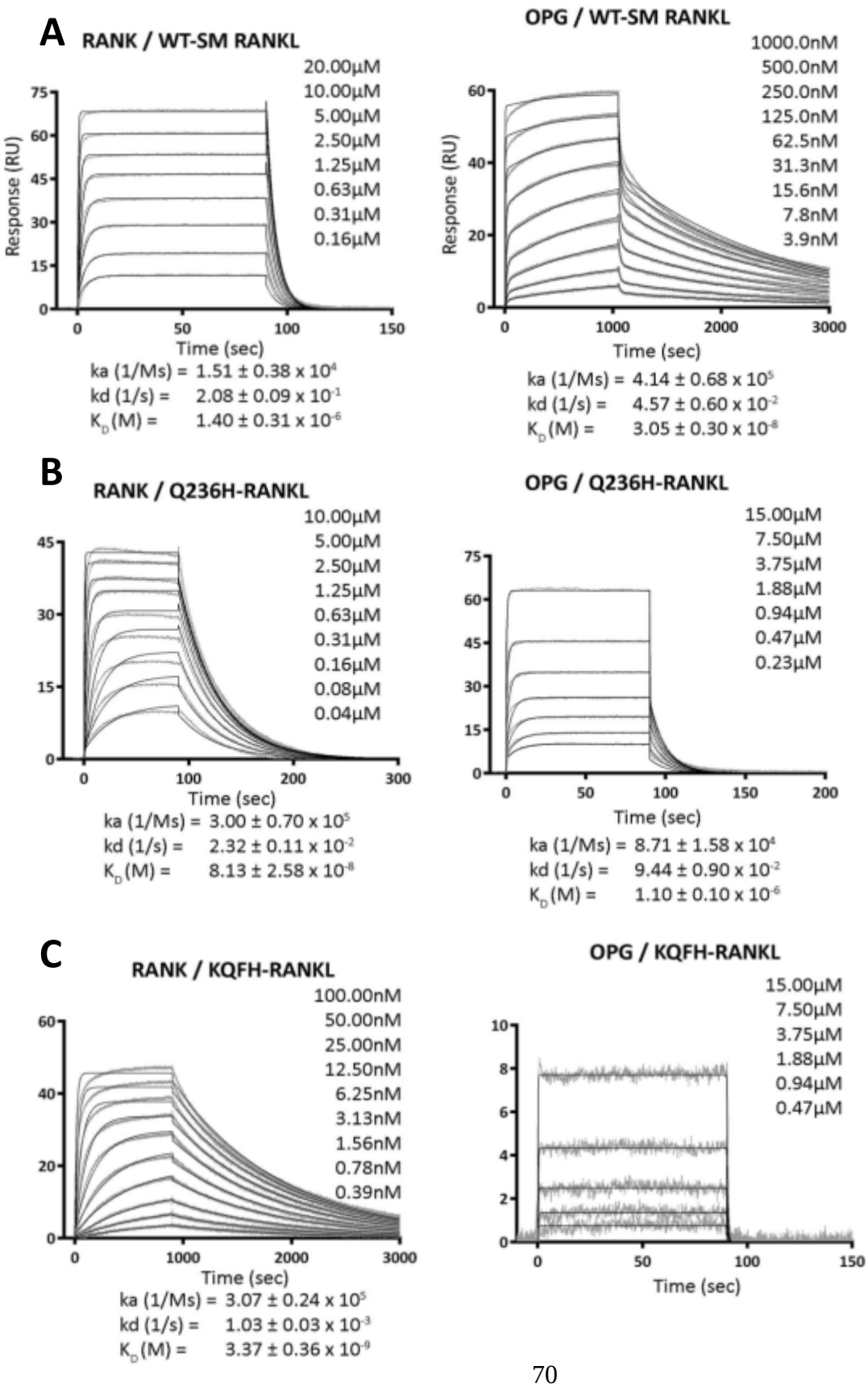
A
RANK / WT-SM RANKL
20.00µM
10.00µM
5.00µM
2.50µM
1.25µM
0.63µM
0.31µM
0.16µM
Response (RU)
Time (sec)
ka (1/Ms) = 1.51 ± 0.38 x 10^4
kd (1/s) = 2.08 ± 0.09 x 10^-1
K_D (M) = 1.40 ± 0.31 x 10^-6
OPG / WT-SM RANKL
1000.0nM
500.0nM
250.0nM
125.0nM
62.5nM
31.3nM
15.6nM
7.8nM
3.9nM
Response (RU)
Time (sec)
ka (1/Ms) = 4.14 ± 0.68 x 10^5
kd (1/s) = 4.57 ± 0.60 x 10^-2
K_D (M) = 3.05 ± 0.30 x 10^-8
B
RANK / Q236H-RANKL
10.00µM
5.00µM
2.50µM
1.25µM
0.63µM
0.31µM
0.16µM
0.08µM
0.04µM
Time (sec)
ka (1/Ms) = 3.00 ± 0.70 x 10^5
kd (1/s) = 2.32 ± 0.11 x 10^-2
K_D (M) = 8.13 ± 2.58 x 10^-8
OPG / Q236H-RANKL
15.00µM
7.50µM
3.75µM
1.88µM
0.94µM
0.47µM
0.23µM
Time (sec)
ka (1/Ms) = 8.71 ± 1.58 x 10^4
kd (1/s) = 9.44 ± 0.90 x 10^-2
K_D (M) = 1.10 ± 0.10 x 10^-6
C
RANK / KQFH-RANKL
100.00nM
50.00nM
25.00nM
12.50nM
6.25nM
3.13nM
1.56nM
0.78nM
0.39nM
Time (sec)
ka (1/Ms) = 3.07 ± 0.24 x 10^5
kd (1/s) = 1.03 ± 0.03 x 10^-3
K_D (M) = 3.37 ± 0.36 x 10^-9
OPG / KQFH-RANKL
15.00µM
7.50µM
3.75µM
1.88µM
0.94µM
0.47µM
Time (sec)

Figure 2.12

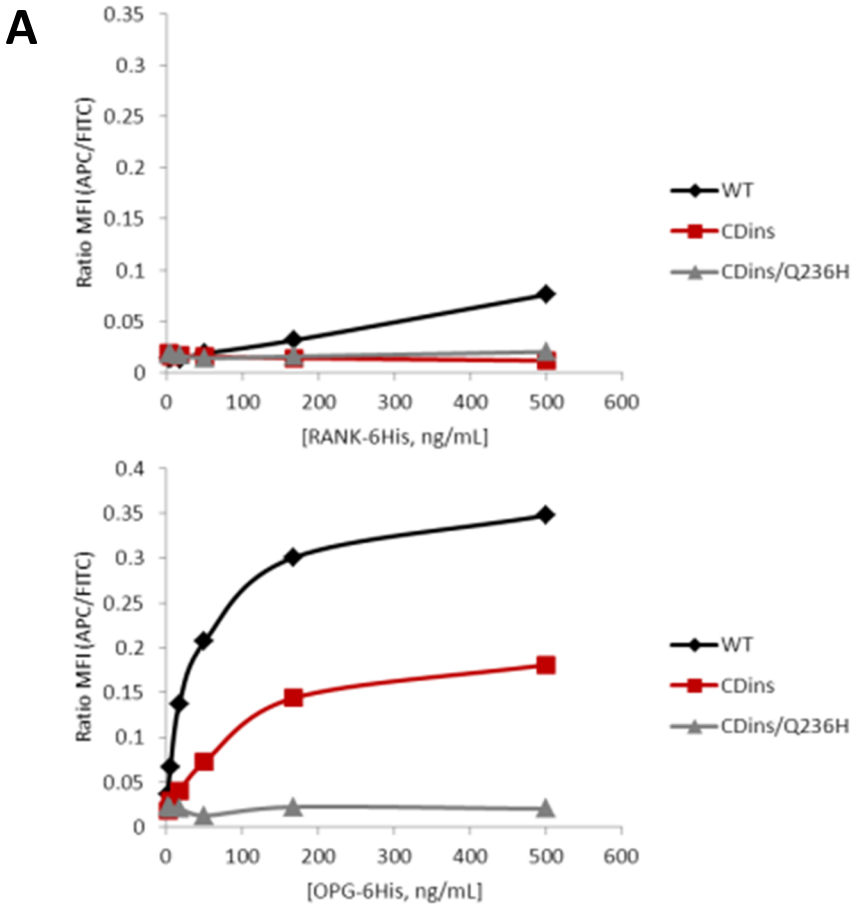
A
Ratio MFI (APC/FITC)
0.35
0.3
0.25
0.2
0.15
0.1
0.05
0
0
100
200
300
400
500
600
[RANK-6His, ng/mL]
WT
CDins
CDins/Q236H
Ratio MFI (APC/FITC)
0.4
0.35
0.3
0.25
0.2
0.15
0.1
0.05
0
0
100
200
300
400
500
600
[OPG-6His, ng/mL]
WT
CDins
CDins/Q236H

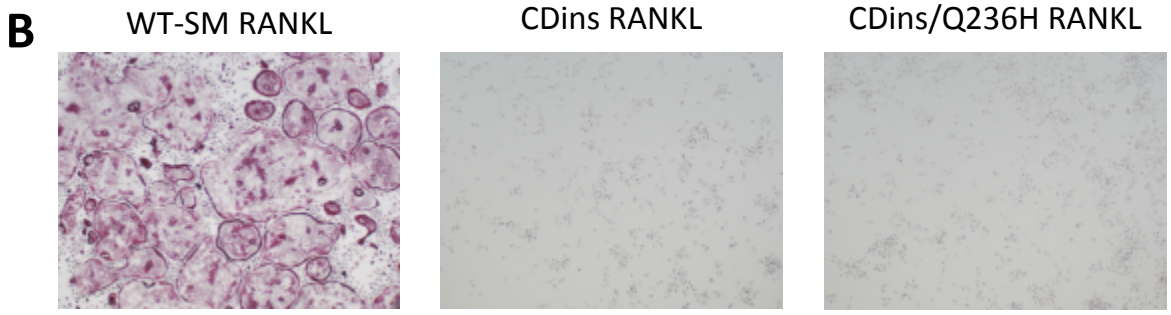
B
WT-SM RANKL
CDins RANKL
CDins/Q236H RANKL

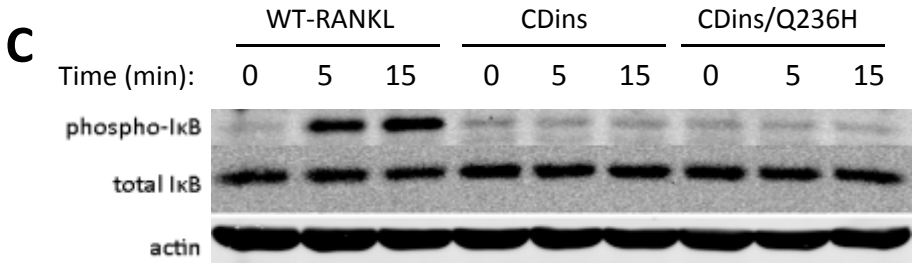
C
WT-RANKL
CDins
CDins/Q236H
Time (min):
0
5
15
0
5
15
0
5
15
phospho-IκB
total IκB
actin

Figure 2.13

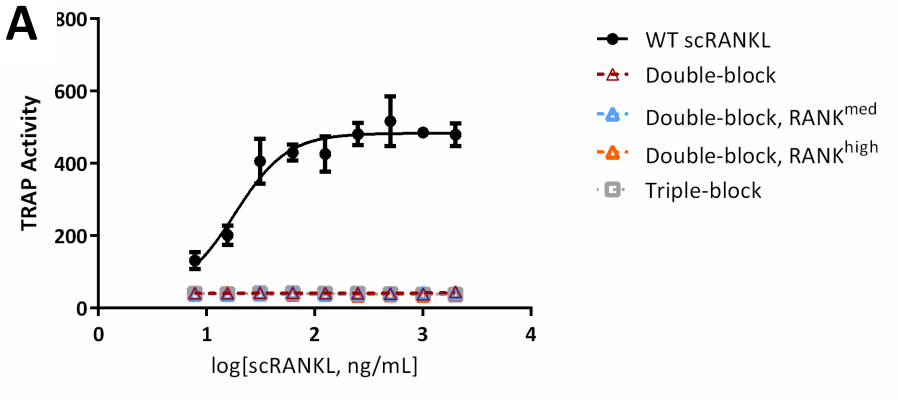

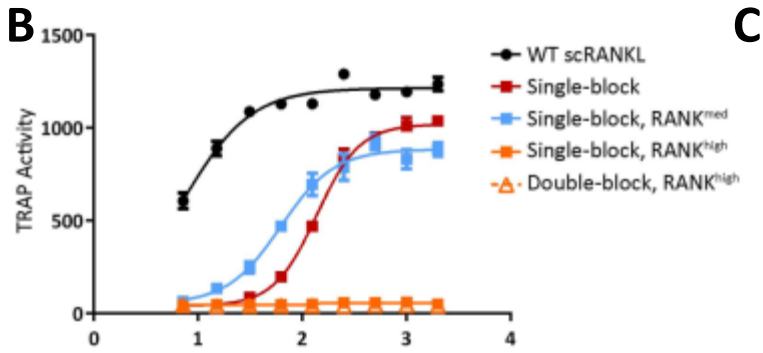

C

	EC50 (ng/mL)	% of WT Max
WT scRANKL	13.3 ± 8.3	100%
Single-block	240.4 ± 145.9	84.5 ± 0.6%
Single-block, RANK^{med}	91.3 ± 41.6	63.7 ± 13.9%
Single-block, RANK^{high}	N/A	N/A
Double-block, RANK^{high}	N/A	N/A

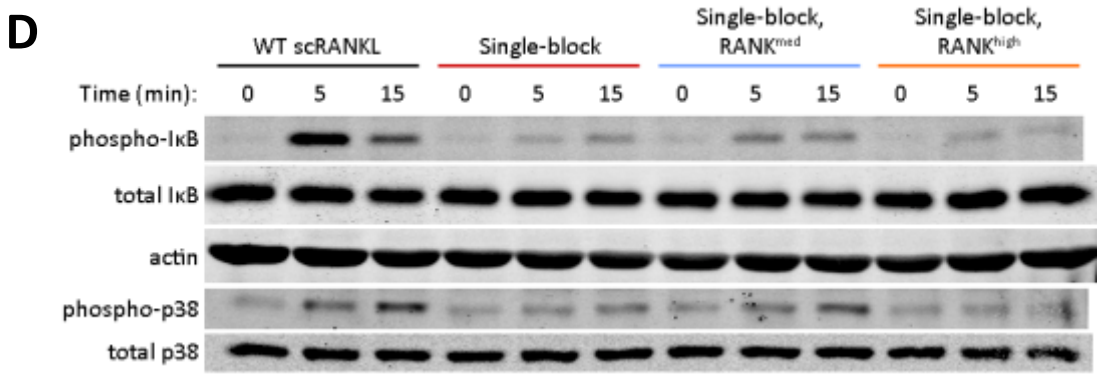

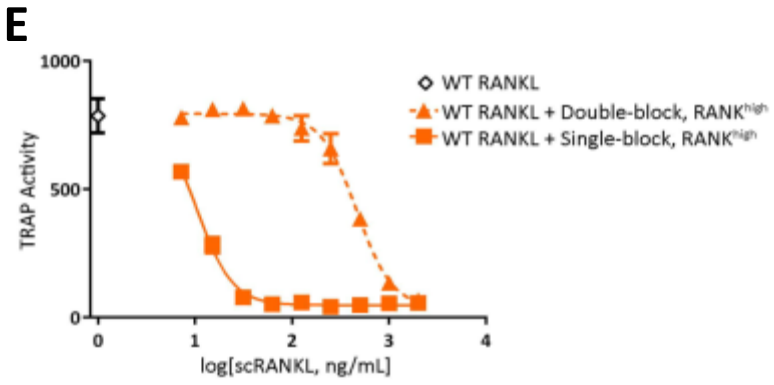

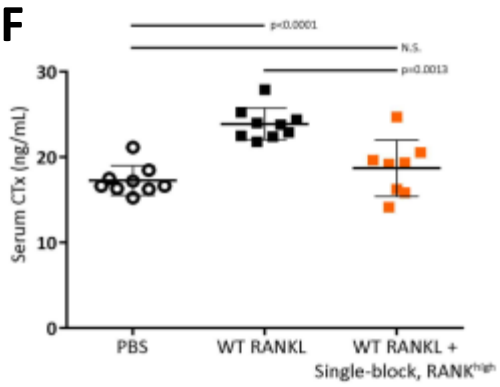

Chapter 3

Optimized RANKL/RANK Binding Kinetics Exert a Biphasic Effect on Osteoclast Formation and Function

Julia T. Warren, Corinne E. Decker, Wei Zou, Nidhi Rohatgi, Steven L. Teitelbaum,

Manuscript in preparation, November, 2013.

3.1 Abstract

The interaction between Receptor Activator of NF-κB Ligand (RANKL) and its receptor RANK is essential for the differentiation and bone resorbing capacity of the osteoclast. Osteoprotegerin (OPG), a soluble homodimer, acts as a decoy receptor for RANKL and thus inhibits osteoclastogenesis. An imbalance in the RANKL/RANK/OPG axis, with decreased OPG and/or increased RANKL, is associated with diseases that favor bone loss, including osteoporosis. Recently, we established a yeast surface display system and screened libraries of randomly mutated RANKL proteins to identify mutations that abolish binding to OPG while preserving recognition of RANK. These efforts yielded several RANKL variants possessing substantially higher affinity for RANK compared to their wild-type (WT) counterpart. Using recombinant RANKL mutant proteins, we find those with increased affinity for RANK produce more robust signaling in osteoclast lineage cells and have greater osteoclastogenic potential. Our results are the first to document gain of function RANKL mutations. They indicate that the physiological RANKL/RANK interaction is not optimized for maximal signaling and function, perhaps reflecting the need to maintain receptor specificity within the tumor necrosis factor superfamily (TNFSF). Instead, we find, a biphasic relationship exists between RANKL/RANK affinity and osteoclastogenic capacity. In our panel of RANKL variants, this relationship is driven entirely by manipulation of the kinetic off-rate. Our structure-based and yeast surface display-derived insights into manipulating this critical signaling axis may aid in the design of novel anti-resorptive therapies as well as provide a paradigm for design of other receptor-specific TNF superfamily ligand variants.

3.2 Introduction

The tumor necrosis factor superfamily (TNFSF) is composed of 19 different type II transmembrane ligands whose involvement in homeostasis and disease is wide-ranging (*1*). Many of these cytokines target or are produced by cells of the immune system, and participate in development and function of hematopoietic lineage cells (*2*-*9*). TNFSF cytokines act by binding to and inducing signals downstream of TNF-receptor superfamily (TNFRSF) members (*10*, *11*). Additionally, there are several examples within TNFRSF of decoy receptors whose binding can modulate the activity of these cytokines (*12*). Due to their diverse roles in human disease, there are currently several therapies aimed at targeting these receptor/ligand pairs (*13*, *14*).

The control of skeletal mass is regulated in part by the bone resorptive osteoclast, whose differentiation and function rely on the TNFSF cytokine receptor activator of NF-kB ligand (RANKL) (*15*). By interacting with its receptor RANK, RANKL induces signaling to NF-kB, MAP kinases, and NFATc1 among others (*16*, *17*). These crucial signaling events are blocked by osteoprotegerin (OPG), a secreted decoy receptor that binds RANKL and prevents its interaction with RANK (*18*, *19*). RANKL-mediated signaling promoting osteoclast formation and function, in excess of the bone anabolic osteoblast, is associated with many diseases including osteoporosis, inflammatory osteolysis, and skeletal metastasis (*20*). Therefore, understanding the molecular events initiating signal transduction remains key to the development of future therapeutics targeting this signaling axis.

Most TNFSF members exist as homotrimers in solution (*21*), and it is largely assumed that the trimeric clustering of receptors is the primary initiating event for signal induction. We have recently developed a novel inhibitor of RANKL-induced osteoclast formation and function relying on the manipulation of receptor oligomerization (see Chapter 2). In the process of

engineering a single-chain RANKL capable of antagonizing RANK signaling, we generated a panel of increased affinity RANKL mutants that allowed our construct to out-compete wild-type (WT) RANKL binding. In the present exercise, we sought to understand the relationship between binding affinity and biological function downstream of receptor ligation. We utilized our panel of RANKL mutants with RANK affinities increased by 15- to 500-fold. Increased RANKL affinity for RANK displays a biphasic effect on osteoclastogenesis *in vitro*, reaching optimal activity at approximately 15-fold higher affinity than WT. These findings provide insights into the relationship between affinity and agonist function, raising the possibility that variants with even higher affinities may display antagonistic properties relevant for the design of future TNFSF-based therapies.

3.3 Materials and Methods:

Production of mammalian RANKL protein: Constructs used for transient transfection of RANKL (see Chapter 2) or OPG (*22*) were previously described. For mammalian protein production, suspension adapted 293-Freestyle cells (Life Technologies) were maintained in serum-free Freestyle 293 expression medium (Life Technologies) according to the manufacturer's protocol. Cells were seeded at a density of $0.5x10^6$/mL and transfected the next day using the cationic lipid polyethylenimine(*23*). Supernatant was harvested four and seven days after transfection, 0.22uM filtered and equilibrated by the addition of 1/10 volume 10X phosphate buffered saline (Gibco) and 10mM imidazole. The protein was captured on Ni-NTA Superflow resin (Qiagen) and washed using 10mM imidazole in PBS. Protein was eluted in steps from 25-500mM imidazole. Fractions containing purified protein were identified on coomassie stained SDS-PAGE. Positive fractions were pooled and concentrated using a disposable YM30 centricon (Millipore). All proteins were sterile filtered for use in cell culture.

Surface Plasmon Resonance (SPR): All SPR experiments were performed on a Biacore T-100 (GE Healthcare) using CM5 sensor chips and HBS-EP buffer. To confirm receptor recruitment using scRANKL variants, 4,000 RU of WT-scRANKL or variant scRANKL were coupled to individual lanes, leaving one reference flow cell uncoupled. Experiments to determine kinetic affinity constants of RANKL variants for RANK or OPG were performed and analyzed as previously described (*22*).

Generation of osteoclasts from primary bone marrow macrophages: Long bones of eight week-old mice were flushed and the marrow subjected to red blood cell lysis. The remainder of the whole marrow was cultured on petri dishes maintained at 37°C with 6% CO2 in alpha-mem containing 10% inactivated fetal bovine serum, 100 U/ml penicillin, 100 μg/ml streptomycin, (α-

10 medium) supplemented with 1:10 CMG (conditioned medium supernatant containing recombinant M-CSF)(*24*). Osteoclasts were differentiated in α-10 medium with 1:50 CMG and the relevant RANKL variant. Alternatively, osteoclasts were differentiated in the presence of 100ng/mL of mutant RANKL with varying concentrations of monomeric OPG.

Detection of osteoclast formation: Cells were fixed in 4% paraformaldehyde in PBS for 15 minutes and stained for the tartrate resistant acid phosphatase (TRAP) using a kit (Sigma. Quantitative assessment of TRAP activity was performed using the fluorescent phosphatase substrate ELF-97 (Molecular Probes). Fixed cells were incubated with 100uM ELF-97 in 90mM citrate buffer pH=4.8, 80mM sodium tartrate for 15 minutes at room temperature. The reaction was stopped by the addition of sodium hydroxide and fluorescence was visualized using the 345/530 excitation/emission filter on a Spectramax M2 plate reader.

Quantitative real-time PCR: To quantitate mRNA markers of osteoclast formation, RNA was isolated from cultured cells according to the manufacturer's protocol (Qiagen RNeasy miniprep kit). Equal amounts of RNA were used to perform reverse transcription (Bio-rad iScript) and quantitative real-time PCR was performed using Eva Sso fast qPCR Sybr green kit (Bio-rad) using a 7500 fast machine (ABI). Data was analyzed according to the delta-delta Ct method and normalized to a control containing no RANKL addition (labeled BMM). Primers used were as follows: CatK (Forward: 5'-ATGTGGGTGTTCAAGTTTCTGC-3', Reverse: 5'-CCACAAGATTCTGGGGACTC-3'), NFATc1 (Forward: 5'-CCCGTCACATTCTGGTCCAT-3', Reverse: 5'-CAAGTAACCGTGTAGCTGCACAA-3'), TRAP (Forward: 5'-CAGCTCCCTAGAAGATGGATTCAT-3', Reverse: 5'GTCAGGAGTGGGAGCCATATG), beta3 (Forward: 5'-TTCGACTACGGCCAGATGATT-3', Reverse: 5'-GGAGAAAGACAGGTCCATCAAGT-3').

Detection of Collagen Fragments from Culture Supernatant: Pre-osteoclasts were generated form primary bone marrow macrophages in the presence of wild-type RANKL and lifted with trypsin/EDTA. Equal numbers of pre-osteoclasts were plated on bovine bone slices in the presence of RANKL variants at 100ng/mL or doses for two additional days. The release of collagen peptides into the culture supernantant was detected by ELISA according to the manufacturer's protocol (IDS).

3.4 Results

Osteoclast formation in vitro *driven by RANKL mutants:* In Chapter 2 of this thesis, we reported the affinity maturation of RANKL for its signaling receptor RANK using yeast surface display. We estimated the affinities of several RANKL mutants using titration curves generated on the surface of RANKL-displaying yeast cells, showing a range from 15- to 500-fold increase relative to wild-type. Of note, these variants were identified on a background of two mutations that allowed for the increased production of our proteins of interest without affecting the affinity for RANK. These two mutations (C220S and I246E) were termed "solubility mutants," hence RANKL containing only these two mutations will be referred to as solubility-mutant WT RANKL (WT-SM). Importantly, both WT RANKL and WT-SM RANKL are equally capable of forming osteoclasts *in vitro* (Supplemental Figure 3.S1A).

First, we confirmed the affinities for RANK and OPG of each RANKL variant using surface plasmon resonance (Table 1). As described above (see Chapter 2, Figure 2.11), the single point mutant Q236H increased the affinity for RANK by approximately 15-fold while a quadruple mutation (K194E/Q236H/F269Y/H270 or "KQFH") increased the affinity by roughly 500-fold. Here we show that K194E alone also increases the affinity for RANK, though less than 2-fold (Table 1). The combination of K194E/Q236H ("KQ") increases binding to the receptor by 20-fold, and K194E/Q236H/F269Y ("KQF") by 50-fold. Thus, we have established a panel of RANKL variants ranging from a slight increase in affinity up to a 500-fold increase in binding to RANK. We also confirmed that all proteins containing the Q236H mutation have dramatically reduced binding to OPG. Interestingly, the single point mutant K194E decreases binding to OPG by approximately 4-fold.

Next, we sought to determine the osteoclastogenic capacity of our RANKL variants with increased affinity for RANK. To this end, we cultured bone marrow macrophages with M-CSF and increasing concentrations of RANKL, then stained for mature cells (Figure 3.1A). Osteoclastogenesis was quantitated using a TRAP activity assay to fit EC_{50} values of each RANKL variant. (Figure 3.1B,C). A single point mutation added to WT-SM, K194E-SM, is approximately twice as efficient at generating mature osteoclasts. Q236H-SM possessing a 15-fold increase in affinity for RANK, displayed the most robust increase in activity (compare average WT-SM EC50 = 9.78ng/mL versus Q236H-SM EC50 = 1.46 ng/mL). Interestingly, further increases in affinity up to 50-fold higher than WT RANKL did not more efficiently promote osteoclastogenic potency. Moreover, KQFH-SM RANKL, with a 500-fold increase in affinity for RANK, does not generate osteoclasts as efficiently as Q236H-SM, though is still outperforms WT-SM RANKL. In agreement with osteoclast formation as assessed by TRAP stain and TRAP activity, osteoclastogenic markers induced by RANKL variants show a similar affinity-dependent biphasic effect (Figure 3.1D,E). Hence, RANKL/RANK affinity exerts a biphasic effect of RANKL affinity for RANK on osteoclast formation *in vitro*, such that extremely high binding is not as optimal as an intermediate increase.

Resistance of RANKL mutants to exogenously added OPG. During the development of a single-chain RANKL inhibitor possessing altered RANK affinities, we sought to simultaneously decrease the capacity of the RANKL variants to bind the decoy receptor OPG. To that end, the mutations we OPG affinities of mutations we identified substantially decreased as assessed by yeast surface display and confirmed by SPR (Table 1). We next sought to determine if these mutants are more resistant to the addition of exogenous OPG in osteoclastogenic conditions *in vitro*. Interestingly, the solubility mutations which did not affect binding to RANK, exhibit a

roughly 10-fold decrease in OPG affinity (Supplemental Figure 3.S1B). In TRAP activity assays for osteoclast formation, we observed a functional consequence of this affinity change results in a 6-fold greater resistance to the addition of monomeric, cytokine-binding OPG fragment. Specifically, the OPG IC_{50} inhibiting WT RANKL-induced osteoclastogenesis is 141.6ng/mL, while the OPG IC_{50} inhibiting WT-SM RANKL is 824.3ng/mL. Representative TRAP stained images of bone marrow macrophages cultured in the presence of increasing amounts of OPG with a constant amount of each RANKL variant demonstrate that all mutations incorporating Q236H are completely resistant to the effects of OPG (Figure 3.2). RANKL K194E-induced osteoclastogenesis was inhibited slightly at the highest doses of the decoy receptor, though not sufficient to permit the assessment of an IC_{50} value given the range of OPG concentrations used. Therefore, despite the similar binding footprints of OPG and RANK on the cytokine RANKL, it is possible to impose opposite effects on cellular function using receptor selective mutations.

Altered signaling to key osteoclastogenic mediators is enhanced by high affinity RANKL variants. To determine whether the osteoclastogenic effects of progressively increasing RANKL affinity for RANK reflects altered signaling, we stimulated bone marrow macrophages with RANKL variants. We then assessed the phosphorylation of two crucial signaling events in osteoclast differentiation, namely phosphorylation of NF-kB and the MAP kinase, p38 (Figure 3.3A,B; Supplemental Figure 3.S1C). The signaling induced by Q236H-SM and KQFH-SM RANKL is more robust than that of WT-SM RANKL, and maximizes earlier. As with osteoclast formation, KQFH-SM RANKL is not as potent as Q236H-SM RANKL at phosphorylating these key osteoclastogenic molecules. Thus, like osteoclastogenesis, per se, the RANKL/RANK interaction optimizes signal transduction at intermediate, rather than extremely high, affinities.

Enhanced osteoclast function in vitro *with increased RANKL affinity variants*. RANKL not only promotes osteoclast formation, but also stimulates the resorption of bone by the mature cell. To determine if osteoclast function is also dictated by RANK/RANKL affinity, we cultured bone marrow macrophages on plastic in equal amounts of WT-RANKL for four days to generate pre-osteoclasts. We then lifted and plated an equal number of cells on bovine bone slices in low- or high-dose RANKL variants. After 24 hours, we assessed collagen fragment release into the media (Figure 3.4; Supplemental Figure 3.S1D). Despite normalized osteoclast numbers, Q236H-SM RANKL activates mature cells to resorb bone more than WT-SM RANKL, indicating that this variant not only enhances differentiation but also functional activity.

3.5 Discussion

From the discovery of lymphotoxin-beta and the TNF/TNFR1/TNFR2 ligand/receptor pairs almost thirty years ago, the role of TNFSF members in human disease has continued to grow. The expanding role of this protein family has also led to an increased interest in targeting cytokine or receptor to modulate autoimmunity, anti-tumoral activity, and bone mass. Current FDA-approved drugs comprise antibodies or receptor-Fc fragments that act by functionally removing the cytokine from the system (*13*). However, several TNFSF members bind more than one receptor (*1*), and there are circumstances in which the specific targeting of the actions of an individual receptor would be desirable. These and other aspects of this complex protein family may contribute in part to the disparities sometimes observed between pre-clinical and clinical trials focused at neutralizing cytokine.

A striking example is TNF-alpha, whose initial blockade in the pre-clinical multiple sclerosis model, experimental autoimmune encephalitis, was protective (*25*). However, some patients with multiple sclerosis treated with Lenercept (soluble-TNFR IgG-fusion protein) experienced an increased number of disease exacerbations with more severe neurological deficits (*26*). Additionally, pre-clinical studies using various models of sepsis yielded dramatically different results following TNF cytokine neutralization (*27*) depending in part on the model utilized. Indeed, clinical trials based on the endotoxin murine model of sepsis suggested that TNF blockade may be beneficial for survival, though the human experience did not propagate these results (*28*). Indeed, a protective effect of TNFR2 and detrimental effect of TNFR1 signaling has been implicated not only in septic shock (*29, 30*), but also in LPS-, RANKL-, or TNFa-mediated bone resorption (*31-33*). Thus, recent efforts using antibodies specifically

targeting TNFR1 may help provide impetus for the design of future therapeutics aimed at receptor specific targeting (*34*).

An alternative to antibody-mediated modulation of these signaling pathways is the development of receptor-selective cytokine mutants. Our present study elucidates the *in vitro* functional outcomes of modulating RANKL affinity for its signaling receptor RANK and its decoy receptor OPG. We show that initially, moderate increases in affinity for RANK lead to a substantial increase in function as measured by osteoclast formation, signaling, and bone resorption *in vitro*. However, further increases to very high affinity RANKL mutants produce less efficient downstream actions. To our knowledge, this is the first evidence that RANK signaling can be optimized by increasing affinity. However, there is not a linear relationship between affinity and functional outcome. This observation is, however, consistent with previous studies exploring the relationship between T-cell receptor (TCR): peptide-MHC affinity and biological events (*35-37*). Additionally, there is some evidence that there may be a non-linear relationship between TNF receptor binding and functional outcome (*38*), though the reported affinities do not represent single-site binding events, making interpretation of this data difficult.

Our results suggest that the use of forward-genetic approaches to identify novel mutations within the TNFSF can allow for the generation of receptor-selective, highly efficient agonists. The supposition that selective inhibition and/or activation of TNF receptors may be beneficial is supposed by the effect of TNFR2 agonism on the complications of experimental type I diabetes (*39, 40*). A scenario in which signal-transduction optimized, TNFR2 agonist that does not bind to and alter the TNFR1 pathway could provide a novel avenue for the treatment this or other autoimmune and cardiovascular diseases. This strategy could be applicable to several other TNFSF ligand/receptor pairs. Because of the non-linear relationship between RANKL/RANK

affinity and function, the development of receptor agonists within the protein family through non-biased, forward genetic approaches may necessitate the use of functional screens rather than affinity-based screens (*41*).

3.6 References

1. T. Hehlgans, K. Pfeffer, The intriguing biology of the tumour necrosis factor/tumour necrosis factor receptor superfamily: players, rules and the games, *Immunology* **115**, 1–20 (2005).

2. V. Upadhyay, Y.-X. Fu, Lymphotoxin signalling in immune homeostasis and the control of microorganisms, *Nat. Rev. Immunol.* **13**, 270–279 (2013).

3. L. Summers deLuca, J. L. Gommerman, Fine-tuning of dendritic cell biology by the TNF superfamily, *Nat. Rev. Immunol.* **12**, 339–351 (2012).

4. M. Croft, The role of TNF superfamily members in T-cell function and diseases, *Nat. Rev. Immunol.* **9**, 271–285 (2009).

5. N. L. Vujanovic, Role of TNF superfamily ligands in innate immunity, *Immunol. Res.* **50**, 159–174 (2011).

6. M. Zhu, Y.-X. Fu, The role of core TNF/LIGHT family members in lymph node homeostasis and remodeling, *Immunol. Rev.* **244**, 75–84 (2011).

7. F. Mackay, P. Schneider, Cracking the BAFF code, *Nat. Rev. Immunol.* **9**, 491–502 (2009).

8. G. Zauli, P. Secchiero, The role of the TRAIL/TRAIL receptors system in hematopoiesis and endothelial cell biology, *Cytokine Growth Factor Rev.* **17**, 245–257 (2006).

9. D. Jiang, Y. Chen, H. Schwarz, CD137 induces proliferation of murine hematopoietic progenitor cells and differentiation to macrophages, *The Journal of Immunology* **181**, 3923–3932 (2008).

10. L. Cabal-Hierro, P. S. Lazo, Signal transduction by tumor necrosis factor receptors, *Cell. Signal.* **24**, 1297–1305 (2012).

11. J. Li, Q. Yin, H. Wu, Structural basis of signal transduction in the TNF receptor superfamily, *Adv. Immunol.* **119**, 135–153 (2013).

12. J.-L. Bodmer, P. Schneider, J. Tschopp, The molecular architecture of the TNF superfamily, *Trends Biochem. Sci.* **27**, 19–26 (2002).

13. B. B. Aggarwal, S. C. Gupta, J. H. Kim, Historical perspectives on tumor necrosis factor and its superfamily: 25 years later, a golden journey, *Blood* **119**, 651–665 (2012).

14. M. Croft, C. A. Benedict, C. F. Ware, Clinical targeting of the TNF and TNFR superfamilies, *Nat Rev Drug Discov* **12**, 147–168 (2013).

15. D. V. Novack, S. L. Teitelbaum, The osteoclast: friend or foe? *Annu Rev Pathol* **3**, 457–484 (2008).

16. H. C. Blair, L. J. Robinson, M. Zaidi, Osteoclast signalling pathways, *Biochem. Biophys. Res. Commun.* **328**, 728–738 (2005).

17. M. Asagiri, H. Takayanagi, The molecular understanding of osteoclast differentiation, *Bone* **40**, 251–264 (2007).

18. W. S. Simonet *et al.*, Osteoprotegerin: a novel secreted protein involved in the regulation of bone density, *Cell* **89**, 309–319 (1997).

19. K. Yamaguchi *et al.*, Characterization of structural domains of human osteoclastogenesis

inhibitory factor, *J. Biol. Chem.* **273**, 5117–5123 (1998).

20. R. Hanada, T. Hanada, J. M. Penninger, Physiology and pathophysiology of the RANKL/RANK system, *Biol. Chem.* **391**, 1365–1370 (2010).

21. H. Wu, S. G. Hymowitz, in *Handbook of Cell Signaling*, R. Bradshaw, E. Dennis, Eds. (Academic Press, 2009), vol. 1, pp. 265–275.

22. C. A. Nelson, J. T. Warren, M. W.-H. Wang, S. L. Teitelbaum, D. H. Fremont, RANKL employs distinct binding modes to engage RANK and the osteoprotegerin decoy receptor, *Structure/Folding and Design* **20**, 1971–1982 (2012).

23. A. R. Aricescu, W. Lu, E. Y. Jones, A time- and cost-efficient system for high-level protein production in mammalian cells, *Acta Crystallogr. D Biol. Crystallogr.* **62**, 1243–1250 (2006).

24. S. Takeshita, K. Kaji, A. Kudo, Identification and characterization of the new osteoclast progenitor with macrophage phenotypes being able to differentiate into mature osteoclasts, *J Bone Miner Res* **15**, 1477–1488 (2000).

25. K. Selmaj, C. S. Raine, A. H. Cross, Anti-tumor necrosis factor therapy abrogates autoimmune demyelination, *Ann. Neurol.* **30**, 694–700 (1991).

26. TNF neutralization in MS: results of a randomized, placebo-controlled multicenter study. The Lenercept Multiple Sclerosis Study Group and The University of British Columbia MS/MRI Analysis Group, *Neurology* **53**, 457–465 (1999).

27. J. A. Lorente, J. C. Marshall, Neutralization of tumor necrosis factor in preclinical models of sepsis, *Shock* **24 Suppl 1**, 107–119 (2005).

28. D. Rittirsch, L. M. Hoesel, P. A. Ward, The disconnect between animal models of sepsis and human sepsis, *J. Leukoc. Biol.* **81**, 137–143 (2007).

29. D. R. Ebach, T. E. Riehl, W. F. Stenson, Opposing effects of tumor necrosis factor receptor 1 and 2 in sepsis due to cecal ligation and puncture, *Shock* **23**, 311–318 (2005).

30. J. J. Peschon *et al.*, TNF receptor-deficient mice reveal divergent roles for p55 and p75 in several models of inflammation, *J. Immunol.* **160**, 943–952 (1998).

31. Y. Abu-Amer, F. P. Ross, J. Edwards, S. L. Teitelbaum, Lipopolysaccharide-stimulated osteoclastogenesis is mediated by tumor necrosis factor via its P55 receptor, *J. Clin. Invest.* **100**, 1557–1565 (1997).

32. Y. Abu-Amer *et al.*, Tumor necrosis factor receptors types 1 and 2 differentially regulate osteoclastogenesis, *J. Biol. Chem.* **275**, 27307–27310 (2000).

33. K. Nagano *et al.*, The tumor necrosis factor type 2 receptor plays a protective role in tumor necrosis factor-α-induced bone resorption lacunae on mouse calvariae, *J. Bone Miner. Metab.* **29**, 671–681 (2011).

34. R. E. Kontermann *et al.*, A humanized tumor necrosis factor receptor 1 (TNFR1)-specific antagonistic antibody for selective inhibition of tumor necrosis factor (TNF) action, *J. Immunother.* **31**, 225–234 (2008).

35. A. S. Chervin *et al.*, The impact of TCR-binding properties and antigen presentation format on T cell responsiveness, *The Journal of Immunology* **183**, 1166–1178 (2009).

36. M. Irving *et al.*, Interplay between T cell receptor binding kinetics and the level of cognate

peptide presented by major histocompatibility complexes governs CD8+ T cell responsiveness, *Journal of Biological Chemistry* **287**, 23068–23078 (2012).

37. D. A. Schmid *et al.*, Evidence for a TCR affinity threshold delimiting maximal CD8 T cell function, *The Journal of Immunology* **184**, 4936–4946 (2010).

38. Y. Mukai *et al.*, Structure-function relationship of tumor necrosis factor (TNF) and its receptor interaction based on 3D structural analysis of a fully active TNFR1-selective TNF mutant, *J. Mol. Biol.* **385**, 1221–1229 (2009).

39. D. Faustman, M. Davis, TNF receptor 2 pathway: drug target for autoimmune diseases, *Nat Rev Drug Discov* **9**, 482–493 (2010).

40. L. Ban *et al.*, Selective death of autoreactive T cells in human diabetes by TNF or TNF receptor 2 agonism, *Proceedings of the National Academy of Sciences* **105**, 13644–13649 (2008).

41. A. M. Levin *et al.*, Exploiting a natural conformational switch to engineer an interleukin-2 'superkine', *Nature* **484**, 529–533 (2012).

3.7 Figure Legends

Table 3.1. Kinetic affinity parameters of RANKL mutants binding to monomeric RANK or OPG were determined using SPR. *Previously reported (see Chapter 2). Values represent the averages of three independent experiments.

Figure 3.1. Osteoclastogenic potential of RANKL variants. (A)The capacity of mutant RANKL proteins to generate osteoclasts from bone marrow macrophages was assessed by TRAP stain using increasing amounts of purified RANKL protein. (B) Titration curves of osteoclastogenesis were fit using a four-parameter dose-response curve. (C) EC_{50} values calculated from the curve fits in (B). Assessment of osteoclastogenic markers by real-time detection of NFATc1 (D) or β3 integrin (E) mRNA levels.

Figure 3.2. Ability of monomeric OPG to inhibit RANKL-induced osteoclast formation. Varying amounts of monomeric OPG were added to cultures containing 100ng/mL of each RANKL variants and osteoclasts were stained for TRAP.

Figure 3.3. Signaling downstream of RANKL variants. (A) Bone marrow macrophages were serum starved and stimulated with 100ng/mL WT-SM, Q236H-SM, or KQFH-SM RANKL. The phosphorylation of NF-kB and p38 were assessed by western blot. (B) Densitometry of western blots depicted in (A).

Figure 3.4. Activation of mature osteoclasts by RANKL variants. After several days in culture with WT RANKL, osteoclasts were plated in equal numbers on bovine bone slices and stimulated with WT-SM, Q236H-SM, or KQFH-SM. The release of collagen fragments (CTx) was measured after 24 hours.

Supplemental Figure 3.S1. Comparison of WT RANKL and WT-SM RANKL. Differences and similarities between the ability of WT RANKL and WT-SM RANKL to induce

osteoclastogenesis (A), resist the inhibitory activity of OPG (B), initiate RANK signaling (C) and resorb bone *in vitro* (D).

Table 3.1 Kinetic affinity parameters of RANKL variants binding to monomeric RANK and OPG

					RANK			OPG
RANKL:	194	236	269	270	K_D (uM)	k_{on} ($M^{-1}s^{-1}$)	k_{off} (s^{-1})	K_D (uM)
WT-SM*	K	Q	F	H	1.403	1.51×10^5	0.208	0.031
K194E-SM	E	Q	F	H	0.899	1.13×10^5	0.101	0.119
Q236H-SM*	K	H	F	H	0.081	3.00×10^5	0.023	1.095
KQ-SM	E	H	F	H	0.067	1.74×10^5	0.017	3.087
KQF-SM	E	H	Y	H	0.029	1.67×10^5	0.005	7.022
KQFH-SM*	E	H	Y	Y	0.003	3.07×10^5	0.001	N.D.

Figure 3.1

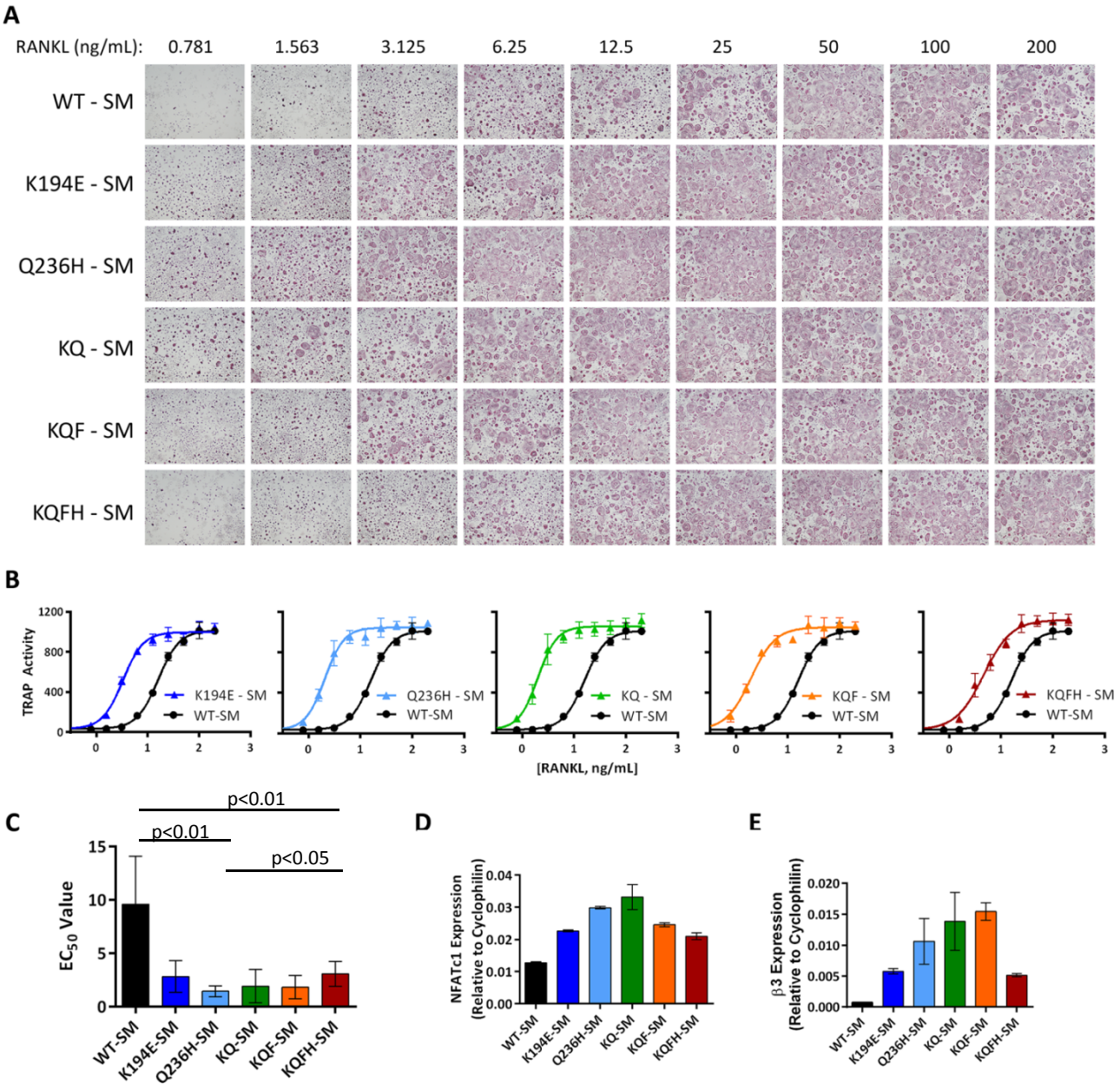
A
RANKL (ng/mL): 0.781 1.563 3.125 6.25 12.5 25 50 100 200
WT - SM
K194E - SM
Q236H - SM
KQ - SM
KQF - SM
KQFH - SM
B
TRAP Activity
K194E - SM
WT-SM
Q236H - SM
KQ - SM
KQF - SM
KQFH - SM
[RANKL, ng/mL]
C
p<0.01
p<0.01
p<0.05
EC50 Value
WT-SM
K194E-SM
Q236H-SM
KQ-SM
KQF-SM
KQFH-SM
D
NFATc1 Expression (Relative to Cyclophilin)
E
β3 Expression (Relative to Cyclophilin)

Figure 3.2

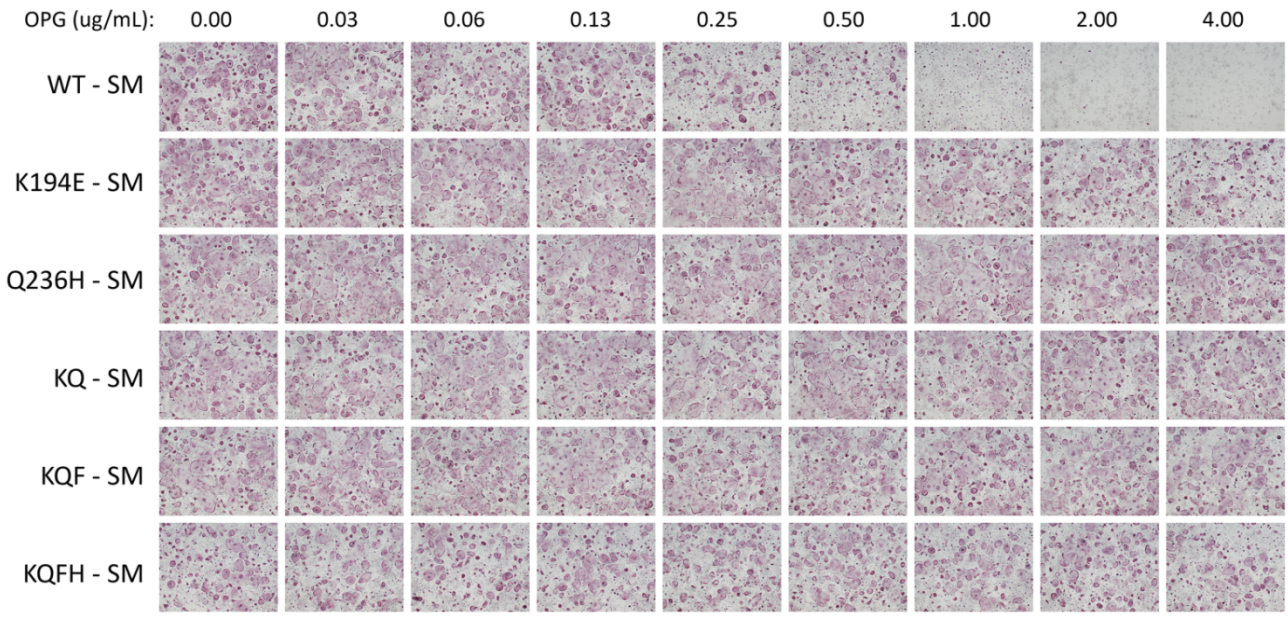
OPG (ug/mL):
0.00
0.03
0.06
0.13
0.25
0.50
1.00
2.00
4.00
WT - SM
K194E - SM
Q236H - SM
KQ - SM
KQF - SM
KQFH - SM

Figure 3.3

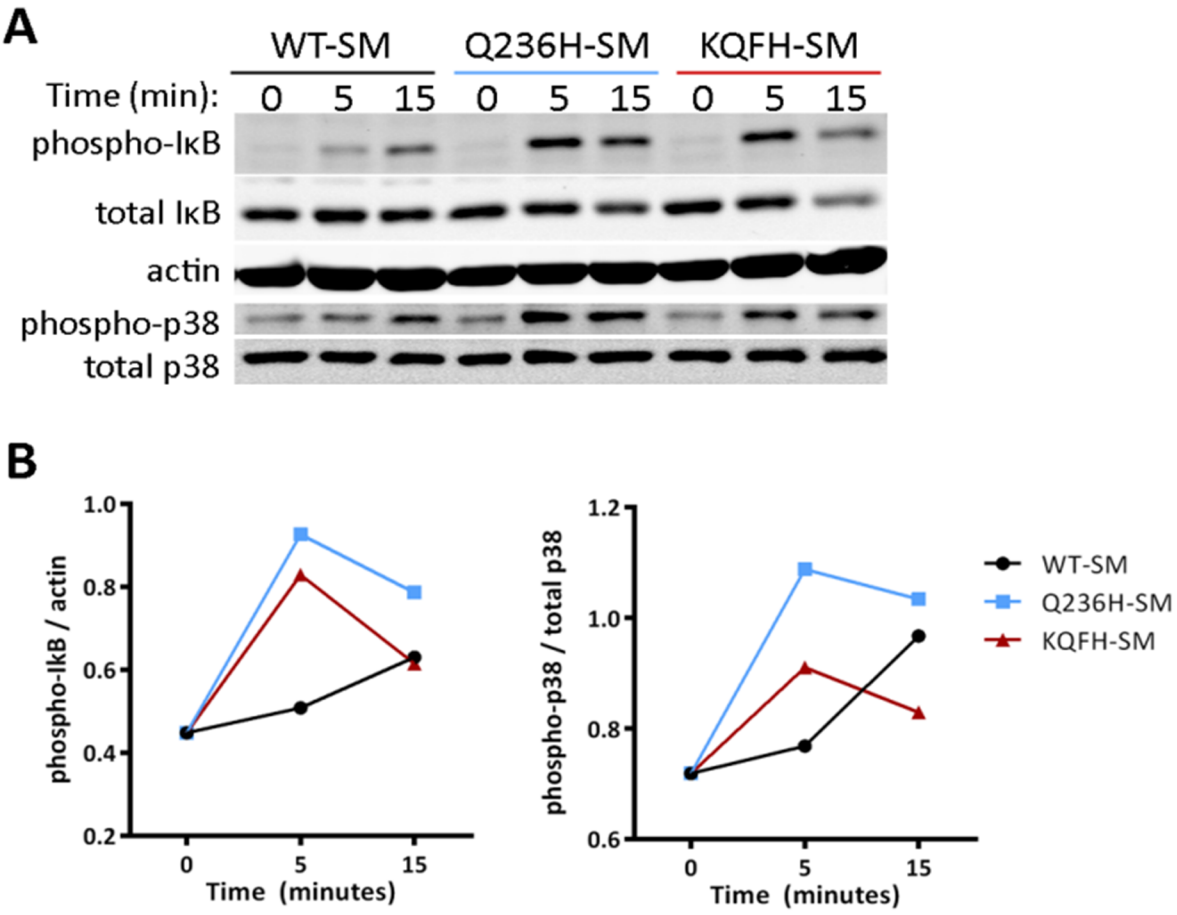
A
WT-SM
Q236H-SM
KQFH-SM
Time (min):
0 5 15 0 5 15 0 5 15
phospho-IκB
total IκB
actin
phospho-p38
total p38
B
phospho-IkB / actin
1.0
0.8
0.6
0.4
0.2
0 5 15
Time (minutes)
phospho-p38 / total p38
1.2
1.0
0.8
0.6
0 5 15
Time (minutes)
WT-SM
Q236H-SM
KQFH-SM

Figure 3.4

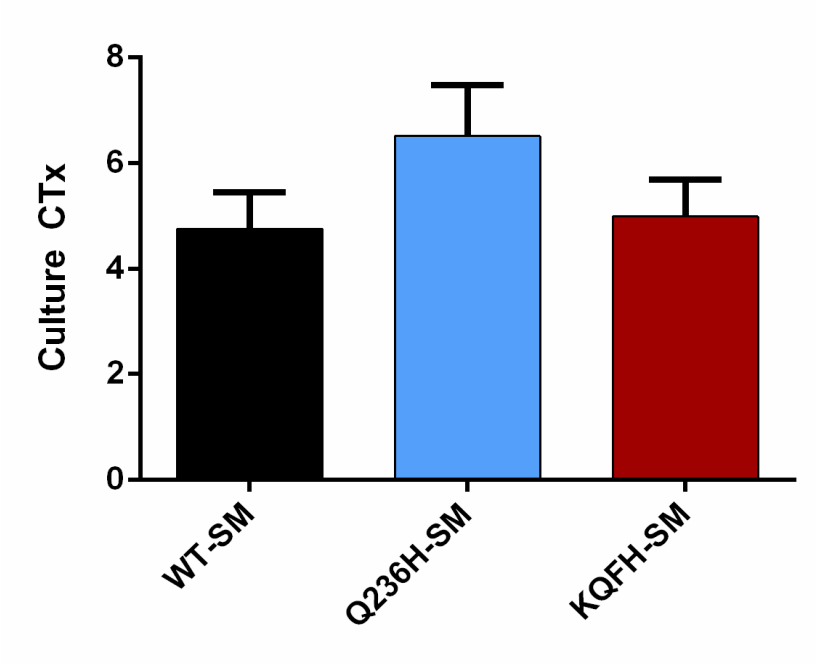

Supplemental Figure 3.S1

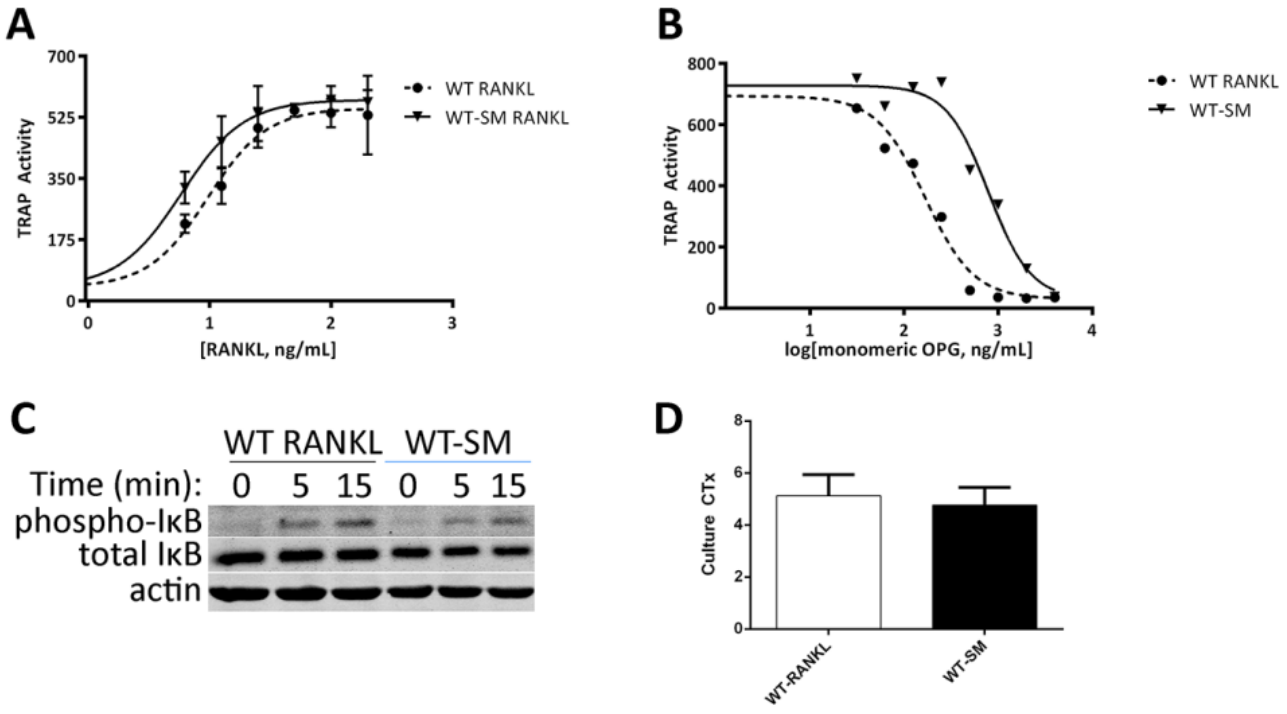

Chapter 4

Conclusions and Future Directions

4.1 Conclusions

Generation of single-chain RANKL: The primary aim of this thesis was to provide evidence for the receptor oligomeric state of RANK receptor necessary and sufficient to induce pro-osteoclastogenic signals. A secondary goal was to use this information to develop a novel strategy for RANK inhibition, which may be broadly applicable to TNF receptor superfamily inhibition. Despite the assumption that trimeric TNFSF ligands act by clustering three receptors to initiate signal transduction, evidence suggesting the importance of ligand-independent receptor association (*1*-*3*), the formation of signaling-competent receptor dimers (*4*), or higher-order clustering (*5*-*8*) has challenged this simple model. Within RANK signaling, reports have suggested both ligand-independent receptor association (*9*) and signaling through dimeric receptors (*10*), though these studies are accompanied by the major caveats inherent with receptor overexpression or the use of artificial chimeric constructs.

To circumvent the need for overexpressed or chimeric receptor, we approached the question of receptor recruitment using manipulation of the cytokine itself. Because the N- and C-termini of RANKL are located in close physical proximity (*11*), we were able to covalently link each monomer together using glycine/serine repeats. We demonstrated that this single-chain version of RANKL (scRANKL) was equally capable of generating osteoclasts and had the predicted molecular weight of a trimer without evidence of monomeric species on reducing gel.

Probing the signaling-competent receptor oligomeric state of RANK: With this tool in hand, we generated single- and double-blocked versions of scRANKL capable of only recruiting two or one RANK receptors, respectively. To this end, we identified mutations in RANKL that prevent RANK binding. Initial studies using monomeric RANK to assess decreased binding indicated that the RANKL variant R222Q may be an appropriate mutation to use for this purpose. However, binding studies using an Fc-tagged version of RANK increased the sensitivity of the assay, allowing us to elucidate that, although the affinity of R222Q was substantially lower than WT RANKL, its binding to RANK was not

absent. Therefore, we used the co-crystal structure of RANK/RANKL to design loop insertion mutants in the hopes that these variants would prevent receptor recruitment. Most promising was the CD loop of RANKL, which contains an i+3 beta turn making it possible that amino acids inserted proximal to this ordered structural region would yield a RANK null-binding version. Indeed, all mutations with no detectable binding to RANK-Fc contained various insertions in the CD-loop. Interestingly, the analogous loop in human RANKL (termed the DE loop) is the target of the RANKL-neutralizing therapeutic monoclonal antibody Denosumab (*12*). These findings have important implications for the general applicability of this single-chain approach to studying receptor oligomerization, as steric hinderance of receptor docking to generate a complete null-binder rather than to rely on individual point mutations.

Having identified a RANK receptor blocking mutant, we generated single- and double-block scRANKL and assessed osteoclastogenesis. Formation of mature cells by each scRANKL variant demonstrate that single-block, with two available receptor recruitment sites, is capable of generating osteoclasts while double-block is not. This suggests that the occupancy of RANKL by three RANK receptors is not absolutely required to induce osteoclastogenic signals, while recruitment of at least two receptors is necessary. The number of osteoclasts generated by single-block scRANKL was never as high as that generated by WT scRANKL, and the EC_{50} value of single-block was increased 20-fold indicating that this state of receptor oligomerization is sub-optimal. Because we had generated a version of scRANKL capable of binding receptor yet unable to induce osteoclastogenic signals, we asked if this protein could act as an inhibitor of WT RANKL-induced osteoclastogenesis. Its inability to do so likely reflects the loss of avidity relative to WT RANKL, prompting us to utilize yeast surface display to identify RANKL mutants with increased affinity for RANK. We demonstrated that the use of progressively decreasing amounts of monomeric RANK in combination with OPG competition could facilitate the isolation of variants with a range of affinities for RANK, including one RANKL mutation with a 500-fold increase in affinity driven largely by prolonged off-rate. Importantly, these mutations do not meaningfully recognize the decoy receptor OPG.

The inclusion of medium- or high-affinity variants into the intact binding sites in scRANKL allowed us to observe that single-block RANKL with an increase in affinity at these two receptor recruitment sites generates fewer osteoclasts. Indeed, the ability of single-block scRANKL to generate osteoclasts may be facilitated by the rapid off rate at the two receptor binding sites. This may allow for the recruitment of additional RANK receptor, ultimately leading to higher order clustering. Our observation that increasing the time required for single-block scRANKL variants to dissociate diminishes osteoclastogenesis supports this model. Finally, single-block RANKL with high affinity at the intact sites is an effective inhibitor of RANKL-mediated osteoclast formation.

One important caveat to these experiments is the method used for protein purification and the possibility of ligand heterogeneity. Initial studies using CDins mutant RANKL purified from bacteria demonstrated no detectable binding to RANK-Fc, yet considerable phosphorylation of NF-κB. We found a lack of responsiveness to CDins RANKL-induced signals when using TLR4-KO macrophages, indicating that this phosphorylation was the result of the exquisite sensitivity of macrophages to even minute amounts of LPS carried over during purification. Therefore, we developed a method for producing WT RANKL and scRANKL proteins secreted from mammalian cells into serum-free media. Purification was performed with an attempt to remain LPS-free, necessitating avoidance of a final size exclusion chromatography step. However, when we examined the size exclusion profiles of our scRANKL protein, we observed a small, but significant, higher molecular weight species. This could be explained by two possibilities. First, the solubility mutant version of RANKL contains two predicted glycosylation sites per monomer and migrates as two bands on reducing gel when purified from mammalian cells, but not when purified from bacteria. By two-dimensional gel electrophoresis, the one predicted glycosylation site of murine TNFα was shown to add as much as 10 – 20 kDa of sugar per 17 kDa monomer (*13*) when secreted from stimulated macrophages. Therefore, given the two available glycosylation sites in RANKL, it seems possible that a substantial, though potentially heterogeneous, amount of carbohydrate may be present on scRANKL.

The second possibility is that, by the use of 12 amino acid long linkers between each scRANKL monomer, scRANKL may unfold and re-fold as two or more associated proteins. One argument against this scenario is the RANKL monomer-trimer molar association constant of $6.5 \times 10^{20}\ M^{-2}$, indicating that once a trimer has formed, it is highly unlikely to dissociate from this form (*14*). Therefore, generation of an integrated oligomeric scRANKL species would necessitate the formation of higher order variants during initial protein translation and folding. The relevance of this possibility is to our findings that single-block scRANKL is capable of generating osteoclasts, which is in opposition to the classic model of trimeric receptor clustering as initiating signal transduction. When we performed size exclusion chromatography to isolate a conservatively monomeric species of scRANKL, we still observed osteoclast formation, albeit at levels lower than unsized protein (not shown). Here, scRANKL would have had to unfold post-purification and refold into a dimeric species to allow for the possibility that the higher molecular weight version of scRANKL is a "domain-swapped" variant. Again, given the molar association constant, this scenario seems highly unlikely though cannot be absolutely excluded at this time. Finally, this potential dimeric species of single-block scRANKL would have to consistently fold in such a way that the 120° receptor binding groove geometry was maintained with proper binding site orientation, as it has been shown that the integrity of this groove is important for receptor recruitment (*15*). It is this author's view that our conservative collection of the lowest molecular weight portion of scRANKL during size exclusion chromatography completely removed the glycosylated version of the protein, which may have affected either its binding properties or its solubility in solution throughout the course of *in vitro* experiments thus explaining the reduced osteoclastogenesis when using sized versus non-sized protein.

4.2 Future directions

Optimization of scRANKL protein: To resolve the issue of observed higher molecular weight species of scRANKL, it may be possible to treat scRANKL proteins with inhibitors of glycosylation during transfection and protein production and test the ability of this non-glycosylated version of single-block scRANKL to present as a mono-dispersed fraction on a size exclusion column and/or generate osteoclasts. It may also be possible that there exists an ideal linker length which prevents any potential folded version of scRANKL other than the monomeric version, yet allows for adequate protein expression levels. Lastly, previous reports of single-chain TNF utilized molecular dynamics simulations to provide guidance for optimizing linker length (*4*). As flexible loops that are either too short or too long have been suggested to play a role in the domain swapping of certain proteins (*16*), it may be important to more rigorously determine what version of scRANKL would allow enough flexiblility for proper folding without the possibility of generating oligomerized aggregates.

Clinically Relevant Models of RANKL-driven bone loss: Regardless of whether or not this important issue can be resolved, it remains that single-block scRANKL with high affinity at the intact binding sites is an effective inhibitor of RANKL-mediated osteoclast formation both *in vitro* and *in vivo*. We utilized a rapid bone loss model based on intraperitoneal injection of WT RANKL (*17*) which has limited clinical relevance. It would be interesting to test the ability of single-block, $RANK^{high}$ scRANKL to protect against ovariectomy-induced bone loss, a model used extensively in our laboratory (*18-20*). Additionally, RANKL has been implicated in not only the growth of mammary cancer (*21-24*) but also in the migration (*25-27*) and osteolysis of metastatic breast cancer (*28*). Current evidence suggests that the inhibition of RANKL-mediated signaling may be beneficial at treating breast cancer skeletal metastases (*29*) and it would be interesting to see if our novel scRANKL inhibitor can act in a similar, or perhaps more effective, manner. Indeed, the anti-RANKL monoclonal antibody Denosumab was recently approved for the treatment of breast cancer bone metastases (*30*). Given that the *in vitro* IC_{50} values of

our novel construct are almost 10-fold lower than that of Denosumab (scRANKL inhibitor IC50 = 0.2 nM versus denomsumab IC50 = 1.64nM), it may be possible to achieve therapeutic benefit with substantially lower levels of inhibitor. The further evaluation of single-block, $RANK^{high}$ as an inhibitor of RANKL-mediated pathology *in vivo* will necessitate the determination of phamacodynamic and pharmacokinetic parameters of this protein. Lastly, as all residues involved in generating the blocking and high affinity mutations in murine RANKL are conserved in human RANKL, it would be interesting to generate the human version of this novel inhibitor and test it in the ovariectomized cynomologous monkey model, an important non-clinical animal model for RANKL inhibition (*31*, *32*).

Inhibition of other TNF receptors using the single-chain approach: RANKL is a member of the TNF superfamily and binds to two different receptors (RANK and OPG) with divergent biological effects. Our approach using a combination of blocking and high affinity mutations for RANK together with absent OPG binding, has allowed us to generate an efficient and selective RANK inhibitor. Several other TNFSF members display receptor promiscuity, including TNFα, which is capable of binding TNFR1 and TNFR2. TNFα is involved in a wide variety of pathologies, included rheumatoid arthritis, sepsis, Crohn's disease (*33*). This has led to the development of several TNF antagonists, including an anti-TNF monoclonal antibody (Infliximab, ex) and soluble receptor fragment (Etanercept) (*34*). These therapies, which result in removal of all cytokine-induced signals, are associated with significant morbidity including increased risk for infectious disease and malignancy (*35-37*). This has prompted interest in the selective antagonism of TNFR1 over TNFR2 (*38-41*). Because the binding modes of RANKL with RANK and OPG are very similar to the inferred or reported binding modes of TNFα with TNFR1 and R2 (*42-44*), it seems likely that a similar approach combining steric blockade of receptor docking with forward genetic screens to identify high affinity mutations for TNFR1 that do not recognize TNFR2 may succeed. It is even possible to begin this yeast surface display undertaking with one of several previously described mutations that differentially affect TNFR1 and TNFR2 binding (*45, 46*).

One important caveat to any future use of this single-chain strategy is the necessity for any blocking and high affinity mutations to be located on the same side of the binding groove. Regardless of the orientation of folding (right- or left-handed), having these mutations occupy the same side of the cleft contributed by each monomer ensures that each interface can be individually mutated (Figure 4.1). Our yeast surface display efforts identified four point mutations that increased the affinity for RANK while decreasing the affinity for OPG, three of which are on the same side of the interface as the receptor blocking CD-loop (K194E, F269Y, and H270Y). Fortunately, the fourth mutation, which was not on this side, could equally participate in the formation of a blocking or a high affinity interaction with RANK. For human TNFα, a commonly used TNFR1-selective mutation is R32W/S86T. However, this double point-mutant straddles both sides of the binding groove, making it an unattractive candidate to initiate a yeast surface screen. Alternatively, Y87Q dramatically reduces the affinity for both receptors. Therefore, it is intriguing to speculate that S86T/Y87Q may be an ideal TNFR1 receptor blocking mutation that also decreased TNFR2 affinity, while S86T alone might be a useful mutation to begin a search for TNFα variants with selective increased TNFR1 affinity.

Biphasic effect of RANKL/RANK affinity on osteoclast formation and function: Having identified RANKL mutations with a range of affinities for RANK, but decreased binding to OPG, we tested the ability of each variant to form osteoclasts *in vitro*. We find that increasing the affinity for RANK by 15 – 50 fold leads to optimal activation of RANK as assessed by phosphorylation of downstream signals and EC_{50} values of osteoclast formation. Interestingly, a further increase to 500-fold greater than WT RANKL reverses this trend. Because the differences in affinity between these variants is reflected primarily in an longer off-rate, we can conclude that optimal RANK signaling necessitates not only RANKL association but the ability to dissociate. This phenomenon has been observed in other signaling systems, most notably in T-cell receptor (TCR) signaling (*47-49*). The observation that T-cell triggering occurs in an optimized peptide:MHC affinity window largely guided by variations in off-rate prompted the postulation of a "serial engagement" model (*50*). In this scenario, the relatively rapid

dissociation of TCR from peptide:MHC facilitates the sequential and monovalent triggering of many T-cell receptors. As higher order clustering has been implicated for the signal transduction of other TNFSF members (*5-8*), we posit that RANK signaling is facilitated by the rapid off-rate of WT RANKL, which acts to cluster individual receptors via serial engagement.

High Affinity RANKL Variants: These findings may not only inform our understanding of RANK receptor signaling, they may also serve as the basis for developing novel inhibitors of this pathway. Although the largest increase in affinity for RANK that we identified from yeast surface display was 500-fold, this unbiased form of protein engineering has generated variants with as much as 40,000-fold (*51*) or even 1 million-fold (*52*) higher affinities in other contexts. What might the functional consequences be of similarly affinity-matured variations of RANKL? There is precedent for supraphysiologic binding of TCR to peptide:MHC losing agonist effect (*47*). Additionally, a high-affinity IL-4 variant was converted to an antagonist by substitution of a single amino acid, indicating a decoupling between receptor binding and efficacy (*53*, *54*). The relevance of this finding to TNFα is unclear, as variants have been described with increased affinity leading to disparate effects on *in vitro* function depending on where the mutations clustered on the cytokine (*43*).

Currently, experiments are underway to determine the effect of optimal receptor signaling on osteoclast function *in vivo* using the intraperitoneal IP RANKL injection model described above. Demonstration of enhanced RANKL mediated signaling *in vivo* may provide rational for treating patients with osteoclast-poor osteopetrosis who have mutations in the gene encoding RANKL (*55*). Alternatively, it would be interesting to search for mutations in these conserved, high affinity residues of RANKL in single-nucleotide polymorphism studies to determine whether genetic differences in bone mass and risk for osteoporosis may be linked to mutations that increase receptor binding to an optimized level. Lastly, it would be interesting to explore the mechanism by which WT, intermediate affinity, and high affinity RANKL variants lead to different efficacies. Is RANK receptor internalization necessary for downstream

signaling, and is this event optimal with 10- to 50-fold increases in affinity? Are signaling events beyond receptor proximal targets altered in the context of altered binding kinetics? These and other ongoing studies will add to our knowledge of how signals are initiating upon RANKL ligation of its receptor RANK.

4.3 References:

1. G. Papoff *et al.*, Identification and characterization of a ligand-independent oligomerization domain in the extracellular region of the CD95 death receptor, *J. Biol. Chem.* **274**, 38241–38250 (1999).

2. F. K. Chan *et al.*, A domain in TNF receptors that mediates ligand-independent receptor assembly and signaling, *Science* **288**, 2351–2354 (2000).

3. C. R. Smulski *et al.*, Cysteine-rich domain 1 of CD40 mediates receptor self-assembly, *Journal of Biological Chemistry* **288**, 10914–10922 (2013).

4. V. Boschert *et al.*, Single chain TNF derivatives with individually mutated receptor binding sites reveal differential stoichiometry of ligand receptor complex formation for TNFR1 and TNFR2, *Cell. Signal.* **22**, 1088–1096 (2010).

5. N. Holler *et al.*, Two adjacent trimeric Fas ligands are required for Fas signaling and formation of a death-inducing signaling complex, *Mol. Cell. Biol.* **23**, 1428–1440 (2003).

6. R. M. Siegel *et al.*, SPOTS: signaling protein oligomeric transduction structures are early mediators of death receptor-induced apoptosis at the plasma membrane, *J. Cell Biol.* **167**, 735–744 (2004).

7. H. Wu, Higher-order assemblies in a new paradigm of signal transduction, *Cell* **153**, 287–292 (2013).

8. F. Henkler *et al.*, The extracellular domains of FasL and Fas are sufficient for the formation of supramolecular FasL-Fas clusters of high stability, *J. Cell Biol.* **168**, 1087–1098 (2005).

9. K. Kanazawa, A. Kudo, Self-assembled RANK induces osteoclastogenesis ligand-independently, *J*

Bone Miner Res **20**, 2053–2060 (2005).

10. K. Iwamoto *et al.*, Dimer formation of receptor activator of nuclear factor kappaB induces incomplete osteoclast formation, *Biochem. Biophys. Res. Commun.* **325**, 229–234 (2004).

11. J. Lam, C. A. Nelson, F. P. Ross, S. L. Teitelbaum, D. H. Fremont, Crystal structure of the TRANCE/RANKL cytokine reveals determinants of receptor-ligand specificity, *J. Clin. Invest.* **108**, 971–979 (2001).

12. P. J. Kostenuik *et al.*, Denosumab, a fully human monoclonal antibody to RANKL, inhibits bone resorption and increases BMD in knock-in mice that express chimeric (murine/human) RANKL, *J Bone Miner Res* **24**, 182–195 (2009).

13. A. D. Watts, N. H. Hunt, B. D. Hambly, G. Chaudhri, Separation of tumor necrosis factor alpha isoforms by two-dimensional polyacrylamide gel electrophoresis, *Electrophoresis* **18**, 1086–1091 (1997).

14. D. Willard *et al.*, Expression, purification, and characterization of the human receptor activator of NF-kappaB ligand (RANKL) extracellular domain, *Protein Expr. Purif.* **20**, 48–57 (2000).

15. E. Douni *et al.*, A RANKL G278R mutation causing osteopetrosis identifies a functional amino acid essential for trimer assembly in RANKL and TNF, *Hum. Mol. Genet.* **21**, 784–798 (2012).

16. F. Rousseau, J. Schymkowitz, L. S. Itzhaki, in *Protein Dimerization and Oligomerization in Biology*, J. Matthews, Ed. (Landes Bioscience, 2012), vol. 747, pp. 137–152.

17. Y. Tomimori *et al.*, Evaluation of pharmaceuticals with a novel 50-hour animal model of bone loss, *J Bone Miner Res* **24**, 1194–1205 (2009).

18. C. J. DeSelm, W. Zou, S. L. Teitelbaum, Halofuginone prevents estrogen-deficient osteoporosis in mice, *J. Cell. Biochem.* **113**, 3086–3092 (2012).

19. C. J. DeSelm *et al.*, IL-17 mediates estrogen-deficient osteoporosis in an Act1-dependent manner, *J. Cell. Biochem.* **113**, 2895–2902 (2012).

20. W. Zou *et al.*, Talin1 and Rap1 are critical for osteoclast function, *Mol. Cell. Biol.* **33**, 830–844 (2013).

21. R. Fernandez-Valdivia *et al.*, Developmental Biology, *Developmental Biology* **328**, 127–139 (2009).

22. E. Gonzalez-Suarez *et al.*, RANK ligand mediates progestin-induced mammary epithelial proliferation and carcinogenesis, *Nature* **468**, 103–107 (2010).

23. D. Schramek *et al.*, Osteoclast differentiation factor RANKL controls development of progestin-driven mammary cancer, *Nature* **468**, 98–102 (2010).

24. H.-R. Park *et al.*, Expression of osteoprotegerin and RANK ligand in breast cancer bone metastasis, *J. Korean Med. Sci.* **18**, 541–546 (2003).

25. M. Palafox *et al.*, RANK Induces Epithelial-Mesenchymal Transition and Stemness in Human Mammary Epithelial Cells and Promotes Tumorigenesis and Metastasis, *Cancer Res* **72**, 2879–2888 (2012).

26. D. H. Jones *et al.*, Regulation of cancer cell migration and bone metastasis by RANKL, *Nature* **440**, 692–696 (2006).

27. Z.-N. Tang, F. Zhang, P. Tang, X.-W. Qi, J. Jiang, RANKL-induced migration of MDA-MB-231 human breast cancer cells via Src and MAPK activation, *Oncol Rep* **26**, 1243–1250 (2011).

28. N. Rucci *et al.*, Receptor activator of NF-kappaB ligand enhances breast cancer-induced osteolytic lesions through upregulation of extracellular matrix metalloproteinase inducer/CD147, *Cancer Res* **70**, 6150–6160 (2010).

29. J. R. Canon *et al.*, Inhibition of RANKL blocks skeletal tumor progression and improves survival in a mouse model of breast cancer bone metastasis, *Clin Exp Metastasis* **25**, 119–129 (2008).

30. A. Casas, A. Llombart, M. Martín, Denosumab for the treatment of bone metastases in advanced breast cancer, *Breast* **22**, 585–592 (2013).

31. M. S. Ominsky *et al.*, Denosumab, a fully human RANKL antibody, reduced bone turnover markers and increased trabecular and cortical bone mass, density, and strength in ovariectomized cynomolgus monkeys, *Bone* **49**, 162–173 (2011).

32. P. J. Kostenuik *et al.*, Decreased bone remodeling and porosity are associated with improved bone strength in ovariectomized cynomolgus monkeys treated with denosumab, a fully human RANKL antibody, *Bone* **49**, 151–161 (2011).

33. M. Croft *et al.*, TNF superfamily in inflammatory disease: translating basic insights, *Trends Immunol.* **33**, 144–152 (2012).

34. B. B. Aggarwal, S. C. Gupta, J. H. Kim, Historical perspectives on tumor necrosis factor and its superfamily: 25 years later, a golden journey, *Blood* **119**, 651–665 (2012).

35. T. Bongartz *et al.*, Anti-TNF antibody therapy in rheumatoid arthritis and the risk of serious infections and malignancies: systematic review and meta-analysis of rare harmful effects in randomized controlled trials, *JAMA* **295**, 2275–2285 (2006).

36. E. C. Keystone, Does anti-tumor necrosis factor-α therapy affect risk of serious infection and cancer in patients with rheumatoid arthritis?: a review of longterm data, *J. Rheumatol.* **38**, 1552–1562 (2011).

37. M. Crawford, J. R. Curtis, Tumor necrosis factor inhibitors and infection complications, *Curr Rheumatol Rep* **10**, 383–389 (2008).

38. F. Van Hauwermeiren, R. E. Vandenbroucke, C. Libert, Treatment of TNF mediated diseases by selective inhibition of soluble TNF or TNFR1, *Cytokine Growth Factor Rev.* **22**, 311–319 (2011).

39. R. E. Kontermann *et al.*, A humanized tumor necrosis factor receptor 1 (TNFR1)-specific antagonistic antibody for selective inhibition of tumor necrosis factor (TNF) action, *J. Immunother.* **31**, 225–234 (2008).

40. K. A. Zettlitz *et al.*, ATROSAB, a humanized antagonistic anti-tumor necrosis factor receptor one-specific antibody, *MAbs* **2**, 639–647 (2010).

41. F. Richter *et al.*, Antagonistic TNF receptor one-specific antibody (ATROSAB): receptor binding and in vitro bioactivity, *PLoS ONE* **8**, e72156 (2013).

42. Y. Mukai *et al.*, Solution of the structure of the TNF-TNFR2 complex, *Sci Signal* **3**, ra83 (2010).

43. Y. Mukai *et al.*, Structure-function relationship of tumor necrosis factor (TNF) and its receptor interaction based on 3D structural analysis of a fully active TNFR1-selective TNF mutant, *J. Mol. Biol.* **385**, 1221–1229 (2009).

44. H. Wu, S. G. Hymowitz, in *Handbook of Cell Signaling*, R. Bradshaw, E. Dennis, Eds. (Academic Press, 2009), vol. 1, pp. 265–275.

45. H. Loetscher, D. Stueber, D. Banner, F. Mackay, W. Lesslauer, Human tumor necrosis factor alpha (TNF alpha) mutants with exclusive specificity for the 55-kDa or 75-kDa TNF receptors, *J. Biol. Chem.* **268**, 26350–26357 (1993).

46. T. Nomura *et al.*, Novel protein engineering strategy for creating highly receptor-selective mutant TNFs, *Biochem. Biophys. Res. Commun.* **388**, 667–671 (2009).

47. D. A. Schmid *et al.*, Evidence for a TCR affinity threshold delimiting maximal CD8 T cell function,

The Journal of Immunology **184**, 4936–4946 (2010).

48. M. Irving *et al.*, Interplay between T cell receptor binding kinetics and the level of cognate peptide presented by major histocompatibility complexes governs CD8+ T cell responsiveness, *Journal of Biological Chemistry* **287**, 23068–23078 (2012).

49. A. S. Chervin, D. H. Aggen, J. M. Raseman, D. M. Kranz, Engineering higher affinity T cell receptors using a T cell display system, *J. Immunol. Methods* **339**, 175–184 (2008).

50. S. Valitutti, S. Müller, M. Cella, E. Padovan, A. Lanzavecchia, Serial triggering of many T-cell receptors by a few peptide-MHC complexes, *Nature* **375**, 148–151 (1995).

51. K. Weiskopf *et al.*, Engineered SIRPα variants as immunotherapeutic adjuvants to anticancer antibodies, *Science* **341**, 88–91 (2013).

52. R. A. Buonpane *et al.*, Neutralization of staphylococcal enterotoxin B by soluble, high-affinity receptor antagonists, *Nat. Med.* **13**, 725–729 (2007).

53. N. Kruse, H. P. Tony, W. Sebald, Conversion of human interleukin-4 into a high affinity antagonist by a single amino acid replacement, *EMBO J.* **11**, 3237–3244 (1992).

54. G. Aversa *et al.*, An interleukin 4 (IL-4) mutant protein inhibits both IL-4 or IL-13-induced human immunoglobulin G4 (IgG4) and IgE synthesis and B cell proliferation: support for a common component shared by IL-4 and IL-13 receptors, *J. Exp. Med.* **178**, 2213–2218 (1993).

55. C. Sobacchi *et al.*, Osteoclast-poor human osteopetrosis due to mutations in the gene encoding RANKL, *Nat. Genet.* **39**, 960–962 (2007).

4.4 Figure Legend

Figure 4.1. Receptor interfaces in scRANKL. (A) Each RANKL monomer is labeled "A", "B", or "C" and is shown connected by the Gly/Ser linkers (orange lines). The interfaces capable of accepting RANK receptor have been arbitrarily named "X", "Y", and "Z". The RANKL AA', CD, and GH loops contribute to the side of the interface termed "L", and the DE and EF loops contribute to the side termed "R". Depicted are two possible conformations of scRANKL, one that has folded with a right-handed orientation and one with a left-handed orientation. The possible interfaces with corresponding contributions from each monomer are indicated below the diagram. (B) Single-block scRANKL provides one example of how individually mutated receptors can yield identical binding interfaces regardless of the right- or left-handed nature of scRANKL folding. *Note that CDins from the "L" side of an interface combined with either a WT or Q236H ("Q") contributed from the "R" side comprise a receptor blocking interface, while KFH from the "L" side combined with Q from the R side form a high affinity interface. (C) Single-block, $RANK^{high}$ scRANKL interfaces as in (B).

Figure 4.1

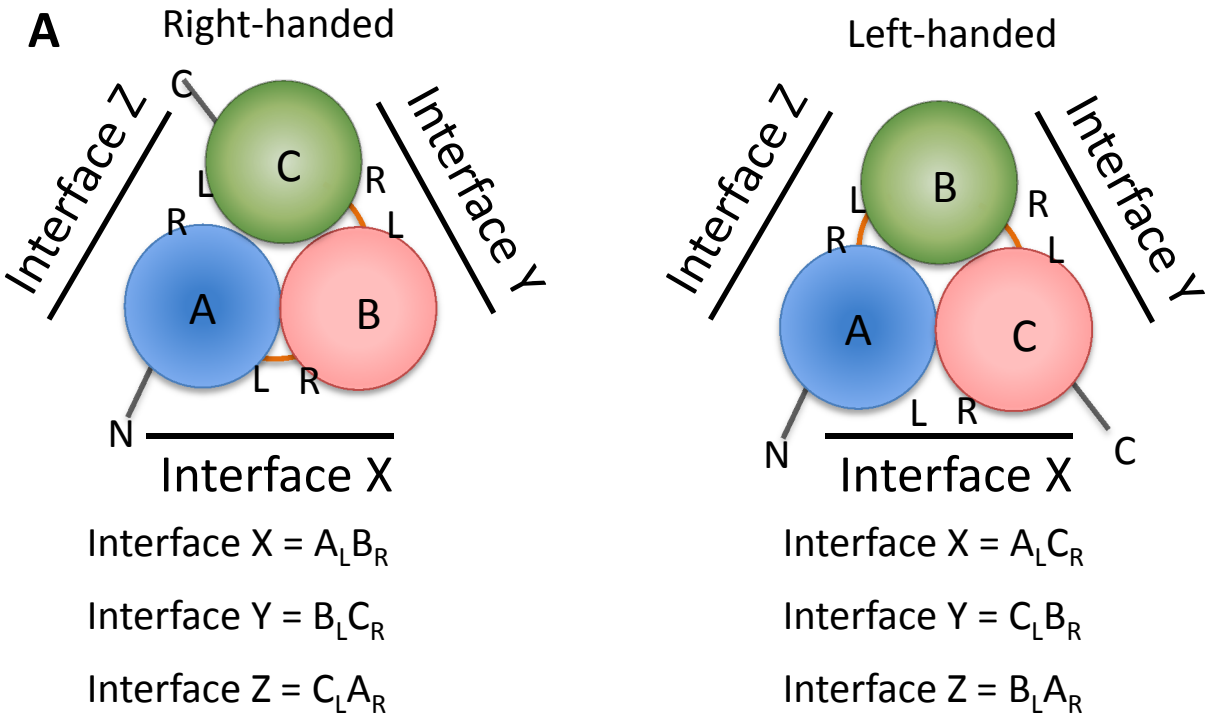

B

Single-block:

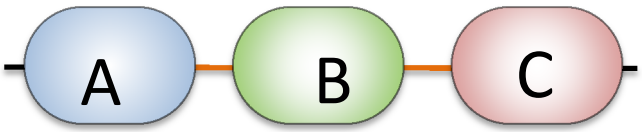

A_L = CDins B_L = WT C_L = WT

A_R = WT B_R = WT C_R = WT

Right Handed:
XYZ = Block – WT – WT

Left Handed:
XYZ = Block – WT – WT

C

Single-block, $RANK^{high}$:

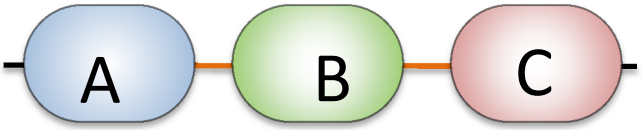

A_L = CDins B_L = KFH C_L = KFH

A_R = Q B_R = Q C_R = Q

Right Handed:
XYZ = Block – High – High

Left Handed:
XYZ = Block – High – High

*CDins/WT or CDins/Q = Block; KFH/Q = High affinity